Université du Québec

Institut National de la Recherche Scientifique

Centre Énergie, Matériaux et Télécomunications

Platinum and Platinum-Ceria Catalysts for the

Electro-oxidation of Ethanol

by

Maria João Vieira Ribeiro Paulo, M.Sc.

A thesis submitted to obtain the

degree of *Philosophiae doctor* (Ph.D.) in Energy and Materials Science

December 2018

Jury Members

President of the jury:	Prof. Daniel Guay (INRS-EMT)
External Examiner:	Prof. Rafik Naccache (U. Concordia)
External Examiner:	Prof. Oumarou Savadogo (E. Polytechnique)
Director of Research:	Prof. Ana Tavares (INRS-EMT)

Abstract

Direct ethanol fuel cells (DEFCs) are a promising system and a potential sustainable power source for portable, mobile, and stationary applications. The successful application of the direct ethanol fuel cells depends on the availability of a catalyst capable of breaking the carbon-carbon (C-C) bond leading to the complete oxidation of this fuel to carbon dioxide and water, releasing 12 electrons through an external circuit. Pure Pt is the state of the art electrocatalyst for the oxidation of ethanol but it suffers from some limitations such as poisoning by CO-intermediates, resulting in a slow ethanol oxidation reaction kinetics and incomplete oxidation with the formation of by-products such as acetaldehyde (two-electron oxidation) or acetic acid (four-electron oxidation).

In this work we aim at increasing the activity of Pt for ethanol oxidation, but using an approach that differs from the traditional which consists of carbon-supported platinum catalysts. Instead, we show that the electrocatalytic activity of unsupported Pt nanoparticles (NPs) for the ethanol oxidation in acid medium can be significantly enhanced by the addition of very small amounts of CeO_2 nanoparticles ($\leq$ 5 wt%).

In order to understand and to compare the effect of ceria on Pt nanoparticles with different particle sizes, catalysts with the same composition were synthesized by two different methods, the Pechini (sol-gel) and reduction (solution-based) methods. Variations explored in this work to control and compare the size of the Pt particles include: a 1, 5 and 10 times dilution of the polymeric matrix for the Pechini method, and the addition of a citrate stabilizer for the reduction method. In the first method, Pt NPs with sizes ranging from 4 to 40 nm were obtained, whereas in the reduction method much smaller nanoparticles, with sizes varying between 2 and 6

nm, were synthesized. Comparative studies on the Pt, Pt-CeO$_2$-1wt% and Pt-CeO$_2$-5wt% catalysts synthesized by both methods revealed the existence of two different effects.

In the Pechini method (larger particles), a strong electronic interaction between the Pt and CeO$_2$ nanoparticles was demonstrated by a systematic shift of the Pt 4f$_{7/2}$ peak to lower binding energies (BE) with the addition of CeO$_2$. As a result, the current density normalized to Pt's electrochemical surface area for ethanol oxidation increased up to 10 × by adding 1 wt% CeO$_2$. This positive effect is however hindered by a high coverage of the Pt nanoparticles surface by CeO$_2$ which results in the decrease of active sites. In this sense the addition of more CeO$_2$ (Pt-CeO$_2$-5wt%) was detrimental for the catalytic activity. Because there is no sharp distinction between the nanoparticle size and ceria effects, there is no evidence of a size effect on the catalysts produced by the Pechini method.

In the reduction method, we observed sharp shifts of the binding energy to higher values of Pt 4f$_{7/2}$ with a decreased of the size of Pt nanoparticles. Assuming the Wertheim's equation that establishes an inverse proportionality between the binding energy and the particle size of spherical-like clusters, there is evidence for the existence of size effect (final state effect). As expected, this relation is even more pronounced on the citrate-stabilized nanoparticles that correspond to the smallest catalysts produced in this work. In this sense we can remark a progressive BE increase from 71.4 eV (Pt-cit) to 71.9 eV (PtCeO$_2$-1wt%-cit) which is inversely related by a decrease in the Pt-cit particle size from 4 (Pt-cit) to 2 nm (PtCeO$_2$-1wt%-cit). The addition of 5wt% CeO$_2$ to Pt-cit corroborates the same trend but its BE varies less than the 1wt% CeO$_2$ since the last two composites show almost the same particle size. Thus, this enhancement is more meaningful on samples containing Pt-CeO$_2$ 1 wt%-cit and in Pt-CeO$_2$-5wt% with current densities for ethanol oxidation of 2.7 Am^{-2} and 4 Am^{-2} respectively. Moreover, PtCeO$_2$-5wt%,

presents the ideal size for ethanol oxidation (3 nm) to which is ascribed the best compromise between structural and electronic effects and/or oxophilicity effects of the Pt surface in order to favor the formation of CO_2.

The [H]NMR analysis of the liquid products obtained from a 5h ethanol oxidation reaction showed different selectivity: $PtCeO_2$-1wt%-cit produced slightly more acetaldehyde than acetic acid, whereas $PtCeO_2$-5wt% produced only a small amount of acetic acid. As $PtCeO_2$-1wt%-cit revealed a higher amount of Ce (III) and liquid products, it is possible that the ethanol oxidation to acetaldehyde and acetic acid, that requires the presence of oxygen-containing species, occurs via Ce_2O_3/CeO_2.

_____ _____

Maria João Paulo   Ana Tavares

Student   Director of Research

Acknowledgements

In first place, am deeply grateful to my professor Ana Tavares, for this experience and learning opportunity (not forgetting my master's) especially for her friendly encouragement during my PhD. This work would not be possible without her generosity, support, kindness and patient guidance… it means a lot.

I am sincerely grateful to my jury members, Professors Daniel Guay, Raffik Nacache and Omarou Savadogo for agreeing to be the reviewers of this work and doing me the honor of being a member in the evaluation of this thesis.

I also want to thanks to professors Ernesto Pereira and Renato Freitas from Sao Carlos University for their collaboration and positive discussions on the publications enrolling this work.

I want to acknowledge to Christophe Chabanier that so kindly helped me with all the characterization techniques as well as Jean-Philippe Masse from École Polytechnique Montréal for the time spent together on TEM.

Also not forgetting my colleagues and friends Spyrus Ntais, Julie Gaudet, Jules Galipaud, Erwan Bertin, Jussara Carneiro, Francesca Capitanio, Sebastian Garbarino and Caludie Roy with whom I had most of the fruitful and pleasant work discussions.

 I cannot forget the sympathy and professionalism of Hélène Tanguay, Hélène Sabourin and Louise Hudon.

The INRS would not be the same place without all the friends I made there and that filled my days with joyful moments during this long journey with which I learned, laughed and shared meals together! A special thanks to Esen Sokullu, Régis Imbeault, Juliana Barranco, Denis Ferachou, Qiliang Wei, Manoj Mridha, Antonio Benaya, Eva Hemmer, Cybelle Soares, William

Roger, Teresa Simão, Matteo Duca, Ivan Davalos, Hassan Hafez, Marta Quintanilla, and Shadi Rohani.

Pour ma famille au Québec, Lucie, Luc Bergeron merci pour être la et faire partie de ma vie avec beaucoup d'amour! Merci pour votre patience avec les corrections de mon français. Merci infiniment…

At last but not the least, I want to acknowledge my family my parents, my mother, my grandmother, for their unconditional love and support. To Bruno, the person I most admire in life and that hold my hand through it. Finally, a special acknowledgement to my baby Martin, for teaching me every day the true meaning of the scientific methodand for teaching me what it means a true engagement with life. Thank you.

Table of Contents

List of Figures

XIV

List of Tables

1. Introduction

1.1. CO_2 cycle

Carbon dioxide from human and animal respiration is sent into the atmosphere, and then recycled into oxygen by plants in the process of photosynthesis. This cycle that operates on a daily basis, is changing over decades and centuries. Before the widespread use of fossil fuels, the composition of the atmosphere was balanced between CO_2-absorbing, oxygen-producing plants, and CO_2-producing, oxygen-absorbing animals. But exploiting and burning of fossil fuels in large quantities is effectively creating a huge input of carbon dioxide. Before the 18th century, our atmosphere typically contained about 280 parts per million of carbon dioxide. With the spread use of the fossil fuels since industrial era, the amount of CO_2 rised, reaching the value of 400 parts per million. In 2014, the CO_2 concentrations crossed 400 ppm in the atmosphere for the first time (410ppm) in at least 2.5 million years, Figure 1. 1
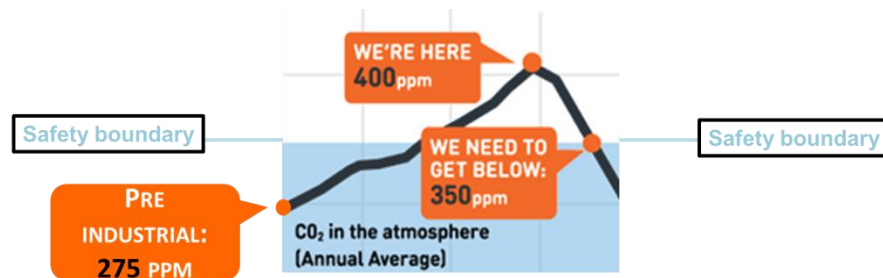
Figure 1. 1 – CO_2 limit levels and safety boundaries[1].

Recent studies state that, CO_2 levels increased 100 ppm over the last century with consequent temperature increase of about 0.8 °C over this period. Thus, if we eliminate further emissions of CO_2 we would obtain near constant temperatures for many centuries[2]. The rapid

growth in demand for animal-based agriculture has put other greenhouse gases like methane and nitrous oxide into the atmosphere. The contribution of agriculture causes about 15% of global emissions[1,2]. Burning fossil fuels remains by far the biggest single contributor to the problem, causing 57% of global emissions[1]. In fact, carbon dioxide stays active in the atmosphere much longer than methane and other greenhouse gases. The consequences of this negative effect are visible as in the greenhouse effect, which causes the temperature of the atmosphere to rise as the levels of CO_2 rise.

Alternative organic liquid fuels, resulting from vegetable and animal wastes, represent energy incomes that are continuously replenished and renewed[3]. Biomass wastes derived from domestic, commercial and industrial activities can be converted to ethanol. These include municipal solid wastes (paper, cloth, garden debris) and commercial and industrial wastes (paper, packing materials, textiles, demolition wood). Ethanol is a liquid hydrocarbon, and just like gasoline, it can be distributed via the existing infrastructure and does not require advanced mobile storage containers as it is the case with compressed H_2. Different from methanol whose low boiling point, inflammability, toxicity are harmful to the user if leakage occurs during fuel cell use, ethanol it is non-toxic. Moreover, it is reported that excessive inhalation of methanol can lead to permanent blindness or have an adverse effect on the optical nerve[4].

Table 1 – The several sources of ethanol, the energy ratio output/input and their commercialization status[4].

Source type	Sources	Energy (output/input)	Commercialization stage
Food crops	Corn Wheat Barley Sugarcane Sugar beet Cassava Sorghum	1.4 < corn < 2.8 8 2	Commercial plants of ethanol mainly from corn (US) and sugarcane (Brazil).
Inedible parts of plant - cellulosic ethanol (non-food crops)	Corn stover Wheat straw Rice straw Sugarcane bagasse	5.2 – 5.54 5.2 32	Pre-commercial stage or pilot scale.
Cellulosic ethanol + waste (non-food crops)	Switch grass Forest residue Agricultural waste Municipality waste	2-36	Pilot scale.

The energy output/input ratio, Table 1, is the ratio of the energy content in ethanol to the energy content in fossil fuels used to produce ethanol from the respective biomass. As an example, ethanol produced from corn using fossil fuels as source of electricity, can achieve an energy output/input ratio of 2. However, this energy balance calculated from the output/input ratio is much better if ethanol is produced from cellulosic feedstock such as corn stover, wheat straw or sugarcane bagasse. If process residues and co-products are taken into account for generating electricity (or process heat), the energy output/input ratios obtained can increase from 5.2 to 32 as shown in Table 1. Even more interestingly, ethanol can be produced from non-edible parts of the plans such as switch grass, forest residues and municipality waste. The energy

output/input ratio for these sources may vary from 2 to 36 depending on the effectiveness of the pre-treatment to breakdown the cellulosic structure, and also on the utilization of the residual matter for electricity/heat generation. However this last process is still at its pilot scale or demonstration level.

By the other way, using ethanol with gasoline as a vehicle fuel has greenhouse gas (GHG) emissions benefits, considering the life cycle steps required for gasoline production. Even for the common case of corn-ethanol, the carbon dioxide (CO_2) released when ethanol is used in vehicles, is re-cycled to grow crops that capture that same amount of CO_2[5]. As a result, ethanol tolerant vehicles that can run on high-level blends of ethanol produce less net CO_2 than conventional vehicles. A 2012 study by Argonne National Laboratory, found that when these entire fuel life cycles are considered, using corn-based ethanol in place of gasoline reduces life cycle GHG emissions on average by 34%. The future use of cellulosic ethanol may potentially reduce the GHG emissions by up to 108%, since ethanol produced from cellulosic material reduce petroleum inputs substantially[6] but it is not as far technologically advanced as corn from agriculture[7].

The complete combustion (production of CO_2) of both fuels, gasoline and ethanol, is shown by the following equations[8] 1.1 and 1.2:

$$C_8H_{18}\,(l) + 12.5O_2(g) \rightarrow 8CO_2(g) + 9H_2O(l) + heat\ (\Delta H = 3500 kJ/mol) \qquad \text{(Equation 1.1)}$$

$$C_2H_6O\,(l) + 3O_2\,(g) \rightarrow 2CO_2\,(g) + 3\,H_2O\,(l) + heat\ \ (\Delta H = 1300\ kJ/mol) \qquad \text{(Equation 1.2)}$$
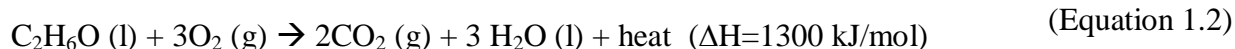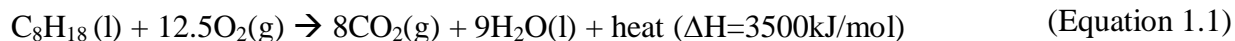
In general most countries try to move away from the dependence on traditional petroleum based fossil fuels in favor of more sustainable options. For instance, in Brazil, since 1976 there are no light vehicles running on pure gasoline. Since 1993, this blend was fixed by law at 22% anhydrous ethanol for the entire country[9]. Other countries such as the USA and more recently in

France (with the E85 fuel containing 85% of ethanol), ethanol is already distributed through the fuel station network for use in conventional automobiles with internal combustion engines (flex-fuel vehicles)[10]. Canada is also requiring renewable content in fuels and it is committed to reducing its total greenhouse gases emissions by 17% from 2005 to 2020 which is estimated to result in a cumulative reduction of 47.4 million tons of CO_2[5]. In long term, the combination of ethanol (a renewable resource) and fuel cell (a promising and attractive technology) can bring benefits, not only lowering GHG emissions but also increasing the air quality and energy security while creating economic opportunities from the social point of view[11].

1.2. Direct Ethanol Fuel Cells

Fuel cells are electrochemical devices designed to convert the chemical energy of a fuel into electricity. One of the main reasons for studying direct energy conversion is to seek out new and better ways to convert our present forms of primary energy (thermal, radiant, mechanical and chemical) into electricity, while improving conversion efficiency.

Fuel cells can help to reduce our dependence on fossil fuels and diminish poisonous emissions into the atmosphere, since they have higher electrical efficiency compared to heat engines[12]. The efficiency of any energy conversion device is defined as the ratio between useful energy output and energy input. In practice a fuel cell has an efficiency of 50-60% whereas an internal combustion engine is less than 35% efficient[13]. An internal combustion engine (ICE) that drives cars is limited by the Carnot cycle which means that the engine's conversion of heat into work, should depend on the temperatures T_h and T_c (hot and cold respectively). Most efforts to improve the efficiency of the ICE's go into increasing the temperature of the heat source, but at very high

temperatures, the metal of the engine begins to soften[14]. However not all the supplied heat can be converted to mechanical energy[15] due to heat and friction losses[16]. In addition the CO_2 emissions of a car are proportional to its fuel consumption. However the devices that convert a fuel's chemical energy directly into electrical energy, such as fuel cells, are not limited by the Carnot efficiency and can exceed it. A scheme of a Direct Ethanol Fuel Cell is shown in

Figure **1. 2**.
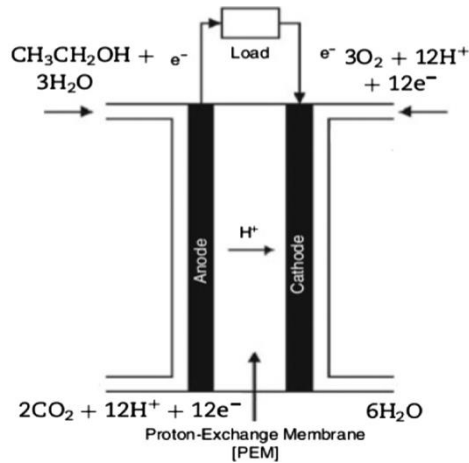
Figure 1. 2 – Direct ethanol fuel cell (acid) from Zakaria *et al.* [17]

The two half and overall reactions occurring in a direct ethanol fuel cell (DEFC) in acid medium at 25 °C are[18] written in equations 1.3 and 1.4. The overall reaction is summed up in equation 1.5.

Anode $C_2H_5OH + 3H_2O \rightarrow 2CO_2 + 12H^+ + 12e^-$ $E^0 = 0.084V$ (Equation 1.3)

Cathode $2O_2 + 12H^+ + 12e^- \rightarrow 6H_2O$ $E^0 = 1.23V$ (Equation 1.4)

Overall $C_2H_5OH + 3O_2 \rightarrow 2CO_2 + 3H_2O$ $E^0 = 1.146$ (Equation 1.5)
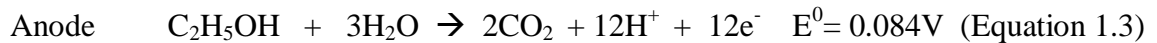
The fuel (ethanol) is oxidized at the anode producing 12 H^+ (Equation1.3) that are conducted through an electrolyte to the cathode. At the cathode, the protons will react with oxygen and, thus, water is produced (Equation 1.4). The 12 electrons that are released upon the oxidation of ethanol travel through an external circuit to the cathode, closing the electrical circuit. Inside the fuel cell, the ionic current is transported by migration and diffusion of the 12 H^+ cations in the electrolyte. The overall reaction to produce electricity is shown in Equation 1.5 and the cell voltage in theory is 1.145 V (at 25 °C) i.e. if all the ethanol is fully oxidized to CO_2 and water[19]. The Faradic or current efficiency of a fuel cell reaction can be defined as the ratio of the actual number of electrons involved in the oxidation reaction (n_{actual}) to the theoretical number of electrons involved in the complete fuel oxidation reaction (n_{theo}) as given below[4], equation 1.6.

$$Ef (\%)=(n_{actual}/n_{theo}) \times 100 \qquad\qquad \text{(Equation 1.6)}$$

As it will be detailed in section 1.3 the ethanol oxidation at platinum electrodes leads to the formation of other reaction products than CO_2, like acetic acid, acetaldehyde. These reaction products, that involve the transfer of 4 and 2 electrons, respectively, leads to decrease the total efficiency of a DEFC. The theoretical Faradic efficiency of ethanol oxidation can vary from 33% (i.e. $4/12 \times 100 = 33\%$) to 100% (i.e. $12/12 \times 100 = 100\%$) respectively for a 4 electrons (partial oxidation to acetic acid, i.e., $C_2H_5OH + H_2O \rightarrow CH_3COOH + 4H^+ + 4e^-$) and 12 electrons (complete oxidation to CO_2 i.e. $C_2H_5OH + 3H_2O \rightarrow 2CO_2 + 12H^+ + 12e^-$). Therefore, it is very important to identify the reaction intermediates and products in order to formulate the best catalyst. In practice, most of the DEFC at lab scale produce power densities of around 10% of that obtainable from the corresponding H_2 fuel cell[20] with 100% complete oxidation reaction. Even if considering complete oxidation of ethanol to CO_2 and working at a cell voltage of 0.5 V

and with a current density of 100 mA/cm^2, a DEFC would result in an efficiency of 40%, which is in the same range of efficiency of a diesel internal combustion engine[20,21]. In a DEFC, however, it is yet not clear if the reduced current density is due to incomplete oxidation or ethanol crossover, or to both. The concept of ethanol crossover will be further detailed but briefly it consists on that amount of ethanol that is transported, together with protons, through the membrane from the anode to the cathode without taking part in the electrochemical reactions. This creates a mix-potential and reduces the efficiency and the overall cell performance[20,21]. The electrolyte is usually a solid polymer electrolyte membrane (PEM). The oxygen reduction and the ethanol oxidation occur on the two electrode assembled on both sides of this membrane. Currently the only commercial available membrane is Nafion® but ethanol and methanol crossover issues have prompted the development of composite membranes consisting of a polymer and inorganic components (*e.g.* nafion-composites or other ionomer membranes)[22]. Both proton conductivity and alcohol permeability increase with temperature in a DEFC but the higher the temperature of the alcohol solution the more severe the membrane swelling which leads to increased fuel crossover[23,24]. In order to increase the performance of direct alcohol fuel cells (DAFCs) and to reduce the alcohol crossover modified nafion membranes have been attempted as for example, the incorporation of titanate nanotubes in the nafion matrix[23,24] . The membranes for PEM fuel cells may be suitable for low (~40−60°C) or high (in the 100−200 °C)[18,25-29] temperature or even at more intermediate temperatures. Nowadays it is necessary to look for membranes that are less permeable to alcohols and work at higher temperatures (80−120 C) to increase the rate of the electrochemical reactions involved (oxidation of alcohol and reduction of oxygen) and to manage better the heat produced[10]. An example of a polarization curve for a direct ethanol fuel cell, on the range 80-130 °C (intermediate), is shown in Figure 1.3.
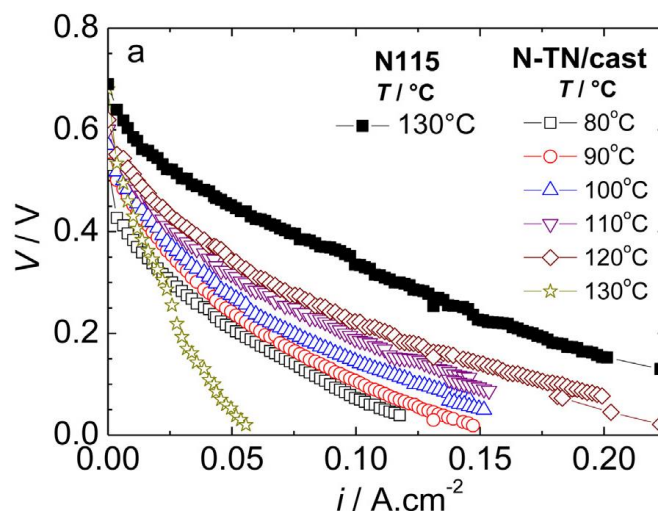
Figure 1. 3 – Polarization curves of DEFC as a function of temperature for Nafion-titania composite membranes.[24]

As can be observed in Figure 1.3, increasing the temperature, increases the DEFC performance using Nafion-Titania composite membranes from 80 ºC to 120 ºC, whereas at T=130ºC the lowest DEFC performance is observed. The authors report that this temperature-limit the membrane's thermal stability is compromised resulting in ethanol crossover within the membrane of the DEFC. As a matter of fact, the fuel crossover in DEFC is responsible for approximately 50% of the reduction of the DEFC performance[23,30]. By the other way, both ethanol oxidation and oxygen reduction reactions are kinetically very slow[31]. In the current work, we synthesize Platinum based nanoparticles to electrocatalyze the ethanol electro-oxidation reaction, equation (1.5).

Platinum is the state of art catalyst for several electrochemical reactions, not only because of its stability in both acidic and basic medium, but also because of its reactivity toward most of the oxidation and reduction reactions of a large number of molecules[18,32].

In order to reduce fuel cell costs, efforts are primarily being made on reducing the Pt loading in the electrodes[33]. For the platinum group metals (Pt, Ir, Os, Ru, Rh, and Pd) the content and loading have to be low to achieve system cost targets. For automotive fuel cells systems the Pt loading varies from 0.15 to 0.3 mg_{Pt}/cm^2 [34]. For instance by the year 2020 the target value is expected to be as low as 0.125 mg_{Pt}/cm^2 for a H_2/O_2 PEM fuel cell operating at 80°C and a Pt mass activity of 0.44 A/mg[34,35].

1.3. Ethanol oxidation mechanism on Platinum

Oxidation of alcohols, aldehydes, ketones and carboxylic acids are among the most extensively studied reactions on small organic molecules (SOM) on transition metal surfaces such as Pt. The reaction pathways and product selectivity observed during the decomposition of alcohols and aldehydes depend on the transition metal[36]. Figure 1.5 shows the whole schematic process of ethanol partial and total oxidation on Pt.
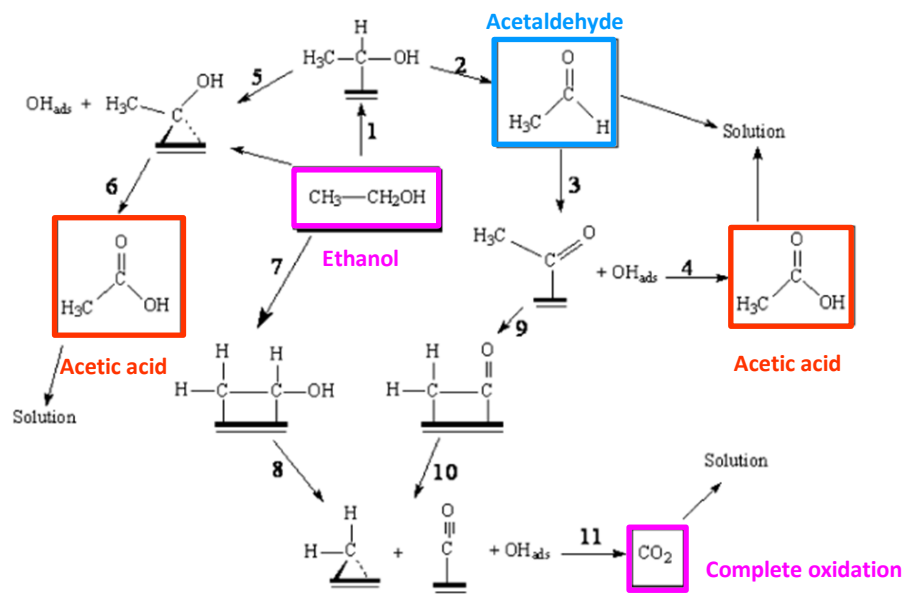
Figure 1. 4. – Ethanol oxidation reaction and intermediates by-products on Pt, adapted from ref [36].

Ethanol can be first adsorbed on the surface of a Platinum site followed by the α-C-H dissociation, leading to the formation of adsorbed acetaldehyde (step 1) that can be released in the solution (step 2)[36,37]. These are the simplest and fastest steps, which justify the high amounts of acetaldehyde usually obtained by electrolysis. Acetaldehyde can be re-adsorbed according to step 3 and interact with adsorbed OH generating acetic acid in step 4[36]. This product can be also formed through steps 5 and 6 but it is apparently less probable. On the contrary to acetaldehyde, acetic acid is not desirable since it is extremely stable (non-reactive specie) in acid solution impeding the total ethanol oxidation toward CO_2[38]. Acetaldehyde may react with the Pt surface to be oxidized to CO_2. Many catalyst materials have been investigated so that ethanol is selectively oxidized to CO_2 instead of partially oxidized to acetic acid and/or acetaldehyde, the main products in most of the DEFCs. In section 1.6 we will show examples on the ethanol oxidation reaction products.

It is also well known that CO irreversibly adsorbs on the Pt surface, blocking the active sites in the final step. CO strongly binds to platinum with time until total saturation. This phenomenon is known as platinum poisoning. Consequently, the attachment of a CO molecule onto the catalyst reduces the surface available for ethanol oxidation. The presence of adsorbed CO can be explained by two distinct sequences: steps 7 and 8 or steps 9 and 10. In the first case, one molecule of ethanol must adsorb on Pt by the two C-H groups leading to the rupture of the bond between two C atoms[36]. The second one implies the rupture of the C-H bond of the intermediate form after the acetaldehyde adsorption. Finally, the CO_{ads} species can react with adsorbed OH to form CO_2 completing the total ethanol oxidation.

It is obvious that an ideal catalyst for ethanol oxidation would be one that results in the selective formation of $CH_2CH(OH)_{ads}$ species by the cleavage of C-H bonds (step 7) followed by C-C bond cleavage (step 8) and subsequent oxidation of intermediates to CO_2 in the presence of adsorbed OH[39]. To overcome this problem, a second metal which helps Pt to become CO-tolerant, is added to platinum. The second metal should either be able to form oxygenated species (metal-OH) at potentials lower than that for pure Pt or electronically weaken the platinum to CO bond. This would lead to a more complete ethanol oxidation than on a pure platinum catalyst[40,41].

Among the metals that can be used, Ru[42] has been extensively used due to the easy formation of Ru-OH species at low potentials. For example, Iwasita studied the activity of PtRu electrodeposits with different compositions toward the electrochemical oxidation of ethanol. As shown in Figure 1.6, the catalysts with low Ru content exhibit a very low activity.
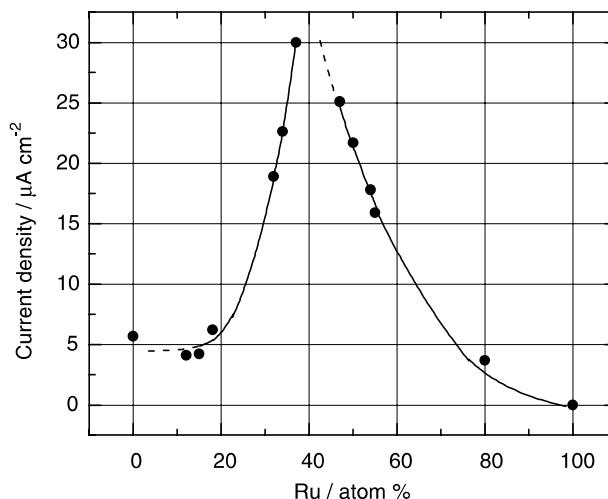
Figure 1. 5 – Catalysis of EtOH electro-oxidation by PtRu: the influence of catalyst composition. [43]

At low Ru concentration, there are not enough Ru sites to effectively assist the oxidation of adsorbed residues and the oxidation current remains almost at the levels obtained for pure Pt. For a Ru content higher than 20 at%, the current densities increase steeply. A Pt:Ru ratio of 60:40 seems to be close to the optimum composition for the ethanol oxidation. Ru concentrations higher than ca. 40 at% cause the current to fall. This effect can be rationalized in terms of an inhibition of ethanol adsorption, which is probably due to the diminution of Pt sites. Therefore, the presence of small amounts of Ru has no effect on the ethanol oxidation current. The promoting current density of Ru starts at a minimum concentration of 20%.

A series of PtM alloys were tested by Beden[44] to study the oxidation of small organic molecules in acid and basic media. The authors conclude that from all metals (Ru, Sn, Re, Pb) alloyed with Pt, Ru provided a higher catalytic activity in all the tested experimental conditions. However, the limited availability of Ru may become a significant problem before PEMFC systems can be placed on the market. Due to the limited availability of Ru, it is necessary to find alternative metals at a lowest potential possible. Many other Pt-based catalysts, with a good CO

tolerance and that can provide OH, have thus been proposed as alternatives to PtRu[45] which are Pt-SnO[36], Pt-WO$_3$[46], Pt-ZrO$_2$[47], Pt-TiO$_2$[48] . Indeed the addition of other oxophilic elements to Pt, in the form of an alloy or a co-deposit also yields to a significant improvement in the CO-tolerance relative to pure Pt[49]. Consequently, it is generally accepted that complete ethanol electro-oxidation, cannot be performed on Pt only and the operating mechanisms behind the role of the second element are presented in the next paragraph.

1.4. Bifunctional and electronic effects

The "bifunctional effect" was initially proposed in the 70s by Watanabe and Motoo[42] to explain the CO oxidation on PtRu catalysts. In this mechanism, platinum is the catalytic material that breaks the C-C chemical bond in ethanol, while ruthenium provides oxidizing species releasing the adsorption sites of platinum occupied by CO (Equation 1.6). Specifically, ruthenium is known to easily bond hydroxyl species (OH$_{ads}$) at a more negative potential than Pt (Equation1.7). The adsorbed OH reacts with the adsorbed CO on the Pt neighbor oxidizing it (Equation1.8). In this way the CO is transformed in CO$_2$, and the platinum sites become again available to adsorb ethanol[49]:

Adsorption: $Pt + CO \rightarrow Pt\text{-}CO_{ads}$ (Equation 1.6)

Water activation: $Ru + H_2O \rightarrow Ru\text{-}OH_{ads} + H^+ + e^-$ (Equation 1.7)

CO to CO$_2$ conversion: $Pt\text{-}CO_{ads} + Ru\text{-}OH_{ads} \rightarrow Pt + Ru + CO_2 + H^+ + e^-$ (Equation 1.8)
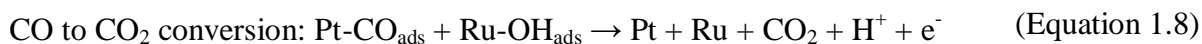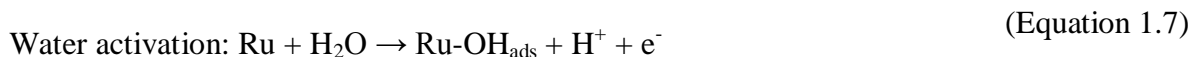
The "electronic effect" can also be used to explain the mechanism on bimetallic catalysts. This theory is related with the modification of the Pt electronic properties by its co-catalyst. Some authors also call it « ligand effect » since it resembles what occurs when a ligand is bound to an inorganic complex[50]. It has been proposed that in the electronic effect, the CO tolerance is

associated with an energy shift of the Pt 5d electronic states caused by the second element. As explained in Figure 1. 6 a) and b), a linear or bridge-bonded CO species are formed on the Pt catalyst surface[51-54]. Such strong binding between the metal and CO, has been explained by the electron donation of two electrons from the 5σ carbon monoxide orbital, Figure 1. 6 a) to the metal, and subsequent transfer of the same two electrons from the d metal atomic orbital to the antibonding $2\pi^*$ CO orbital[49], Figure 1. 6 b). This electron transfer is known as back-donation.
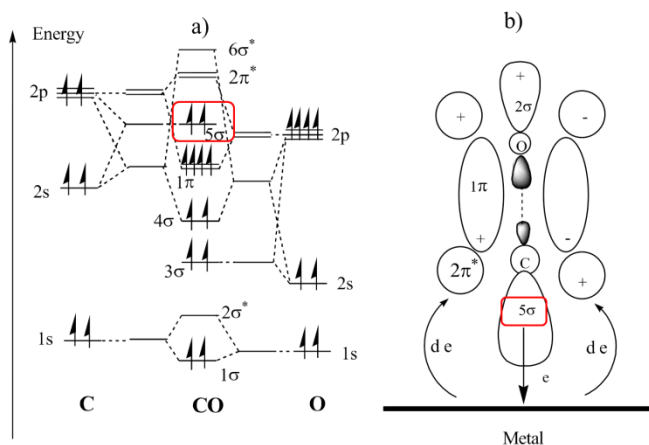
Figure 1. 6 – a) The energy level of carbon monoxide molecules, and b) the formation of the strong metal-carbon monoxide bonding (back-donation) [49].

The proximity of the second metal (the co-catalyst) modifies the electronic structure of Pt. For example, in a presence of less electronegative metals, the electronic density around Pt will increase, increasing the back donation effect. In this way, the strength of the C-O bond will decrease, and the CO will be activated for further oxidation to CO_2 so that it desorbs from Pt surface. As a result the Pt–CO interactions will become weakened and the poisoning effect on Pt is diminished.

15

1.5. The Pt particle size effect

The first direct evidence reported for the effect of the Pt particle size on the binding energy studied by X-Ray photoelectron Spectroscopy (XPS) was done by Mason et al.[55] in 1977. The author wrote that "The effects of cluster size on electronic structure are manifested by the variations in core spectra". Since then, it has been generally accepted that the electrocatalyst size effect certainly exists and in this case, for the electro-oxidation of alcohols and their derivatives on the Pt electrocatalyst surface.

Arenz et al.[56] recently showed that the rate of CO_2 production is strongly dependent on the size of Pt nanoparticles in the order of $1 \leq 2 < 5 << 30$ nm. However, they ascribed their results to the number of defects, which were abundant on the surface of large particles and played a beneficial role in CO oxidative removal. In another study[57], the catalytic activity of a series of Pt/MWCNTs with average particle size of 1.7, 2.4, and 4.0 nm were tested toward alcohol electro-oxidation reactions, (methanol, ethanol and ethylene glycol) following similar conclusions. The authors reported that the catalytic activities had a strong dependence on their Pt particle size: as the size decreased, the alcohol electro-oxidation increased but this benefit was limited to a stronger CO adsorption on the smaller Pt nanoparticles. Bergamaski et al.[58] found that the optimum particle size for methanol electro-oxidation to CO_2 was 3–10 nm, and the loss in efficiency mostly occurred on either too small or too large particles. The authors point out the critical desorption of formaldehyde by-product to the solution once out of this range. Interestingly, in another study[59] on ethanol oxidation in platinum nanoparticles in the 2−6 nm range, showed that the Pt catalytic activity (in both the gas and liquid phases) is highly dependent on the size, but not the selectivity. Acetaldehyde was then a general major product.

The effect of particle size on the current density of the ethanol oxidation reaction (EOR) has been less studied than in methanol but Perez et al.[60] studied the electroactivity of particles with diameter inferior to 5 nm. The author that extensively studied the effect of the particle size on EOR found a maximum current density of 32 mAcm^{-2} when the Pt (carbon supported) particle size was 2.6 nm for ethanol oxidation. The origin of this particle size effect appears to be due to the stronger adsorption of oxygenated intermediate species on the smaller particles.

1.6. State of the art catalysts for DEFCs

Studies performed in the last two decades reported a wide spectrum of CO_2 yields for the ethanol oxidation reaction. An overview about some publications dealing with ethanol oxidation reaction in acidic media and their key findings are briefly presented in Table 1.1[15].

Table 1. 1 – Some of the most representative publications on the ethanol oxidation yields by means of CO_2, acetic acid (AA) and acetaldehyde (AAL) in acidic medium. The results are shown for the best catalyst of each publication.

Catalyst	Method	Pt loading	Setup	T (ºC)	Main product	CO_2 yield	Ref.
Polyc. Pt	smooth polycrystalline Pt	-	3-Electrode cell	10	AAL, AA	n.a.	[61]
Pt Ru, Pt40% Pt-20% Ru/Vulcan XC 72	Comercial (Mateck)	Anode and Cathode: 2 mg Pt/ cm^2	DEFC	145	CO_2	>95%	[62]
$Pt_xRu_{(1-x)}$, (1.0<x<0.5)	potentiostatic co- deposition	-	3-Electrode cell	5-40	CO_2	n.a.	[63]
Polyc. Pt	smooth polycrystalline Pt disk	-	3-Electrode cell	25	AA, AAL	Aprox 10%	[64]
Pt/C	Commercial 20 wt % metal, E-TEK Inc.)	28 μgPt/cm^2	3-Electrode cell	23-30-60	AA, AAL	Aprox. 7.5%	[27]
Pt/C, PtRu/C, PtSn(9:1)/C	"Bönneman" method	1.5 mg/cm^2	3-Electrode cell, DEFC	50-110	AA, AAL	n.a.	[65]
Pt/C	"Bönneman" method	Anode: 3 mgPt/cm^2, Cathode: 2 mgPt/cm^2	DEFC	80	AA	20%	[66]
Pt/C	Commercial (Pt 20%, Alpha Aesar, Pt:Ru, E-TEK)	Anode and Cathode: 4 mg Pt/cm^2	DEFC	90	CO_2	86%	[67]
PtSn/C, PtRu/C	Commercial (Johnson Matthey Corp.)	Anode :1.33m gPt/cm^2 for PtSn/C and PtRu/C Cathode: 1.0 mg Pt/cm^2.	DEFC	90	AA	n.a.	[68]

Pt/C Pt/CNT Pt/CNT/PANI	NaBH$_4$ reduction method	Pt : 40%	3-Electrode cell	Room T	n.a	n.a.	[69]
PtSn(M) M= Ni, Co	"Bönneman" method	2mg/cm^2	DEFC	80	n.a	n.a.	[70]
PtSnCe (Pt=68wt% Sn=22wt% Ce=10wt%)	Polymeric precursor method	1mg/cm^2	DEFC	100	CO$_2$ Acetic acid	n.a	[71]

The most remarkable characteristic from Table 1.1 is that the highest CO$_2$ yields are reported for DEFCs and not for model electrodes in a three electrodes setup[62]. Rao et al.[67] proposed that the intrinsic anodic oxidation conditions within a PEMFC anode, mainly residence time (several weeks of operation) and Pt catalyst loading (4 mg cm^{-2}), enhance the C-C cleavage rate. Behm *et al.*[72]showed that the main parameter to affect C-C bond breaking in ethanol oxidation is temperature. Higher temperatures lead to an enhanced CO$_2$ efficiency (up to 50%) because the C-C bond dissociation was reported to be as high as 90% at 250 °C[15]. In a recent review paper[73], it is also reported that Pt completely oxidizes ethanol to CO$_2$ but rather in small amount. At higher temperature, Pt alone has a higher conversion to CO$_2$ than other catalysts at 80 °C but this value remains below 20%. However,it is important to mention that mechanical and thermal stability, along with high ionic conductivity, have to be met with the membrane material in a DEFC. The fraction of ethanol that is converted to CO$_2$ is also influenced by other different parameters such as ethanol concentration. Camara and Iwasita[64] found that the production of acetic acid and acetaldehyde depends strongly on the ethanol concentration. Total oxidation to CO$_2$ and high yields of acetic acid was only observed at ethanol concentrations below 0.1 M. With increasing ethanol concentration, the oxidation to acetaldehyde becomes the main reaction. This is one of the keys to the complete oxidation to CO$_2$ i.e. to find a way to selectively produce

acetaldehyde (aldehydes) even before undergoing the C-C cleavage of the ethanol structure. If this cleavage does not occur, then the non-oxidized acetic acid may form in abundance which is a dead-end procuct[70]. The same strategy is followed by Beyhan *et al.*[70] that studied several combinations of trimetallic catalysts from the PtSnM family (M=Ni, Co, Rh, Pd) in order to find out the best catalyst for acetaldehyde yield. The authors found out that both Ni and Co can promote the high yields of acetaldehyde that can be further oxidized to CO_2. Thus, both PtSnNi/C and PtSnCo/C produced a four times higher catalytic activity than PtSn/C bimetallic catalyst. Still in the field of rare earths, De Souza *et al.*[71] investigated the ethanol oxidation reaction using $PtSnCeO_2$/C electrocatalysts observing a current density 50% higher than that observed for commercial PtSn/C. Their tests in DEFC also showed a power density 40% higher than for the same commercial PtSn/C electrodes. The authors found that for PtSn/C electrocatalysts acetaldehyde and acetic acid were the main products while on $PtSn/CeO_2$/C electrocatalysts produced CO_2 and acetic acid. It is very interesting to note that PtSn/C lead to acetaldehyde, which involves only two electrons per ethanol molecule while the presence of cerium was necessary to convert ethanol preferably to acetic acid which in the end resulted in the best performance for PtSnCe/C catalyst. Data from FTIR suggested that the presence of Sn and Ce either favor CO oxidation, since they produce an oxygen-containing species to oxidize acetaldehyde to acetic acid but the authors do not exclude the possibility of a change in the platinum electronic density due to both elements.

1.7. Platinum and ceria catalysts

Pt is recognized to be the best monometallic catalyst for oxidation of small organic molecules in acid medium. However, certain metal oxides such as RuO_2,[74] WO_3[46], ZrO_2[47], TiO_2[48], and CeO_2[75-77], have been found to enhance the catalytic activity of Pt for ethanol or methanol electro-oxidation through synergetic interactions. Nobel metal-ceria based catalysts are among the systems known to exhibit strong catalyst and co-catalysts interactions[78]. Yao *et al*[79] showed in 1984, that ceria was a chemically active component in such catalysts where it appeared to play the role of an oxygen storage component, releasing stored oxygen during fuel-rich cycles, thus facilitating oxidation of hydrocarbons and CO. Therefore, CeO_2 have been proposed as Pt co-catalyst for the oxidation of small organic molecules[80] and many authors have already verified that CO oxidation to CO_2 is strongly promoted on Pt partially covered by CeO_2[78,81-83]. In addition, this rare earth costs 4 times less than ruthenium, 10 times less than iridium, 15 times less than palladium, and 35 times less than rhodium or Pt[84].

De Souza *et al.* already reported on a progressive increase in the Platinum's catalytic performance toward ethanol oxidation[85] from 0 to 25 wt% of Ce and then from 50 to 70 wt% although there is no specification on the products obtained, Figure 1. 7. The authors also reported a Pt particle size of 3 nm for all the Pt-CeO_2 electrocatalysts.
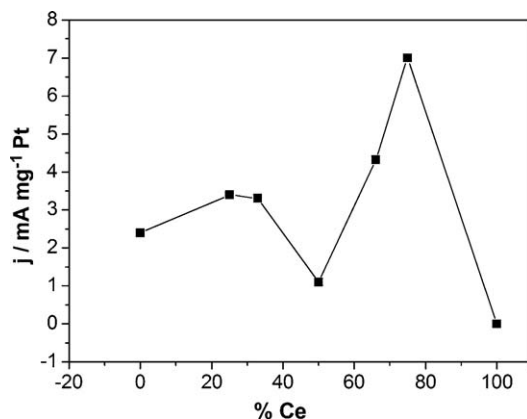
Figure 1. 7 – Ethanol electrocatalytic activity as a function of % Ce in Pt-CeO$_2$ catalysts[67].

The Pt performance is enhanced even at Ce contents as low as 25 wt%. The dependence of the current density with %Ce show two maxima, Figure 1. 7. Both enhancements can be attributed to a higher CO tolerance but it is not clear if it is because of bifunctional or electronic effects. For a Ce content of 50% the current decreases substantially, and the authors correlated it to the lower specific surface area of Pt of the catalyst. This behavior is completely different from that observed for Pt-Ru catalysts, where the current densities on catalysts with a Ru content higher than 25% increase steeply, and a Pt:Ru ratio of 60:40 seems be the optimum for ethanol oxidation[43], Figure 1.6. The authors conclude that ceria's behaviour may not be described only by bifunctional mechanism as in PtRu. In a published study[86] on the methanol oxidation on PtCeO$_2$ with only 9 wt% of ceria, the composite catalyst exhibited a better activity (20 mA/cm^2 with chronoamperometry at 0.5 V vs SCE) and stability than did the unmodified Pt/C (1 mA/cm^2 with chronoamperometry at 0.5 V vs SCE. For a matter of comparison, the authors reported a commercial PtRu with electrochemical activity of 30 mA/cm^2 under the same conditions.

Corradini et *al.*[87] synthesized by the Polyol method, Pt with rare earths (Lanthanides, Ln) catalysts with the same general composition Pt=85 and Ln=15 wt%, including cerium, for ethanol oxidation reaction. The obtained current density follows the order Pt/C < Pt–Eu < Pt–La ~ Pt–Pr ~ Pt–Ce indicating that cerium is the lanthanide with best current density competing with praseodymium (Pr) both reaching approximately a current density of 0.01 mAcm^{-2} (chronoamperometry at 0.6 V vs RHE). In another work also dedicated to ethanol oxidation, Cordeiro *et al.*[88]compared oven-dried $PtCeO_2$ samples at different temperatures, where the amount of ceria is twice more the amount of Pt. The authors reported that ceria increased two times more the Pt current (chronoamperometry at 0.5 V vs RHE), which was attributed to the heat treatment at 400 ºC. This temperature allowed a suitable crystallite size (8.1nm) and a proper bandgap size of 3.43 eV for optimal electron conduction. Wang et *al.*[89] synthesized Pt-CeO_2 catalysts by CBPLD under different pressures finding out that at 0.5 Torr the current density reached its maximum of 15 mA cm^{-2} (chronoamperometry at 0.6 V vs Ag/AgCl) due to a higher ESA of the Pt, which exposed a larger number of active sites for surface reactions.

In fact, ceria's enhanced ability to adsorb, dissociate and release oxygen via the Ce^{4+}/Ce^{3+} redox cycle[80] may justify in many cases its co-catalytic effect. Ceria may adopt several non-stoichiometric oxides between two limit compositions CeO_2 (Ce^{4+}) and Ce_2O_3 (Ce^{3+}) or in general, $Ce_xO_{2-x.}$ Its defects are oxygen vacancies, acting as an oxygen buffer[80,90] facilitating the incorporation of oxygen into the Pt surface. Thus, ceria can be regenerated due to the oxygen mobility inside its structure[80] and this microstructure changes could be behind the enhanced catalytic effect of ceria[91]. The role of low amounts of CeO_2 in the Pt catalyst with respect to alcohol's oxidation is not well established. Many alternatives to PtRu have been published on the methanol oxidation on a series of Pt-CeO_2 catalysts. Kakati on its recent review[91] "Anode

Catalysts for Direct Methanol Fuel Cells in Acidic Media: Do We Have Any Alternative for Pt or Pt–Ru?" further explains that CeO_2 should be « designed » for synergic interactions with Pt nanoparticles in order to minimize side effects of CeO_2 low electronic conductivity. In addition, since ceria is insoluble in dilute acidic solutions, it provides an anticorrosion property to the carbon material. Apart from this corrosion resistance, CeO_2 serves as an anchor to prevent agglomeration of Pt nanoparticles, thereby enhancing methanol and ethanol oxidation activity[86,91].

In this work, several Pt-CeO_2 catalysts have been prepared and their performance has been studied toward the electrochemical oxidation of ethanol.

1.8. Objectives

Most of the studies in the literature, report on PtCeO_2 with CeO_2 > 10 to 25 wt%. Also, most of the studies are devoted to the methanol oxidation. To the best of our knowledge there is a gap of studies on the effect of very small of ceria (CeO_2 < 5wt%) on the electrocatalytic activity of Pt toward ethanol oxidation in acid medium. The only approach found on this sense, dates from 1978, where Georg-M. Schwab[92] reported on a system consisting of a semiconductor supported by a metal material termed as an "inverse supported catalyst" (for several catalytic reactions). The author reports that in this situation, the electronic effects on the catalysts are larger than in the usual "normal supported catalysts" because the number of free electrons in a metal is several orders of magnitude higher than in semiconductor. Naturally, this interaction mainly involves those Pt particles in close contact with ceria[93]. Furthermore, we aim to clarify the influence of the particle size and synergic effect of ceria on the particle's electrocatalytic reactivity. Since size effects also influence the activity of Pt toward ethanol oxidation, PtCeO_2 catalysts covering a large span of particle sizes (from 2 to 40 nm) will be investigated. Detailed

physicochemical investigation of the catalysts is carried out by X-ray diffraction (XRD), X-Ray Photoelectron Spectroscopy (XPS), Transmission Electron Microscopy (TEM) in order to understand the effect of the catalyst's particle size, morphology and binding energy shifts (electronic effects) and the ethanol oxidation reaction. Since the catalytic activity and selectivity of metal nanoparticles can be tuned by interactions with other nanoparticles[94], the main objective of this work is to investigate the addition of very small amounts of CeO_2 ($\leq$ 5 wt%) on the electrocatalytic activity of Pt. We will also aim to further understand the discernible changes in particle electronic and structural properties of these catalysts as function of the particle size and associated binding energies.

1.9. Structure of the thesis

This thesis is organized in 5 different chapters. In **chapter 1**, an introduction to the direct ethanol fuel cells applications and on the state of the art Pt based catalysts is presented. This description is also extended to the context of the bifunctional, electronic and particle size effects. In **chapter 2**, the synthesis of the $PtCeO_2$ with $CeO_2 \leq 5$ wt% by the Pechini and Reduction methods are detailed followed by a description of the experimental conditions and techniques. The results obtained for the Pechini method are summarized in **chapter 3** while those from the Reduction method are presented in **chapter 4**. Finally **chapter 5** presents the conclusion and a description of future work that will need to be performed. A summary in French is available in **section A1**.

1.10. References

1.   https://350.org/science/.

2.   Harde H. Scrutinizing the carbon cycle and CO2 residence time in the atmosphere. Global and Planetary Change 2017;152:19-26.

3.   Duff SJB, Murray WD. Bioconversion of forest products industry waste cellulosics to fuel ethanol: A review. Bioresource Technology 1996;55:1-33.

4.   Badwal SPS, Giddey S, Kulkarni A, Goel J, Basu S. Direct ethanol fuel cells for transport and stationary applications – A comprehensive review. Applied Energy 2015;145:80-103.

5.   https://www.ec.gc.ca/energie-energy/default.asp?lang=En&n=828C9342-1.

6.   Farrell AE, Plevin RJ, Turner BT, Jones AD, O'Hare M, Kammen DM. Ethanol Can Contribute to Energy and Environmental Goals. Science 2006;311:506-8.

7.   https://www.afdc.energy.gov/vehicles/flexible_fuel_emissions.html

8.   https://oss.adm.ntu.edu.sg.

9.   https://en.wikipedia.org/wiki/Ethanol_fuel_in_Brazil#cite_note-Lei8723-16.

10.   Lamy C, Coutanceau C, Leger JM. The direct ethanol fuel cell: a challenge to convert bioethanol cleanly into electric energy. Catalysis for sustainable energy production 2009:1-46.

11.   Demirci UB. Direct liquid-feed fuel cells: Thermodynamic and environmental concerns. Journal of Power Sources 2007;169:239-46.

12.   Carrette L, Friedrich KA, Stimming U. Fuel Cells – Fundamentals and Applications. Fuel Cells 2001;1:5-39.

13.   Zhang J. PEM fuel cell electrocatalysts and catalyst layers: fundamentals and applications: Springer Science & Business Media; 2008.

14.   http://wiki.kidzsearch.com/wiki/Heat_engine.

15.   Friedl J, Stimming U. Model catalyst studies on hydrogen and ethanol oxidation for fuel cells. Electrochimica Acta 2013;101:41-58.

16.   Rebhan E. Efficiency of nonideal Carnot engines with friction and heat losses. American Journal of Physics 2002;70:1143-9.

17.   Zakaria Z, Kamarudin SK, Timmiati SN. Membranes for direct ethanol fuel cells: An overview. Applied Energy 2016;163:334-42.

18.   Lamy C, Belgsir EM. Other direct-alcohol fuel cells. In: Handbook of Fuel Cells: John Wiley & Sons, Ltd; 2010.

19.   Soloveichik GL. Liquid fuel cells. Beilstein journal of nanotechnology 2014;5:1399.

20.   Wang J. Barriers of scaling-up fuel cells: cost, durability and reliability. Energy 2015;80:509-21.

21.   Deluga G, Salge J, Schmidt L, Verykios X. Renewable hydrogen from ethanol by autothermal reforming. Science 2004;303:993-7.

22.   Andreadis G, Tsiakaras P. Ethanol crossover and direct ethanol PEM fuel cell performance modeling and experimental validation. Chemical Engineering Science 2006;61:7497-508.

23.   Ahmed M, Dincer I. A review on methanol crossover in direct methanol fuel cells: challenges and achievements. International Journal of Energy Research 2011;35:1213-28.

24.   Matos BR, Isidoro RA, Santiago EI, et al. Nafion–titanate nanotubes composites prepared by in situ crystallization and casting for direct ethanol fuel cells. International Journal of Hydrogen Energy 2015;40:1859-67.

25.   Pletcher D. Electrocatalysis: present and future. Journal of Applied Electrochemistry 1984;14:403-15.

26. Perez JM, Beden B, Hahn F, Aldaz A, Lamy C. "In situ" infrared reflectance spectroscopic study of the early stages of ethanol adsorption at a platinum electrode in acid medium. Journal of Electroanalytical Chemistry and Interfacial Electrochemistry 1989;262:251-61.

27. Wang H, Jusys Z, Behm RJ. Ethanol Electrooxidation on a Carbon-Supported Pt Catalyst: Reaction Kinetics and Product Yields. The Journal of Physical Chemistry B 2004;108:19413-24.

28. Wang H, Jusys Z, Behm RJ. Ethanol electro-oxidation on carbon-supported Pt, PtRu and Pt3Sn catalysts: A quantitative DEMS study. Journal of Power Sources 2006;154:351-9.

29. Wang H, Jusys Z, Behm RJ. Ethanol and Acetaldehyde Adsorption on a Carbon-Supported Pt Catalyst: A Comparative DEMS Study. Fuel Cells 2004;4:113-25.

30. DeLuca NW, Elabd YA. Polymer electrolyte membranes for the direct methanol fuel cell: A review. Journal of Polymer Science Part B: Polymer Physics 2006;44:2201-25.

31. Ramanujan D, Bernstein WZ, Benjamin W, et al. A Framework for Visualization-Driven Eco-Conscious Design Exploration. Journal of Computing and Information Science in Engineering 2015;15:041010--9.

32. Sharma S, Singh P, Hegde MS. Electrocatalysis and redox behavior of Pt2+ ion in CeO2 and Ce0.85Ti0.15O2: XPS evidence of participation of lattice oxygen for high activity. Journal of Solid State Electrochemistry 2011;15:2185-97.

33. Holton OT, Stevenson JW. The Role of Platinum in Proton Exchange Membrane Fuel Cells. Platinum Metals Review 2013;57:259-71.

34. https://wwwenergygov/sites/prod/files/2014/02/f8/fctt_roadmap_june2013pdf.

35.   Gasteiger HA, Kocha SS, Sompalli B, Wagner FT. Activity benchmarks and requirements for Pt, Pt-alloy, and non-Pt oxygen reduction catalysts for PEMFCs. Applied Catalysis B: Environmental 2005;56:9-35.

36.   Simões FC, dos Anjos DM, Vigier F, et al. Electroactivity of tin modified platinum electrodes for ethanol electrooxidation. Journal of Power Sources 2007;167:1-10.

37.   Vigier F, Coutanceau C, Perrard A, Belgsir EM, Lamy C. Development of anode catalysts for a direct ethanol fuel cell. Journal of Applied Electrochemistry 2004;34:439-46.

38.   Figueiredo MC, Santasalo-Aarnio A, Vidal-Iglesias FJ, et al. Tailoring properties of platinum supported catalysts by irreversible adsorbed adatoms toward ethanol oxidation for direct ethanol fuel cells. Applied Catalysis B: Environmental 2013;140–141:378-85.

39.   Moghaddam RB, Pickup PG. Support Effects on the Oxidation of Formic Acid at Pd Nanoparticles. Electrocatalysis 2011;2:159.

40.   Mann J, Yao N, Bocarsly AB. Characterization and Analysis of New Catalysts for a Direct Ethanol Fuel Cell. Langmuir 2006;22:10432-6.

41.   Iwasita T, Pastor E. A dems and FTir spectroscopic investigation of adsorbed ethanol on polycrystalline platinum. Electrochimica Acta 1994;39:531-7.

42.   Watanabe M, Motoo S. Electrocatalysis by ad-atoms. Part III. Enhancement of the oxidation of carbon monoxide on the platinum ruthenium ad-atoms. Electroanalytical Chemistry and lnterfacial Electrochemistry 1975;60:275-83.

43.   Camara GA, de Lima RB, Iwasita T. Catalysis of ethanol electrooxidation by PtRu: the influence of catalyst composition. Electrochemistry Communications 2004;6:812-5.

44.   Beden B, Kadirgan F, Lamy C, Leger JM. Electrocatalytic oxidation of methanol on platinum-based binary electrodes. Journal of Electroanalytical Chemistry and Interfacial Electrochemistry 1981;127:75-85.

45.   Parsons R, VanderNoot T. The oxidation of small organic molecules: A survey of recent fuel cell related research. Journal of Electroanalytical Chemistry and Interfacial Electrochemistry 1988;257:9-45.

46.   Zhang D-Y, Ma Z-F, Wang G, Konstantinov K, Yuan X, Liu H-K. Electro-Oxidation of Ethanol on Pt-WO3/C Electrocatalyst. Electrochemical and Solid-State Letters 2006;9:A423-A6.

47.   Bai Y, Wu J, Xi J, et al. Electrochemical oxidation of ethanol on Pt–ZrO2/C catalyst. Electrochemistry Communications 2005;7:1087-90.

48.   He X, Hu C. Building three-dimensional Pt catalysts on TiO2 nanorod arrays for effective ethanol electrooxidation. Journal of Power Sources 2011;196:3119-23.

49.   Ye S. CO-tolerant Catalysts. In: Zhang J, ed. PEM Fuel Cell Electrocatalysts and Catalyst Layers: Springer London; 2008:759-834.

50.   Shukla AK, Aricò AS, El-Khatib KM, Kim H, Antonucci PL, Antonucci V. An X-ray photoelectron spectroscopic study on the effect of Ru and Sn additions to platinised carbons. Applied Surface Science 1999;137:20-9.

51.   Beden B, Bewick A, Kunimatsu K, Lamy C. Infrared study of adsorbed species on electrodes: Adsorption of carbon monoxide on Pt, Rh and Au. Journal of Electroanalytical Chemistry and Interfacial Electrochemistry 1982;142:345-56.

52.   Kabbabi A, Faure R, Durand R, et al. In situ FTIRS study of the electrocatalytic oxidation of carbon monoxide and methanol at platinum–ruthenium bulk alloy electrodes. Journal of Electroanalytical Chemistry 1998;444:41-53.

53.   Beden B, Bewick A, Lamy C. A study by electrochemically modulated infrared reflectance spectroscopy of the electrosorption of formic acid at a platinum electrode. Journal of Electroanalytical Chemistry and Interfacial Electrochemistry 1983;148:147-60.

54.   Rama Rao MV, Shripathi T. Photoelectron spectroscopic study of X-ray induced reduction of CeO2. Journal of Electron Spectroscopy and Related Phenomena 1997;87:121-6.

55.   Mason MG, Gerenser LJ, Lee ST. Electronic Structure of Catalytic Metal Clusters Studied by X-Ray Photoemission Spectroscopy. Physical Review Letters 1977;39:288-91.

56.   Arenz M, Mayrhofer KJJ, Stamenkovic V, et al. The Effect of the Particle Size on the Kinetics of CO Electrooxidation on High Surface Area Pt Catalysts. Journal of the American Chemical Society 2005;127:6819-29.

57.   Li X, Qiu X, Yuan H, Chen L, Zhu W. Size-effect on the activity of anodic catalysts in alcohol and CO electrooxidation. Journal of Power Sources 2008;184:353-60.

58.   Bergamaski K, Pinheiro ALN, Teixeira-Neto E, Nart FC. Nanoparticle Size Effects on Methanol Electrochemical Oxidation on Carbon Supported Platinum Catalysts. The Journal of Physical Chemistry B 2006;110:19271-9.

59.   Sapi A, Liu F, Cai X, et al. Comparing the Catalytic Oxidation of Ethanol at the Solid–Gas and Solid–Liquid Interfaces over Size-Controlled Pt Nanoparticles: Striking Differences in Kinetics and Mechanism. Nano letters 2014;14:6727-30.

60.   Perez J, Paganin VA, Antolini E. Particle size effect for ethanol electro-oxidation on Pt/C catalysts in half-cell and in a single direct ethanol fuel cell. Journal of Electroanalytical Chemistry 2011;654:108-15.

61.   Hitmi H, Belgsir EM, Léger JM, Lamy C, Lezna RO. A kinetic analysis of the electro-oxidation of ethanol at a platinum electrode in acid medium. Electrochimica Acta 1994;39:407-15.

62.   Aricò AS, Cretı̀ P, Antonucci PL, Antonucci V. Comparison of Ethanol and Methanol Oxidation in a Liquid-Feed Solid Polymer Electrolyte Fuel Cell at High Temperature. Electrochemical and Solid-State Letters 1998;1:66-8.

63.   Fujiwara N, Friedrich KA, Stimming U. Ethanol oxidation on PtRu electrodes studied by differential electrochemical mass spectrometry. Journal of Electroanalytical Chemistry 1999;472:120-5.

64.   Camara GA, Iwasita T. Parallel pathways of ethanol oxidation: The effect of ethanol concentration. Journal of Electroanalytical Chemistry 2005;578:315-21.

65.   Lamy C, Rousseau S, Belgsir EM, Coutanceau C, Léger JM. Recent progress in the direct ethanol fuel cell: development of new platinum–tin electrocatalysts. Electrochimica Acta 2004;49:3901-8.

66.   Rousseau S, Coutanceau C, Lamy C, Léger JM. Direct ethanol fuel cell (DEFC): Electrical performances and reaction products distribution under operating conditions with different platinum-based anodes. Journal of Power Sources 2006;158:18-24.

67.   Rao V, Cremers C, Stimming U, et al. Electro-oxidation of Ethanol at Gas Diffusion Electrodes A DEMS Study. Journal of The Electrochemical Society 2007;154:B1138-B47.

68.   Song SQ, Zhou WJ, Zhou ZH, et al. Direct ethanol PEM fuel cells: The case of platinum based anodes. International Journal of Hydrogen Energy 2005;30:995-1001.

69.   De A, Adhikary R, Datta J. Proactive role of carbon nanotube-polyaniline conjugate support for Pt nano-particles toward electro-catalysis of ethanol in fuel cell. International Journal of Hydrogen Energy 2017;42:25316-25.

70.   Beyhan S, Coutanceau C, Léger J-M, Napporn TW, Kadırgan F. Promising anode candidates for direct ethanol fuel cell: Carbon supported PtSn-based trimetallic catalysts prepared by Bönnemann method. International Journal of Hydrogen Energy 2013;38:6830-41.

71.   De Souza RFB, Parreira LS, Silva JCM, et al. PtSnCe/C electrocatalysts for ethanol oxidation: DEFC and FTIR "in-situ" studies. International Journal of Hydrogen Energy 2011;36:11519-27.

72.   Sun S, Halseid MC, Heinen M, Jusys Z, Behm RJ. Ethanol electrooxidation on a carbon-supported Pt catalyst at elevated temperature and pressure: A high-temperature/high-pressure DEMS study. Journal of Power Sources 2009;190:2-13.

73.   Akhairi MAF, Kamarudin SK. Catalysts in direct ethanol fuel cell (DEFC): An overview. International Journal of Hydrogen Energy 2016;41:4214-28.

74.   Chen Z, Qiu X, Lu B, Zhang S, Zhu W, Chen L. Synthesis of hydrous ruthenium oxide supported platinum catalysts for direct methanol fuel cells. Electrochemistry Communications 2005;7:593-6.

75.   Wang J, Xi J, Bai Y, et al. Structural designing of Pt-CeO2/CNTs for methanol electro-oxidation. Journal of Power Sources 2007;164:555-60.

76.   Shen PK, Xu C. Alcohol oxidation on nanocrystalline oxide Pd/C promoted electrocatalysts. Electrochemistry Communications 2006;8:184-8.

77.   Anderson JM, Patel J, Karakoti AS, Greeneltch N, Díaz DJ, Seal S. Aging effects of nanoscale ceria in ceria–platinum composite electrodes for direct alcohol electro-oxidation. Electrochimica Acta 2011;56:2541-5.

78.   Ostroverkh A, Johánek V, Kúš P, Šedivá R, Matolín V. Efficient Ceria–Platinum Inverse Catalyst for Partial Oxidation of Methanol. Langmuir 2016;32:6297-309.

79.   Yao HC, Yao YFY. Ceria in automotive exhaust catalysts. Journal of Catalysis 1984;86:254-65.

80.   Trovarelli A. Catalysis by Ceria and Related Materials: Imperial College Press; 2002.

81.   Idriss H. Ethanol Reactions over the Surfaces of Noble Metal/Cerium Oxide Catalysts. Platinum Metals Review 2004;48:105-15.

82.   Yeung CMY, Yu KMK, Fu QJ, Thompsett D, Petch MI, Tsang SC. Engineering Pt in Ceria for a Maximum Metal−Support Interaction in Catalysis. Journal of the American Chemical Society 2005;127:18010-1.

83.   Hardacre C, Ormerod RM, Lambert RM. Platinum-Promoted Catalysis by Ceria: A Study of Carbon Monoxide Oxidation over Pt(111)/CeO2. The Journal of Physical Chemistry 1994;98:10901-5.

84.   Lide DR. CRC Handbook of Chemistry and Physics, 84th Edition: Taylor & Francis; 2003.

85.   De Souza RFB, Flausino AEA, Rascio DC, et al. Ethanol oxidation reaction on PtCeO2/C electrocatalysts prepared by the polymeric precursor method. Applied Catalysis B: Environmental 2009;91:516-23.

86.   Scibioh MA, Kim S-K, Cho EA, Lim T-H, Hong S-A, Ha HY. Pt-CeO2/C anode catalyst for direct methanol fuel cells. Applied Catalysis B: Environmental 2008;84:773-82.

87.   Corradini PG, Santos NA, Silva GC, Perez J. Pt–rare earth catalysts for ethanol electrooxidation: modification of polyol synthesis. Journal of Solid State Electrochemistry 2016;20:2581-7.

88.   Cordeiro GL, de Camargo EF, Santos MC, et al. Improved Pt/CeO2 Electrocatalysts for Ethanol Electro-oxidation. Int J Electrochem Sci 2018;13:6388-401.

89.   Wang Y, Tabet-Aoul A, Gougis M, Mohamedi M. Cross-beam pulsed laser fabrication of Free-Standing Nanostructured Carbon Nanotubes-Pt-Ceria Anode with unprecedented electroactivity and durability for ethanol oxidation. Journal of Power Sources 2015;273:904-13.

90.   Gu D-M, Chu Y-Y, Wang Z-B, Jiang Z-Z, Yin G-P, Liu Y. Methanol oxidation on Pt/CeO2–C electrocatalyst prepared by microwave-assisted ethylene glycol process. Applied Catalysis B: Environmental 2011;102:9-18.

91.   Kakati N, Maiti J, Lee SH, Jee SH, Viswanathan B, Yoon YS. Anode Catalysts for Direct Methanol Fuel Cells in Acidic Media: Do We Have Any Alternative for Pt or Pt–Ru? Chemical reviews 2014;114:12397-429.

92.   Schwab G-M. Electronics of Supported Catalysts. In: D.D. Eley HP, Paul BW, eds. Advances in Catalysis: Academic Press; 1979:1-22.

93.   Solymosi F. Importance of the Electric Properties of Supports in the Carrier Effect. Catalysis Reviews 1968;1:233-55.

94.   Zwijnenburg A, Goossens A, Sloof WG, et al. XPS and Mössbauer Characterization of Au/TiO2 Propene Epoxidation Catalysts. The Journal of Physical Chemistry B 2002;106:9853-62.

2. Synthesis and characterization techniques

2.1. Introduction

Pt and PtCeO$_2$ nanoparticles with levels of CeO$_2$ 1 or 5 wt% (corresponding to 1.1 and 5.6 at%) were synthesized in this work using two different methods, namely the Polymeric Precursor Method (also known as the Pechini method, which is a sol-gel method) and the Reduction method. The Pechini and reduction methods are two straightforward ways to produce nanoparticles. However, both have their own advantages and disadvantages. The advantages for the first method are: 1) The experimental procedure is a one-step synthesis[1] – which means that metallic Pt is easily obtained by direct oxidation of a polymeric matrix; 2) it is possible to control the particle size and morphology by changing the metal : organic mass ratio in the gel[2]. The main disadvantage pointed to this method is associated with the calcination step at high temperature (typically above 400 °C) which causes coalescence and aggregation of the nanoparticles. For this reason, the chemical reduction method remains the primary method of producing small nanoparticles. It consists on reducing chloroplatinic acid in the presence of a reducing agent as sodium borohydride. Since it is a low temperature technique, it minimizes particle aggregation or clusters sintering and it allows the production of large amounts of product, with relatively narrow particle size distribution[3].

2.2. Synthesis of Pt-CeO$_2$ nanoparticles by the Pechini method (Polymeric Precursor Method)

Pechini proposed this method in 1967[4] which consists on the formation of a polymeric resin (gel) through polyesterification of metal chelate complexes using citric acid and ethylene glycol as a bridging agent. The general purpose is to obtain a polyester resin comprising of randomly carboxylic esters sites (negative charges) to which the metal cations are chelated and cross-linked with the carboxylate groups inside the gel[5], as illustrated in Figure 2. 1. The main advantage of this method is to uniformly "trap" the cations throughout the carboxylic groups of the viscous polymer structure allowing some degree of homogeneity and preventing segregation[6,7]. Paraphrasing P. A. Lessing[7]: "cations need to be frozen in space to prevent extreme segregation". The esterification occurs when the reactants are heated at moderated temperatures (130 °C). Prolonged heating at high temperatures ($\geq$400 °C) causes a breakdown and oxidation of the polymer to produce the nanoparticles.
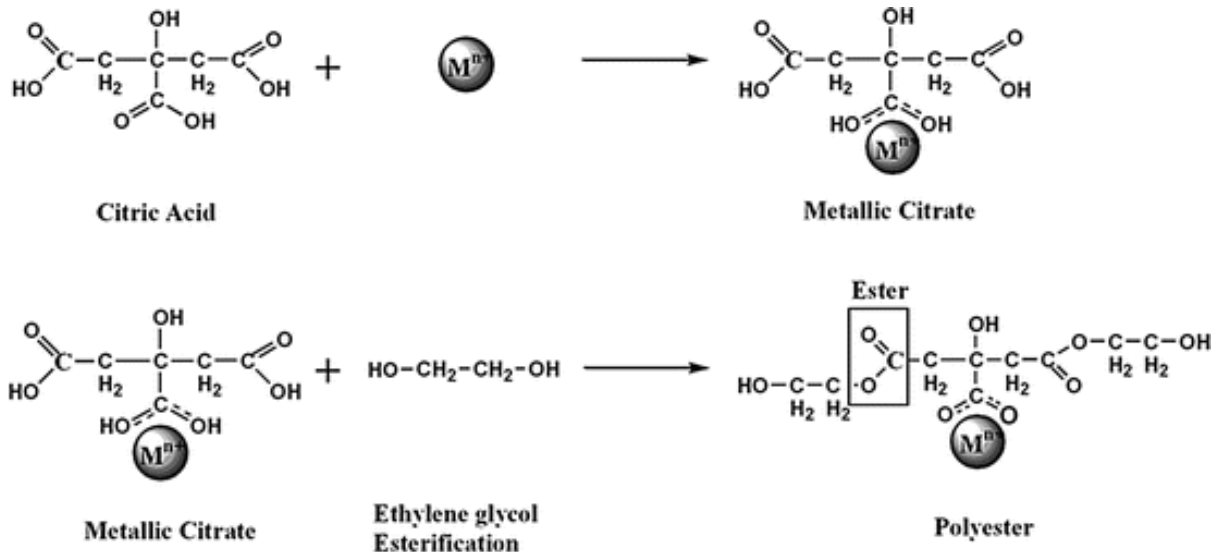
Figure 2. 1 – Scheme of a polyester network with the metallic cations represented as M^{n-} = Pt, Ce produced by Pechini method[5].

Similar to what was proposed by Pechini, in this work, the catalysts are prepared according to the following procedure: citric acid ($Na_3C_6H_5O_7$, 99%, Fischer) is first dissolved in ethylene glycol ($C_2H_6O_2$, 99.8 % Aldrich) at 60^oC, followed by the addition of dihydrogen hexachloroplatinate (IV) (H_2PtCl_6, 99.9%, Alfa Aesar) and ammonium cerium (IV) nitrate (($NH_4)_2Ce(NO_3)_6$, 98.5%, Fischer) with a molar ratio 1:12:96 (metal : citric acid : ethylene glycol) and stirring for 30 minutes. This precursor solution is first jellified at 130 ^oC for 30 minutes to eliminate water, leading to the formation of a high molecular weight polyester through successive esterification reactions[8]. Pechini, in his work, used four times more ethylene glycol with respect to citric acid; in the present work we used eight times more ethylene glycol to increase the solubility of the platinum complex. Thus, we diminished the viscosity of the CA-EG of the Pechini's mixture[9]. By increasing the excess of ethylene glycol to citric acid, we also attempted to uniformly distribute the metallic cations through the polyester network, thus to increase the number of nuclei centers, and to limit the crystallite growth[9]. We also vary the Pt to CA/EG polymer network, from 1 to 10 keeping constant the CA/EG in order to dilute the Pt and Ce in more carboxylic groups. From systems A to C it is expected a decrease of the particle size by increasing the distance between consecutive metallic ions in the polyester resin as illustrated in Figure 2.2.
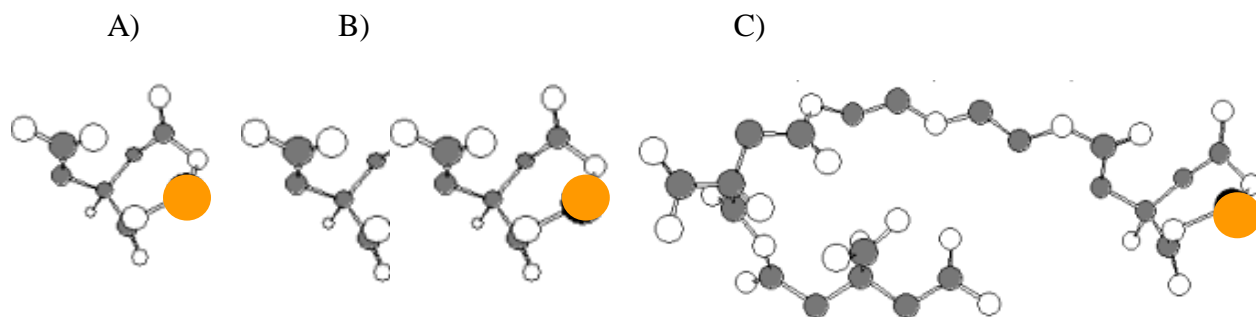
Figure 2. 2. – Scheme illustrating the effect of Pt (orange circles) dilution on the polymer network in the system: A) with 1x, B) with 5x and C) with 10x more polymer dilution.

By providing a thicker organic layer, prior to calcination, we avoid the addition of surfactants thus simplifying the process. However, for the production of crystalline nanoparticles, it is necessary to burn the organic part (the gel). When the heating temperature exceeds 400 ºC, oxidation and pyrolysis of the polymer matrix begin to form a homogeneous crystalline material[8]. Thus, this reactional mixture was first thermally treated at 130ºC for 30 minutes to eliminate water and then at 400 ºC for 4 hours to burn the organic portion. The heating rate was set at 5 ºC min^{-1}. After 4 hours, the powder was brought back to room temperature.

Calcination of a gel will improve the crystallinity of the sample but normally leads to the increase of the crystallite sizes. However, ceria an additive in diesel engines, due to its facility to oxidize carbon[10,11], is known to have an effect in controlling the Pt particle size during the calcination process limiting the particles growth[10,12]. Thus, as will be shown in Chapters 3 and 4, the addition of CeO_2 in wt $\leq 5\%$ is sufficient to cause a significant deagglomeration and decrease of Pt particle size. Table 2.1 summarizes the synthesis conditions and the nominal composition of the catalysts.

Table 2. 1 – Experimental details on the preparation of Pt and PtCeO$_2$ by the Pechini method.

System	Catalyst	Pt:CA:EG (mol)	CeO$_2$ (wt%)	Pt precursor H$_2$PtCl$_6$.6H$_2$O (g)	CeO$_2$ precursor (NH$_4$)$_2$Ce(NO$_3$)$_6$ (g)
A (**1×**)	Pt	1:12:96	-	0.25	-
	PtCeO2-1%	1:12:96	1	0.25	0.003
	PtCeO2-5%	1:12:96	5	0.25	0.0157
B (**5×**)	Pt	0.2:12:96	-	0.05	-
	PtCeO2-1%	0.2:12:96	1	0.05	0.0006
	PtCeO2-5%	0.2:12:96	5	0.05	0.0031
C (**10×**)	Pt	0.1:12:96	-	0.025	-
	PtCeO2-1%	0.1:12:96	1	0.025	0.000302
	PtCeO2-5%	0.1:12:96	5	0.025	0.00157

2.3. Synthesis by the Reduction Method

The reduction method consists in the production of metallic nanoparticles by direct reduction of a precursor metal complex. Depending on the reduction potential of the metal, a number of reducing agents can be proposed for the preparation of metallic nanoparticles, sodium borohydride (NaBH$_4$) being the most common. Ingelsten and coworkers[13] proposed the next reaction for the reduction mechanism of H$_2$PtCl$_6$ carried out in the presence of a an excess of NaBH$_4$, equation 2.1 :

$$PtCl_6^{2-}{}_{(aq)} + BH_4^-{}_{(aq)} + 3H_2O_{(l)} \rightarrow Pt^{(0)} + H_2BO_3^-{}_{(aq)} + 4H^+{}_{(aq)} + 6Cl^-{}_{(aq)} + 2H_{2(g)} \quad \text{(Equation 2.1)}$$

It has been reported that NaBH$_4$ can improve the dispersion and reduce the size of Pt, which in turn will increase the electrochemical active surface area of the Pt catalysts[14]. It is suggested in the literature a n(NaBH$_4$)/n(H$_2$PtCl$_6$) > 6 ensure a complete reduction reaction[15] . In this work the amount of NaBH$_4$ to the platinum complex was increased 20 times with respect to H$_2$PtCl$_6$. Consequently one can take advantage of the positive effect of borohydride as reducing

agent on the electrochemical properties of Pt. It is already reported that increased boron deposition may help in a better dispersion, reduce the size of Pt and raise the electrochemical surface area although this is a singular study[14].

Citrate anion is often used as stabilizer during the synthesis of Pt nanoparticles (NPs) by the reduction method. It is a water-soluble surfactant with small molecular weight[11,12] that stabilizes the Pt nanoparticles in aqueous solution, contributing to a better control of the Pt particle size. The stabilizing effect of sodium citrate is due to its three carboxyl anions which electrostatically interact to the metal ions to accommodate charge without a great increase in its electrostatic energy. Consequently citrate anions are able to sterically prevent the Pt nuclei from ageing by growth and agglomeration[16]. It is important that the steric stabilization of Pt and ceria catalyst by the citrate anion have no adverse effects on the electrocatalyic activity of Pt and PtCeO$_2$ nanocomposites. Figure 2.3 shows a scheme of the steric stabilization of citrate with the conformations of the groups COO$^-$ that may easily stabilize not only Pt but also the positive ions Pt^{2+}, Ce^{4+} and Ce^{3+}.
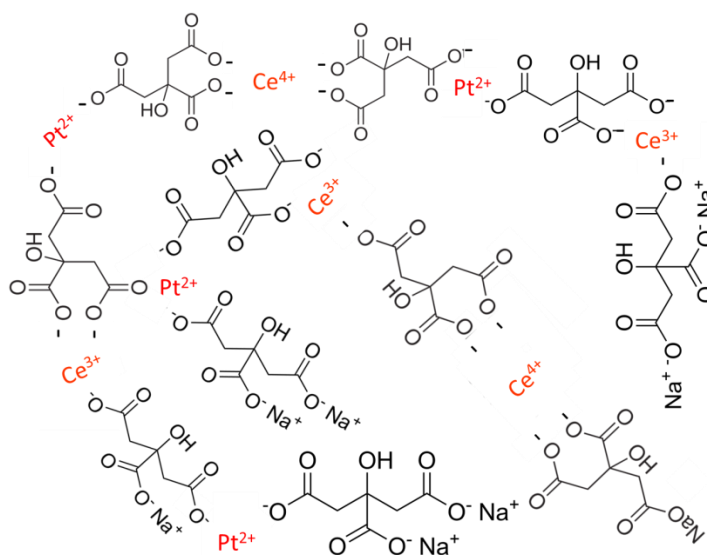
Figure 2. 3 – Platinum sterical stabilization by citrate molecules.

It is not clear however if the citrate modifies the Pt surface and if it affects the ethanol electro-oxidation. In fact there is no clear insight about which anionic stabilizer is really preferred by the transition metal and why[17].

Experimentally, $H_2PtCl_{6\,(aq)}$ (2.5 mL; 0.017 M) was added dropwise to a stirred solution of $NaBH_{4\,(aq)}$ (5 mL; 1.704 M). Deionized water was added to this reactional mixture until a total volume of 10 mL and stirred for more 2h resulting in a black Pt nanoparticle suspension. For the catalysts with citrate, the same procedure was applied on which a 0.6 mL of 50 mM aqueous sodium citrate had previously been added before the $NaBH_{4(aq)}$ aqueous solution.

For the preparation of $PtCeO_2$ nanoparticles with 1 and 5 wt% of ceria the same procedure was applied as for Pt, but with for 1wt% of ceria, a 1 mL of a 4.74×10^{-3} M solution of $(NH_4)_2Ce(NO_3)_6$ was added dropwise after the solution of H_2PtCl_6. For the 5 wt% of ceria, an aliquot of 1mL of a 2.535×10^{-2} M of $(NH_4)_2Ce(NO_3)_6$ solution was added. At the end of the synthesis, each suspension was centrifuged for 30 min. at 13000 rpm and at 10 ºC. The process was repeated 6 times always followed by decanting and washing with deionized water. This concentrated suspension of catalyst, labeled as a stock solution, was stored in a fridge.

2.4. Characterization techniques

Different techniques were used for the characterization of the prepared powder materials. A brief description of each technique follows.

2.4.1. X-ray diffraction

X-Ray diffraction (XRD) is a commonly used technique to elucidate the crystallographic structure of materials. It is based on the fact that the crystals diffract X-rays in a way that is dependent on the periodical arrangement of the atoms in a crystal [18]. An X-ray diffractometer is basically constituted of three main parts: a source of X-ray, a sample holder and an X-ray

detector. The Bragg's law, equation 2.2, relates the conditions upon which the diffraction occurs [18,19] which are given by the wavelength (λ) of the incident radiation and the incidence angle (θ) and the inter-planar spacing (d):

$$\lambda = 2dsin\theta$$

(Equation 2.2)
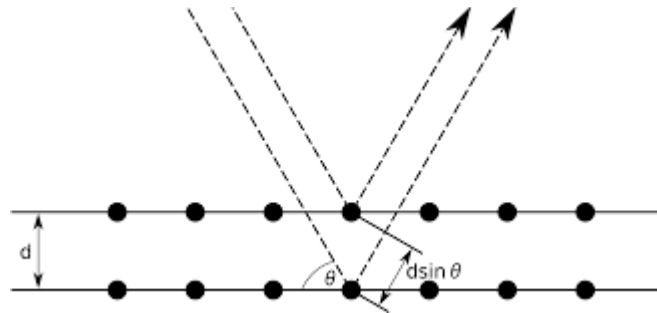
Figure 2. 4 – Bragg's law scheme of the diffracted X-ray in a crystal.[20]

The inter-planar spacing (d) is a function of the Miller indices (hkl) that are used to indicate directions and planes. The lattice parameters (a,b,c) and the angles (α,β,γ) of the crystal system as shown in Figure 2.5.
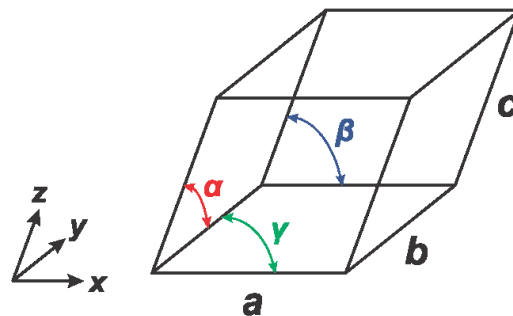
Figure 2. 5 – Lattice parameters (axis) and angles of a unit cell[21].

From the 7 crystal systems, the cubic one ($a = b = c; \alpha = \beta = \gamma = 90°$) is the most relevant for the current work. In this case, the following relation for the inter-planar spacing and the Miller indices can be written [18]:

$$d_{hkl} = \frac{a}{\sqrt{h^2 + k^2 + l^2}} \qquad \text{(Equation 2.3)}$$

A combination of equations 2.2 and 2.3 provides the tool for calculating the lattice parameter of a crystal from the diffraction data, equation 2.4:

$$a_{hkl} = \frac{\lambda\sqrt{h^2 + k^2 + l^2}}{2\sin\theta_{hkl}} \qquad \text{(Equation 2.4)}$$

The diffractograms also provide us with useful information about the crystallite size, which is known to influence peak broadening [18-20], apart from instrumental effects. The crystallite size, this is, the effective thickness of the crystallite in a direction perpendicular to the reflecting planes[1] (D_{hkl}), can be calculated with the help of the Scherrer equation [22,23]:

$$D_{hkl} = \frac{K\lambda}{B_{hkl}\cos\theta} \qquad \text{(Equation 2.5)}$$

Where K is the crystallite shape factor and is equal to 0.9 (for a common spherical shape), and B_{hkl} is the full width at half maximum (FWHM) in radians. Scherrer's equation is valid only for crystallite sizes below 100-200 nm [22].

---

[1] Crystallite size may also be defined as the cube root of volume of the crystallite (20.   Klug HP, Alexander LE. X-ray Diffraction Procedures for Polycrystalline and Amorphous Materials: John Wiley & Sons, Inc.; 1954.). In the present work we will use only the definition presented in the main text.

2.4.1.1. Experimental details

The structure of all catalysts was analyzed using a Bruker AXDS8 instrument with a Cu Kα radiation (λ=1.54184 Å) operating at 40 mV and 40 mA. The diffractograms were collected in the 2θ range between 30° and 90° with a step of 0.05^o and a measuring time of 5 s per step. In the specific case of the nanoparticles prepared by the reduction method, a 15 μL deposition of stock solution was deposited in a glass foil and allowed to dry overnight. EVA V14 software was used to determine the full width half maximum (FWHM) and the lattice parameter.

2.4.2. Transmission Electron Microscopy (TEM)

In TEM, an accelerated electron beam is focused on a sample thin enough (≤100nm) to allow the transmission of the incident electrons. This irradiated sample is in a high vacuum column where the electrons that are transmitted through the sample and are used to produce an image[24]. This means that in order to have a 2-D image of the sample or to observe it on a fluorescent screen, a beam should necessarily be transmitted through the sample without losing energy (direct beam, Figure 2.6). If, by the other way, the electron beam only interacts with the sample it will lead to other signals as electron energy loss, scattering, emission of secondary electrons or characteristic X-rays from the irradiated sample, Figure 2.6.
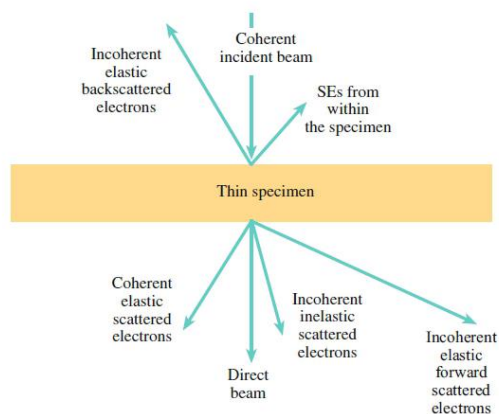
Figure 2. 6 – Electron beam interaction for a thin sample[24].

In many regards, the TEM can be seen as an optical microscope with a much higher imaging resolution, while also providing information about the sample's morphology, structure, grain size, chemical composition and composition distribution [25]. The morphology and microstructure of the Pt and $PtCeO_2$ nanocomposites were investigated by transmission electron microscopy (TEM), Figure 2.6.

2.4.2.1. Experimental Details

Transmission electron micrographs were obtained with a JEOL 2100F equipment operated at 200 kV (Center for Characterization of Microscopic Materials, at Ecole Polytechnique de Montreal). The sample preparation and observations were performed by Mr.Jean-Philippe Masse. The TEM samples were prepared by dipping the copper grids on the powder samples already dispersed in methanol. The software ImageJ was used for the particle size statistics.

2.4.3. X-Ray Photoelectron Spectroscopy (XPS)

2.4.3.1. Background

X-ray photoelectron spectroscopy (XPS), also known as electron spectroscopy for chemical analysis (ESCA) or photoemission spectroscopy (PES), is a characterization technique with high surface sensitivity often employed to study solid surfaces. Although the theoretical background of this technique was described in 1905 by Albert Einstein, it was only in 1954 that the first high-energy-resolution XPS spectrum was reported[26].

In XPS, a beam of X-rays promotes the emission of electrons from the sample, a process that is known as photoemission or as photoelectric effect. The kinetic energy (KE) of these electrons is dependent on their initial energy or the binding energy (BE) that the ejected photoelectron had in the solid relative to the Fermi level of the sample, the energy of the X-ray source ($h\nu$) and the work function (Φ_s, minimum energy required to eject an electron from the surface to the infinity) [25,27,28]:

$$KE = h\nu - BE - \phi_s \qquad \text{(Equation 2.6)}$$

In equation 2.6, Φ_s and $h\nu$ are well known depending on the source (generally aluminum or magnesium), which means that by measuring the kinetic energy of the ejected electrons, we can calculate the binding energy and hence identify and quantify the atoms present in the sample. In practice, KE and φ_s are replaced by the kinetic energy of the electron as measured by the spectrometer and the work function of the spectrometer, respectively which justifies the equation:

$$BE = h\nu - KE \qquad \text{(Equation 2.7)}$$

It is possible to analyze by XPS all elements except hydrogen and helium. Photoelectron spectroscopy can equally probe core-level and valence band electrons. However, the valence

band spectra are typically quite complex because of the large number of valence levels overlapping in a small energy region. On the other hand, in the core-level spectra, the position of atoms from different chemical elements is distinct and usually easy to distinguish. At the same time, differences up to several eV in an element's BE, allow the identification its local chemical environment and the electronic structure. Therefore, in most cases core-level photoelectrons are used for elemental analysis, while small shifts in their BE (known as chemical shifts) can be used to determine the oxidation state. In the former case survey spectra are required, while in the latter case high resolution spectra are needed. The number of ejected photoelectrons reflects itself in a photoelectron peak intensity and therefore the core-level spectra can be used for quantitative analysis. The possibility for each element to produce photoelectrons is taken into account using atomic sensitivity factors (ASF). The ASF strongly depend on the element, the specific core-level shell, and the excitation photon energy.

For electrical insulating samples, the above description is complicated, since the reference Fermi level is neither well defined nor in electrical contact with the spectrometer (this problem is usually referred to as electrostatic charging)[26]. The Fermi level is defined as the highest energy level occupied by an electron in an atom (at absolute zero kelvin). Figure 2.7 illustrates the core level binding energy, the incident X-ray with a certain hv energy, the ejected 1s electron and a core hole that was left behind. On the upper levels we can see valence and conduction bands, and the Fermi level between them, Figure 2.7.
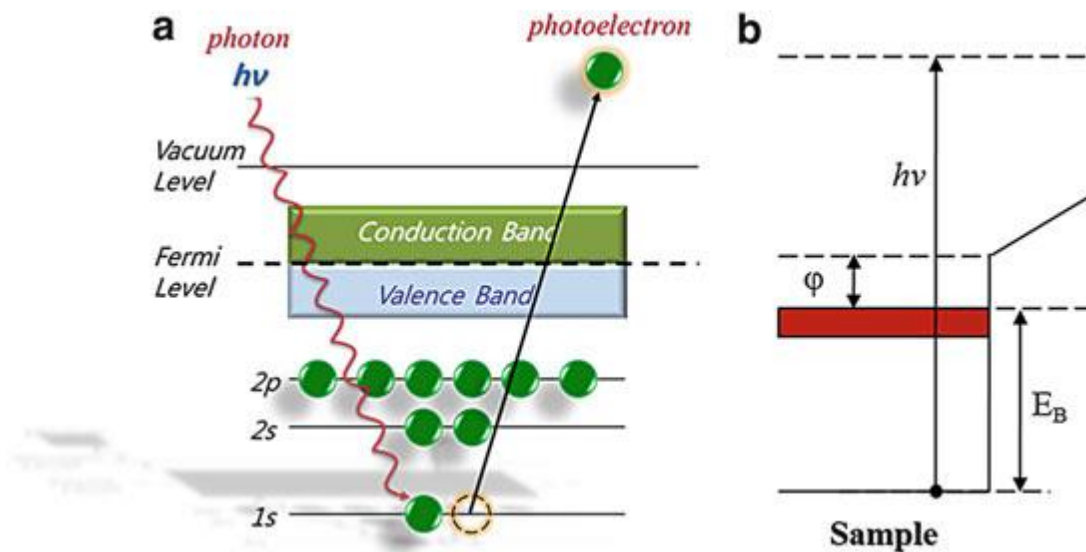
Figure 2. 7 – a) Illustration of the core-level photoelectron emission by the photoelectric effect in a metal; b) Scheme of a core level energy diagram for a sample[26].

The detection limit of this technique is ~0.01-0.1 at% [25]. XPS provides us with information of the first 10 nm depth of the sample even if the X-rays are able to penetrate the sample several micrometers [25]. This is so because the electrons generated deeper than ~ 10 nm do not have enough energy to escape the sample and reach the detector, as they are subjected to multiple inelastic collisions. In fact, even within the 10 first nanometers only the electrons that go through little inelastic collisions will give rise to peaks in the spectra, while the remaining electrons will contribute to the spectral background.

The binding energy of core-level electrons is strongly related to the electron distribution around the core of the atom. The problem is that after photoemission all the remaining electrons are not "frozen" but are influenced by the removal of the photoelectron. Bearing this picture in mind, the BE calculated in a photoemission experiment does not directly reflect the state of the atom before photoemission because it is affected by the redistribution of all the surrounding

electrons. This leads us to the study of the so-called initial and final state effects in following 2.5.2 section.

2.4.3.2. The core level binding energy shifts

The core levels in XPS are the local probes of changes in the electronic structure of an atom in different environments[29]. A core level binding energy shift, takes place due to a modification in an atom's chemical or physical environment[30].

The core level binding energy shifts are intrinsically explained by means of initial-state-final-state approach in the field of photoelectron spectroscopy. Basically, initial-state effects are due to the charge density or other intrinsic properties of the atom prior to photoemission i.e. that was already present on the atom in the ground state. For instance, changes in the electronic structure (due to the chemical or the geometric environment). In resume, initial state effects are generally defined by an electronic type of interaction like a charge transfer between the atom and its environment[26,31].

Final-state effects occur during and following the photoelectron emission and can be caused by core hole screening (or relaxation) after photoemission[32] due to differences in the screening of the core hole created after photoemission. As will be discussed below, the removal of an electron from a particular shell of the atom may induce several types of final states. The effectiveness of the core hole screening depends not only on the particular element (intra-atomic screening) but also on the surrounding environment, i.e., atom coordination number and interaction with the support (extra-atomic screening)[26]. In fact photoelectron spectroscopy is sometimes referred to as a final-state spectroscopy since this technique probe, in addition to the ground state of the atom, the numerous final or ionized-states of the sample[33]. Generally, the

binding energy varies roughly proportionally to the inverse of the cluster or particle size. Wertheim proposed a $e^2/2r$ relationship between the binding energy and particle radius (e is the electron charge)[34] considering that the particle is an isolated sphere. In this sense, the final state effect is analyzed simply by assuming that a single charge is left on the particle which results in a Coulomb energy relation. This justifies the 1/r dependence of the core level shift which is often observed. It is well known that, the smaller the particles, the more significant the influence of the relaxation process will be[35]. It reported that this relaxation is more pronounced on nanoparticles with diameters below 5 nm[36]. However there is no clear consensus about how small the particle should be but it is more likely to exist in the case of the small nanoparticles grown at low temperatures as in reduction method[30,37]. Thus, in this work we compare the small size nanoparticles obtained by reduction method with those of larger size grown at high temperatures as for Pechini method[31].

The knowledge of the electronic properties of the model catalysts is important to understand their chemical reactivity. In this work, since we aim to produce different nanoparticles sizes, core level shifts due to the variations of particle size are considered in the interpretation of XPS spectra. Thus we attempt to understand the chemical (electronic) and the physical effect of the particle size on the observed binding energy shifts.

2.4.3.3. Experimental details

The surface composition of the samples was measured using a VG Escalab 220i-XL instrument equipped with Al Kα (1486.6 eV) polychromatic source operating at 15kV and 26.6 mA. A hemispherical analyzer and a six-channel detector were both used. The pressure inside the analysis chamber was below 1×10^{-9} mbar. A survey from 0 to 1300 eV (100 eV pass energy) was

first acquired and high resolution core level spectra (20 eV pass energy) were then recorded (Pt 4f 68-82 eV; Ce 3d 875-930 eV and C 1s 275-295 eV). In all cases, the energy scale was calibrated for C 1s at 284.5 eV [38]. Each sample was introduced in the chamber just before the analysis and the Ce 3d spectrum was recorded just after the survey spectrum in order to minimize the extent of Ce(IV) to Ce(III) reduction.

For the powder samples (Pechini method) a relatively thick layer of powder was deposited directly on to a carbon cupper conductive double tape which was pilled to a glass and afterwards to the metallic holder. For the reduction method, a 15 µL drop of catalyst was allowed to dry overnight directly in a glass support which was stacked to the metallic holder. In both cases the glass isolates the sample removing a possible differential charge effect between Pt, a conductor and Cerium, a semi-conductor. Thus we avoid a possible difference in the conductivity when both elements are in contact. A high resolution spectrum Ce 3d was also recorded at the end of the analysis to monitor the reduction of Ce (IV) to Ce (III) but no major differences were observed in the spectra. Element quantification was achieved by fitting the core level spectra with mixed Gaussian-Lorentzian functions while considering a Shirley type baseline. The fitting was performed with the help of CasaXPS software. Peak areas were normalized by appropriate atomic sensitivity factors.

2.5. Electrochemical techniques

2.5.1. Cyclic Voltammetry (CV)

Cyclic voltammetry is one of the techniques that is first used when exploring the electrochemical properties of a given system [39,40]. In this technique, the electrochemical potential is continuously varied in the working electrode up to a certain limit, and then it is reversed at the same scan rate to the initial value, while monitoring the changes in current. The potential (E) is usually selected so that the potential interval contains an oxidation and/or reduction process of interest[41]. This is better illustrated in Figure 2.8.
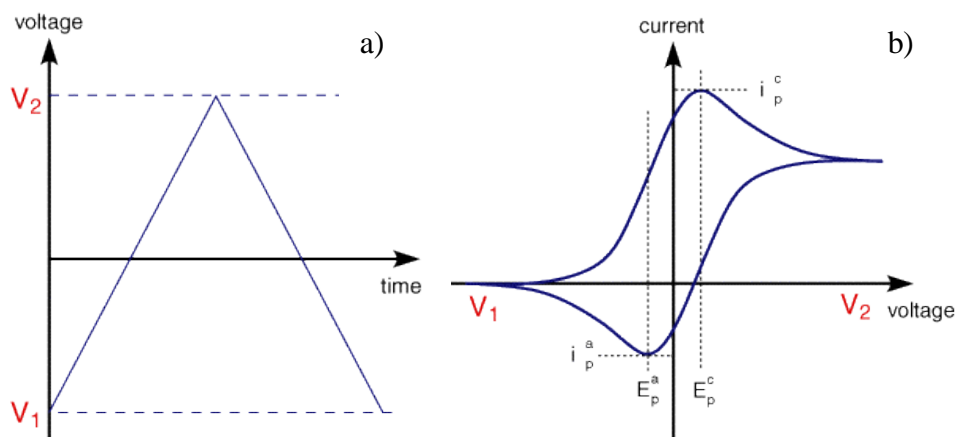
Figure 2. 8 – Variation of the potential with time a) and variation of the current with the potential b)[42].

In the example shown in Figure 2.8 a), the potential increases from the initial value ($E_{initial}$) up to a maximum (E_{max}) at time t_1. At this point the potential switches back and it decreases till reaching the minimum value (E_{min}) at t_2. The potential now increases again till it reaches the final value (E_{final}). The scan rate is given by the variation of the potential with time. The graphical representation of the changes in current, as a result of the changing potential, is typically called a cyclic voltammogram, Figure 2.8 b). In the cyclic voltammograms, the peaks

represent an increase in current toward more positive or negative values, as a result of oxidation [O] or reduction [R] reactions taking place, respectively.

A polycrystalline electrode presents many different exposed crystal faces to a solution, this means that, different sites on the same surface can carry a different charge[43]. The shape of the oxidation current peak in the hydrogen desorption (I > 0) region gives information on the catalyst surface. As can be seen in Figure 2.9, two oxidation peaks are clearly visible, the first one centered at ca. -0.13 V and the second one at ca. -0.01 V which are assigned to surface defects and to short range order (110) and (100) surface domains, respectively[44,45]. On the other hand, a third peak on the hydrogen adsorption region (I < 0) at ca. -0.02 V arises assigned to defective (110) planes following the same trend on the intensity shape as for peaks [46], Figure 2.9.
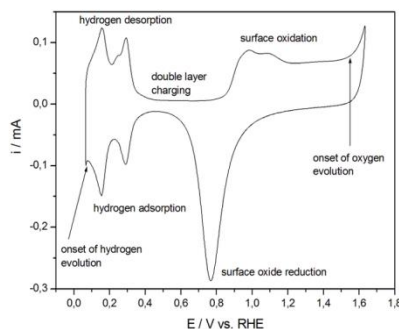
Figure 2. 9 – Characteristics of a double layer charging area in a Pt cyclic voltammetry.

In this sense, a mathematical description of peak current and potential by means of surface area will be presented. Polycrystalline platinum surface have a charge exchanged of 1 H atom per platinum atom, which corresponds to 210 $\mu C/cm^2$ (mean value of the charge contribution for the three single crystal surfaces). Thus, cyclic voltammetry can be used to determine the electrochemical surface area of the Pt electrodes through the amount of charge needed to remove a full hydrogen monolayer adsorbed on a Pt surface. The integration of current

in the anodic scan (i < 0) gives the amount of hydrogen desorbed according to the following reaction:

$$H_{ads} \leftrightarrow H^+ + 1e^-$$
(Equation 2.8)

This charge also contains a contribution due to the double layer charging, which can easily be subtracted as the double layer charging is the same as in the double layer region as illustrated in Figure 2.9. Experimentally the charge involved for the hydrogen desorption reaction is calculated using the following equation 2.9:

$$Q_{Hdes} = \int i(t)dt = \frac{1}{v} \int i(E)dE$$
(Equation 2.9)

where, Q_{Hdes} is the charge corresponding to the integrated current i(t) for a duration t, which corresponds to the integrated current in the potential range considered, i(E), divided by the potential scan rate, v[44,45].

2.5.2. Chronoamperometry

This technique consists in applying a step potential to the working electrode and record changes in current as a function of time, Figure 2.10.
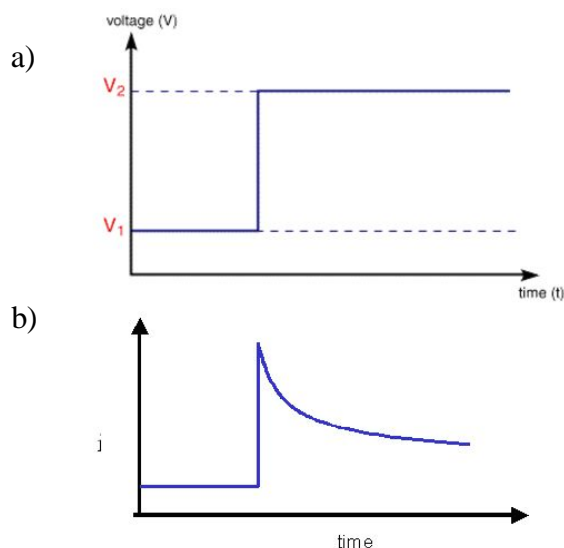
Figure 2. 10 – a) Potential vs time waveform and b) resulting current vs time response.

V_1 is sufficiently negative with respect to V_2 so that the concentration of ethanol on the electrode surface is null and the ionic transport in solution is ruled only by diffusion.

In chronoamperometry, the curves are distorted only at the beginning of the process (t<1ms) corresponding to the charge of the double layer at the time of the imposition of the potential. Afterwards, there is no more capacitive current and one can measure the Faradaic current. Generally, chronoamperometry is very used to test the durability and stability of electrocatalysts in Fuel Cells[39].

2.5.2.1. Experimental details

Electrochemical measurements were carried out in a three-electrode cell by using an Autolab potentiostat/galvanostat PGSTAT 302N equipped with the SCANGEN module. A platinum wire and a Saturated Calomel Electrode (SCE) were used as counter and reference electrodes, respectively. The working electrode is a glassy carbon disk electrode (Metrohm,

Diameter=0.5cm; 0.196 cm^2 geometric area=$\pi*(0.5cm/2)^2$=0.196 cm^2) previously polished with Al$_2$O$_3$ paste and washed in distilled water.

For the preparation of the catalyst ink using the nanoparticles obtained by Pechini method, 0.0025g of catalyst was weighted and dispersed in an Eppendorf with 125μL of ethanol and 25 μL of Nafion® solution. This ink was sonicated for around 30 minutes. An aliquot of 5 μL was deposited on the surface of the glassy carbon electrode surface, and was allowed to dry in air (room temperature) for 20 minutes. The mass of catalyst deposited on the Pt or PtCeO$_2$ electrodes is 0.083 mg. The catalyst loading is then 0.4 mg/cm^2.

For the preparation of the catalyst ink by Reduction method, an aliquot of 15 μL of catalyst was taken from the stock solution and diluted with 125 μL of ethanol and 25 μL of 5 wt% Nafion® solution. This ink was sonicated for around 30 minutes, was and allowed to dry in air (room temperature) for 20 minutes. The mass of catalyst deposited on the Pt or PtCeO$_2$ electrodes is 0.0266 mg. The catalyst loading is then 0.1mg/cm^2. For both methods the catalyst loading is not the same and it is lower comparing with the literature (Table 1.1). However, this difference allows a comparison between the results firstly obtained in powder technique (Pechini method) with the ones secondly obtained in liquid solution (Reduction method) where the nanoparticle size is very small. However as will be seen in the following chapters the results will be normalized so that they can become comparable.

Finally, the cyclic voltammograms tests were recorded in a 0.5 moldm^{-3} H$_2$SO$_4$ electrolyte solution previously purged with nitrogen for 20 minutes at two different scan rates: first at 100 mVs^{-1} and after at 50 mVs^{-1}. The potential range was between -0.2 to 1.2 V and for 20 cycles. Subsequently, the ethanol oxidation was performed under the same conditions but in a 1.0 mol dm^{-3} fuel with 0.5 mol dm^{-3} H$_2$SO$_4$ solution; the data from the 10th cycle is reported.

For each catalyst, the electroactive surface area (ESA) was experimentally determined by recording the CV in a N_2-saturated electrolyte at a scan rate of 50 mV s^{-1} after 10 voltammetric cycles performed between -0.2 V and 1.2 V vs. SCE in order to clean the platinum surface from remaining organic molecules coming from the synthesis and to obtain quasi-constant voltammograms[47].

The chronoamperometry (current-time curves) tests were performed at a constant potential of 0.6V, right after the cyclic voltammetric test and in the same 1.0 mol dm^{-3} ethanol solution / 0.5 mol dm^{-3} H_2SO_4 electrolyte. The chronoamperometric test time was 900 seconds with a previous stabilization time of 30 seconds at a potential of -0.2V.

2.6. Proton Nuclear Magnetic Ressonance Spectroscopy (^{H}NMR)

The composition of the solutions from the chronoamperometric experiments carried out with the catalysts prepared by the reduction method, were analyzed by ^{H}NMR. In nuclear magnetic resonance (NMR) spectroscopy we measure the energy absorption by molecules that have been placed in a strong magnetic field. Instruments known as nuclear magnetic resonance spectrometers allow chemists to measure the absorption of energy by hydrogen-1 nuclei[48]. This technique provides a way to determine structural information with respect to ^{1}H- nuclei within a molecule. Proton NMR spectra of most organic compounds are characterized by chemical shifts in the range +14 to -4 ppm and by spin-spin coupling between protons. As can be seen there are three different types of H atoms. The hydrogen (H) on the (OH) group is not coupling with any other H atoms appearing as a singlet, but the CH_3- and the -CH_2- hydrogens are coupling with each other, resulting in a triplet and quartet respectively (Figure 2.11). The integration curve for

58

each proton reflects the abundance of the individual protons. Figure 2.11 shows an example of H NMR spectrum for ethanol, CH_3CH_2OH.
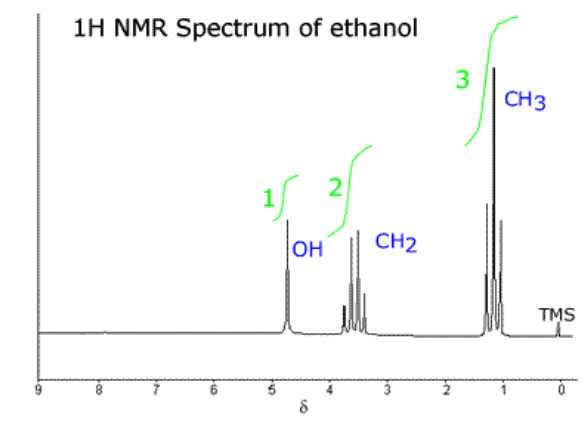
Figure 2. 11 – Example of ^{1}H NMR spectrum of ethanol plotted as signal intensity vs. chemical shift (δ) in ppm[49].

In a given molecule some hydrogen nuclei are in regions of greater electron density than others, and as a result, the nuclei (protons) absorb energy at slightly different magnetic field strengths. The signals for these protons consequently occur at different positions in the NMR spectrum; they are said to have different chemical shifts. In our study of nuclear magnetic resonance (NMR) spectroscopy, we focus our attention on the quantification since the relative magnitudes of the signals (area of the signal) are proportional to the number of hydrogen atoms causing the signal. Thus we compared the proportion of liquid products (acetaldehyde and acetic acid) with respect to the reactant, ethanol. The ration of the integration areas was performed with respect to the ethanol main peak corresponding to CH_3 at 0.89 ppm. For this we previously know that acetic acid acid appears at 1.78 ppm and acetaldehyde at 1.94 ppm, Figure 2.12.
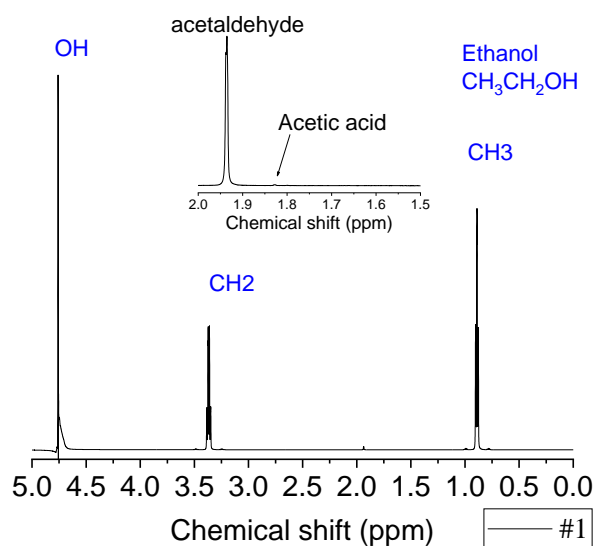
Figure 2. 12 – Example of the chemical shifts observed in this work for Pt (sample #1).

2.6.1. Experimental Details

An aliquot of the solution (500 µL) was taken every hour for a period of 5 hours, this throughout all duration of the chronoamperometry. The overall volume of EtOH/H_2SO_4 solution was 55 mL. Each sample was prepared filling a 5 mm NMR tube with 500 µL of the aliquot and 50 µL of deuterated water as solvent (D_2O, Fisher Scientific, Acros Organics, 99.8 atom%) which was used to align the magnetic field of the spectrometer. The NMR experiments were carried out in a 600 MHz - NMR– varian Inova (performed at UQAM). The integration areas and product ration was performed by Dr. Arnold Alexander. In appendix A2 the 40 H-NMR spectra for the collected samples are shown.

2.7. References

1.   Freitas RG, Santos MC, Oliveira RTS, Bulhões LOS, Pereira EC. Methanol and ethanol electroxidation using Pt electrodes prepared by the polymeric precursor method. Journal of Power Sources 2006;158:164-8.

2.   Adriane V.Rosario ECP. Comparison of the electrochemical behavior of CeO2–SnO2 and CeO2–TiO2 electrodes produced by the Pechini method. Thin solid films 2002:1-7.

3.   Van Rheenen PR, McKelvy MJ, Glaunsinger WS. Synthesis and characterization of small platinum particles formed by the chemical reduction of chloroplatinic acid. Journal of Solid State Chemistry 1987;67:151-69.

4.   Pechini PM. Method of preparing lead and alkaline earth titanates and niobates and coating method using the same to form a capacitor. In: Google Patents; 1967.

5.   Lee H, Hong M, Bae S, Lee H, Park E, Kim K. A novel approach to preparing nano-size Co3O4-coated Ni powder by the Pechini method for MCFC cathodes. Journal of Materials Chemistry 2003;13:2626-32.

6.   Sakka S, Kozuka H. Handbook of sol-gel science and technology. 1. Sol-gel processing: Springer Science & Business Media; 2005.

7.   A. Lessing P. Mixed-Cation Oxide Powders Via Polymeric Precursors; 1989.

8.   Kakihana M. Invited review "sol-gel" preparation of high temperature superconducting oxides. Journal of Sol-Gel Science and Technology 1996;6:7-55.

9.   Tai L-W, Lessing PA. Modified resin-intermediate processing of perovskite powders: Part I. Optimization of polymeric precursors. Journal of Materials Research 1991;7:502-10.

10.   Yao HC, Yao YFY. Ceria in automotive exhaust catalysts. Journal of Catalysis 1984;86:254-65.

11. Tiernan MJ, Finlayson OE. Effects of ceria on the combustion activity and surface properties of Pt-Al2O3 catalysts. Applied Catalysis B: Environmental 1998;19:23-35.

12. Roy S, Saroha AK. Ceria promoted [gamma]-Al2O3 supported platinum catalyst for catalytic wet air oxidation of oxalic acid: kinetics and catalyst deactivation. RSC Advances 2014;4:56838-47.

13. Ingelsten HH, Bagwe R, Palmqvist A, et al. Kinetics of the Formation of Nano-Sized Platinum Particles in Water-in-Oil Microemulsions. Journal of colloid and interface science 2001;241:104-11.

14. Ma H-C, Xue X-Z, Liao J-H, Liu C-P, Xing W. Effect of borohydride as reducing agent on the structures and electrochemical properties of Pt/C catalyst. Applied Surface Science 2006;252:8593-7.

15. Moghaddam RB, Pickup PG. Support effects on the oxidation of ethanol at Pt nanoparticles. Electrochimica Acta 2012;65:210-5.

16. Wiberg KB. The Role of Electrostatic Effects in Organic Chemistry. Journal of Chemical Education 1996;73:1089.

17. Zeng J, Lee JY, Zhou W. Activities of Pt/C catalysts prepared by low temperature chemical reduction methods. Applied Catalysis A: General 2006;308:99-104.

18. Cullity BD. Elements of X-Ray Diffraction. 2 ed: Addison-Wesley Publishing Company, Inc.; 1978.

19. Behrens M, Schlögl R. X-Ray Diffraction and Small Angle X-Ray Scattering. In: Characterization of Solid Materials and Heterogeneous Catalysts: Wiley-VCH Verlag GmbH & Co. KGaA; 2012:609-53.

20.   Klug HP, Alexander LE. X-ray Diffraction Procedures for Polycrystalline and Amorphous Materials: John Wiley & Sons, Inc.; 1954.

21.   http://www.chem.latech.edu/~upali/chem481/chem481c3.htm.

22.   Holzwarth U, Gibson N. The Scherrer equation versus the 'Debye-Scherrer equation'. Nat Nano 2011;6:534-.

23.   Scherrer P. Bestimmung der Größe und der inneren Struktur von Kolloidteilchen mittels Röntgenstrahlen. Gottinger Nachrichten Math Phys 1918;2:98-100.

24.   Williams DB, Carter CB. The Instrument. In: Transmission Electron Microscopy: A Textbook for Materials Science. Boston, MA: Springer US; 2009:141-71.

25.   Baer DR, Thevuthasan S. Chapter 16 - Characterization of Thin Films and Coatings. In: Martin PM, ed. Handbook of Deposition Technologies for Films and Coatings (Third Edition). Boston: William Andrew Publishing; 2010:749-864.

26.   Doh W, Papaefthimiou V, Zafeiratos S. Applications of synchrotron-based X-Ray photoelectron spectroscopy in the characterization of nanomaterials. In: Surface science tools for nanomaterials characterization: Springer; 2015:317-66.

27.   Ratner BD, Castner DG. Electron Spectroscopy for Chemical Analysis. In: Surface Analysis – The Principal Techniques: John Wiley & Sons, Ltd; 2009:47-112.

28.   Ohring M. Chapter 10 - Characterization of thin films and surfaces. In: Ohring M, ed. Materials Science of Thin Films (Second Edition). San Diego: Academic Press; 2002:559-640.

29.   Weinert M, Watson RE. Core-level shifts in bulk alloys and surface adlayers. Physical Review B 1995;51:17168-80.

30.   Radnik J, Mohr C, Claus P. On the origin of binding energy shifts of core levels of supported gold nanoparticles and dependence of pretreatment and material synthesis. Physical Chemistry Chemical Physics 2003;5:172-7.

31.   Henry CR. Surface studies of supported model catalysts. Surface Science Reports 1998;31:231-325.

32.   Hoogewijs R, Vennik J. Auger cross-relaxation energy for metallic sodium, using SCF cluster model calculations. Surface Science 1979;80:503-11.

33.   Egelhoff Jr WF. Core-level binding-energy shifts at surfaces and in solids. Surface Science Reports 1987;6:253-415.

34.   Bagus PS, Nelin CJ, Kay E, Parmigiani F. Reply to the comment by DiCenzo and Wertheim on "core binding energies for clusters⋯". Journal of Electron Spectroscopy and Related Phenomena 1987;43:C13-C8.

35.   Isaifan RJ, Ntais S, Baranova EA. Particle size effect on catalytic activity of carbon-supported Pt nanoparticles for complete ethylene oxidation. Applied Catalysis A: General 2013;464–465:87-94.

36.   Claus P, Brückner A, Mohr C, Hofmeister H. Supported Gold Nanoparticles from Quantum Dot to Mesoscopic Size Scale: Effect of Electronic and Structural Properties on Catalytic Hydrogenation of Conjugated Functional Groups. Journal of the American Chemical Society 2000;122:11430-9.

37.   Ruban A, Hammer B, Stoltze P, Skriver HL, Nørskov JK. Surface electronic structure and reactivity of transition and noble metals. Journal of Molecular Catalysis A: Chemical 1997;115:421-9.

38.   Moulder JF, Sickle WF, Sobol PE, Bomben KD. Handbook of X-ray Photoelectron Spectroscopy: A Reference Book of Standard Spectra for Identification and Interpretation of XPS Data: Physical Electronics Division, Perkin-Elmer Corporation; 1992.

39.   Bard AJ, Faulkner LR. Electrochemical Methods: Fundamentals and Applications 2nd ed: John Wiley & Sons, Inc.; 2001.

40.   Brett CMA, Brett AMO. Electrochemistry: Principles, Methods and Applications: Oxford University Press; 1993.

41.   Compton RG, Banks CE. Understanding Voltammetry. Singapore: World Scientific; 2007.

42.   http://www.ceb.cam.ac.uk/research/groups/rg-eme/teaching-notes/linear-sweep-and-cyclic-voltametry-the-principles.

43.   Bard AJ, Faulkner LR. Electrochemical Methods: Fundamentals and Applications: Wiley; 2000.

44.   Markovic NM, Gasteiger HA, Ross PN. Oxygen Reduction on Platinum Low-Index Single-Crystal Surfaces in Sulfuric Acid Solution: Rotating Ring-Pt(hkl) Disk Studies. The Journal of Physical Chemistry 1995;99:3411-5.

45.   Attard GA, Gillies JE, Harris CA, et al. Electrochemical evaluation of the morphology and enantioselectivity of Pt/graphite. Applied Catalysis A: General 2001;222:393-405.

46.   Gómez R, Clavilier J. Electrochemical behaviour of platinum surfaces containing (110) sites and the problem of the third oxidation peak. Journal of Electroanalytical Chemistry 1993;354:189-208.

47.   Maillard F, Savinova ER, Stimming U. CO monolayer oxidation on Pt nanoparticles: Further insights into the particle size effects. Journal of Electroanalytical Chemistry 2007;599:221-32.

48.   Solomons TWG, Fryhle C, Snyder S. Organic Chemistry, 11th Edition: Wiley; 2012.

49.   https://www.quora.com/Is-it-possible-to-distinguish-between-C2H5OH-and-T-C4H9OH.

3. Pt and PtCeO$_2$ nanoparticles (CeO$_2 \leq$ 5 wt%) synthesized by the Pechini method

3.1. Summary

Pt and PtCeO$_2$ nanoparticles (CeO$_2 \leq$ 5 wt%) were synthesized by Pechini (sol-gel) method. This approach is based on the in-situ polymerization (esterification) between a glycol and a carboxylic acid. The Pechini method has a low environmental impact by minimizing the use of volatile substances and through its polymeric gel network we can obtain a more homogeneous composite system[1-3]. Other advantage of the Pechini method comprises the degree of flexibility on the preparation of the polymer network ratio. In this process, we increased the distance between the Pt nuclei by dilution of the polymer network, avoiding the use of surfactant agents. We diluted five and ten times more than in the original polymer network matrix[1,2] in order to understand how it impacts the Pt particle size and electrochemical activity. Consequently, three series of Pt-CeO$_2$ catalysts with 0, 1 and 5 wt% CeO$_2$ were prepared and tested for the ethanol electro-oxidation in acidic media. No carbon, or any other substrate, was used to support the nanoparticles (NPs), in order to rule out any effect coming from the carbon substrate. It was found that a 10 times diluted pure Pt has a positive impact on its electrochemical activity although for the bimetallic catalysts the ceria effect overcame the dilution effect according with the combined factors. In fact, the combination of the polyester dilution and the presence of ceria may also converge to a reduction of the catalysts particle size under specific conditions by preventing its agglomeration. The TEM images suggest that the dilution seemed to strongly participate at reducing the aggregation, the particle size with consequently "mirroring-type" morphology. By the other way, the ceria addition succeeded at producing smaller

nanocomposites caused by a protective shell. Details on the enhanced catalysts activity are justified by means of TEM, XRD, and XPS data. The electrochemical characterization of ethanol oxidation includes cyclic voltammetry and chronoamperometry techniques.

3.2. Results and discussion

3.2.1. Physicochemical characterization

Figure 3.1 and 3.2 show the diffractograms of all samples prepared using the Pechini method.
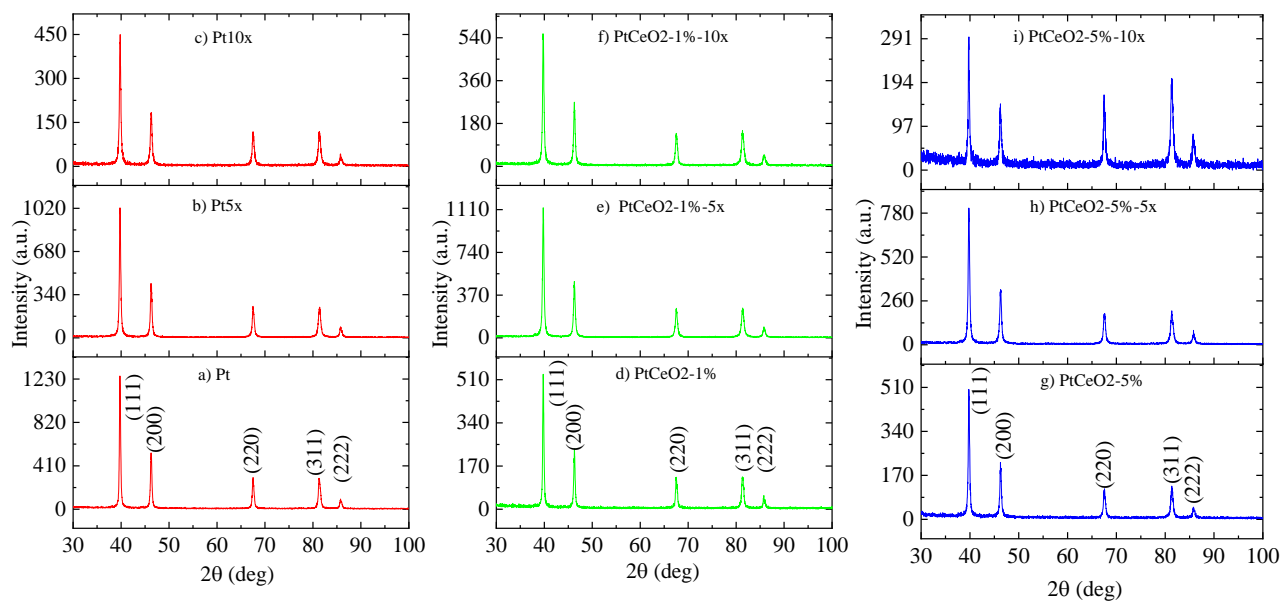
Figure 3. 1 – X-Ray diffraction of pure Pt and nanocomposites samples synthesised by the Pechini method for: **a)-c)** Platinum **d)-f)** PtCeO$_2$-1wt% **g)-i)** PtCeO2-5wt% with zero, five and ten times dilution.

The characteristic peaks of platinum face centered cubic (fcc) phase ($2\theta=39.7°$ (111), $2\theta=46.2°$ (200), $2\theta=67.4°$ (220), $2\theta=81.2°$ (311) and $2\theta=85.7°$ (222); JCPDS#04-0802) are present in all diffractograms of Figure 3.1. The characteristic peaks of CeO_2 structure ($2\theta= 33°$ (200), $2\theta= 47.5°$ (220), $2\theta=56.3°$ (311), $2\theta= 60°$ (222) and $2\theta= 69.4°$ (400); JCPDS#034-0394) are present in all diffractograms of Figure 3.2.
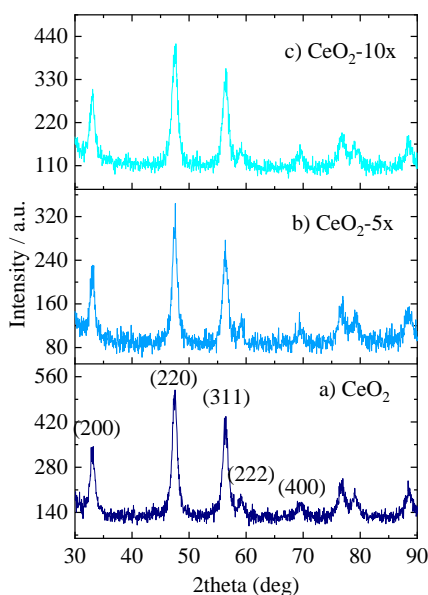
Figure 3. 2 – (a) to (c) X-ray diffraction patterns of CeO_2 nanoparticles synthesised by the polymeric precursor method with $1 \times$, $5 \times$ and $10 \times$ dilution of the cerium precursors in the polyesther gel.

The corresponding lattice parameter values, calculated for each 2θ value, are practically constant and equal to 3.91 Å, for all samples, which is typical of the fcc Pt structure. For the 1 and 5 wt% ceria catalysts it was not possible to observe any of the diffraction peaks related to CeO_2 (JCPDS 34-0394), most probably due to the very low ceria concentration. As for pure platinum, all catalysts show relatively high peak intensity, independent on the dilution factor.

69

The transmission electron microscopy (TEM) was carried out on the prepared samples and selected images are reported in Figure 3.3. The images used for the measured of the particle size shown in the appendix A3.
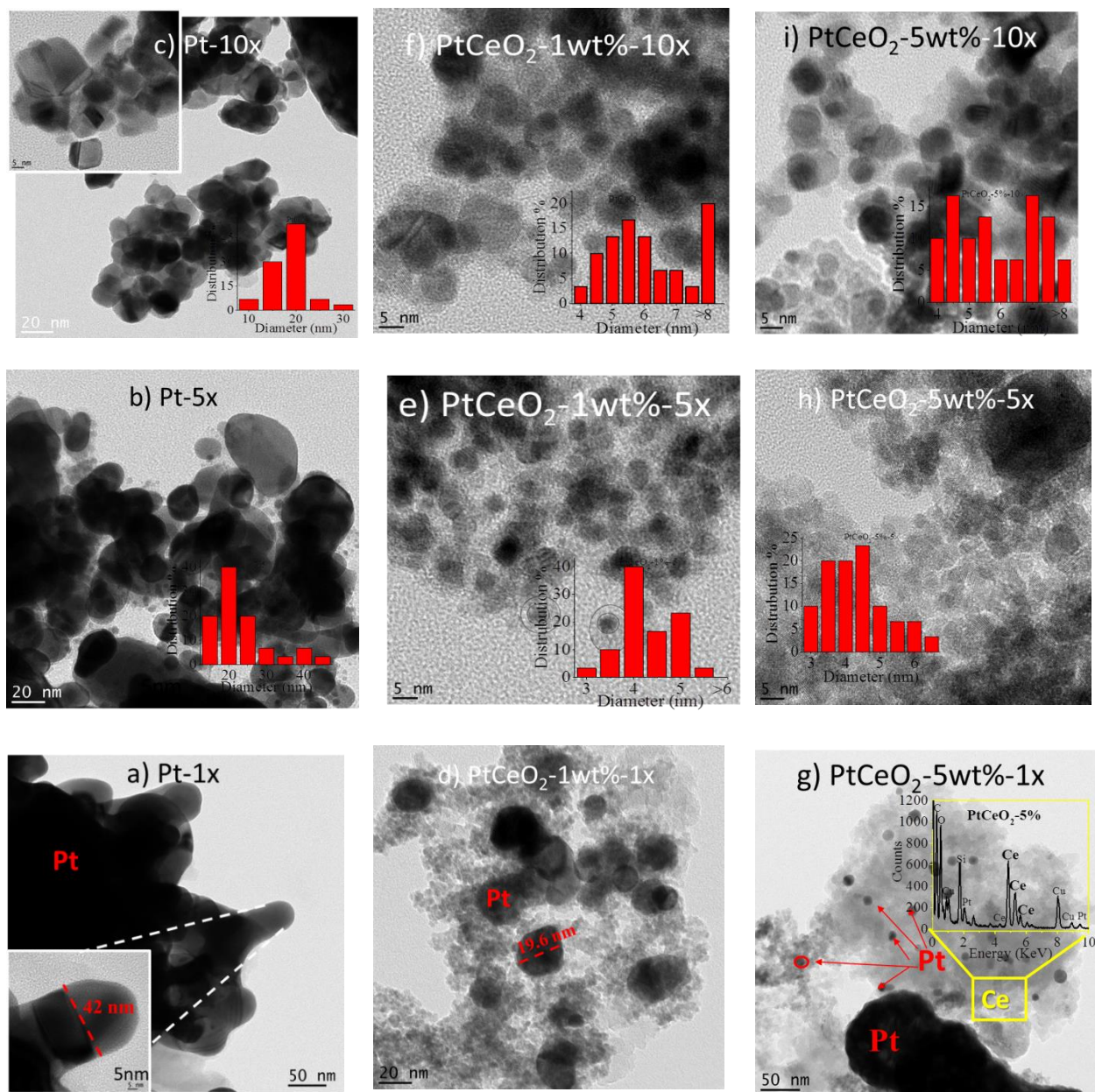
Figure 3. 3 – a) - i) TEM images of Pt (a) to (c), Pt-CeO2 1wt% (d) to (f) and Pt-CeO2 5 wt% (g) to (i) nanoparticles. The statistics for the particle size distribution was done counting 100 particles on images with a 20 nm scale.

As shown in Figure 3.3, Pt 1 × sample is formed by nanoparticles with sizes ≥ 40 nm agglomerated in large clusters. As expected, the samples obtained from the diluted Pt precursor in the polyester polymeric network (Pt 5 × and 10 ×) are formed by smaller (sizes < 40 nm) and less agglomerated nanoparticles. In these cases, the presence of partially burned carbon residues could also inhibit the grain growth. The mean particle size decreases from approximately 42 nm for the sample 1 ×, to 23.1±7.9 and 18.2±4.1 nm for 5 × and 10 × samples, respectively. It is interesting to note that Pt 10 × shows a "mirroring-type" of growth where the planes are seeded together out of the plane (see inset in Figure 3.3.c). The presence of CeO_2, even in very small amounts, also promotes the decrease of the size and the deaglomeration of the Pt nanoparticles as evidenced in Figures 3.3.d and 3.3.g. Individual Pt NPs with ca. 20 nm and 12 nm sizes can now be easily identified in samples Pt-CeO_2 1 × with 1 and 5 wt% CeO_2 respectively. These Pt NPs are dispersed in a CeO_2 "matrix". However, the dilution of the Pt and Ce precursors in polyester polymer matrix revealed to be the most effective way to obtain samples mostly composed of well dispersed and small Pt NP. A strong particle size decrease is indeed observed from 19.6±4.7 nm for Pt-CeO_2-1wt% to 4.3±0.7 nm and 6.5±1.9 nm for the 5 × and 10 × dilutions, respectively (Figures 3.3.d and Figure 3.3.e). Samples PtCeO_2-5 wt%-5 × and 10 × are composed by Pt NPs with sizes slightly higher and with a broader size distribution than in Pt-CeO_2 -1 wt% - 5 × and 10 × (Figures 3.3.g). Because the PtCeO_2-1wt%-10× also shows some particles with the "mirroring-type" of growth, this phenomenon seems to be caused by a dilution effect on Pt nanoparticles and not due to ceria since the mirroring is no longer visible in Pt-CeO_2-5 wt% - 10×.

Synthesis of CeO_2 powders from gels with 1 ×, 5 × and 10 × dilutions, revealed the formation of NPs with average particle sizes between 6 and 8 nm, Figure 3.4. Ceria is an

oxidizing agent known to aid the combustion process lowering the temperature of oxidation of carbon[4]. Thus, the in-situ grown CeO_2 may accelerate locally the calcination process and facilitate the formation of smaller Pt nuclei[5].
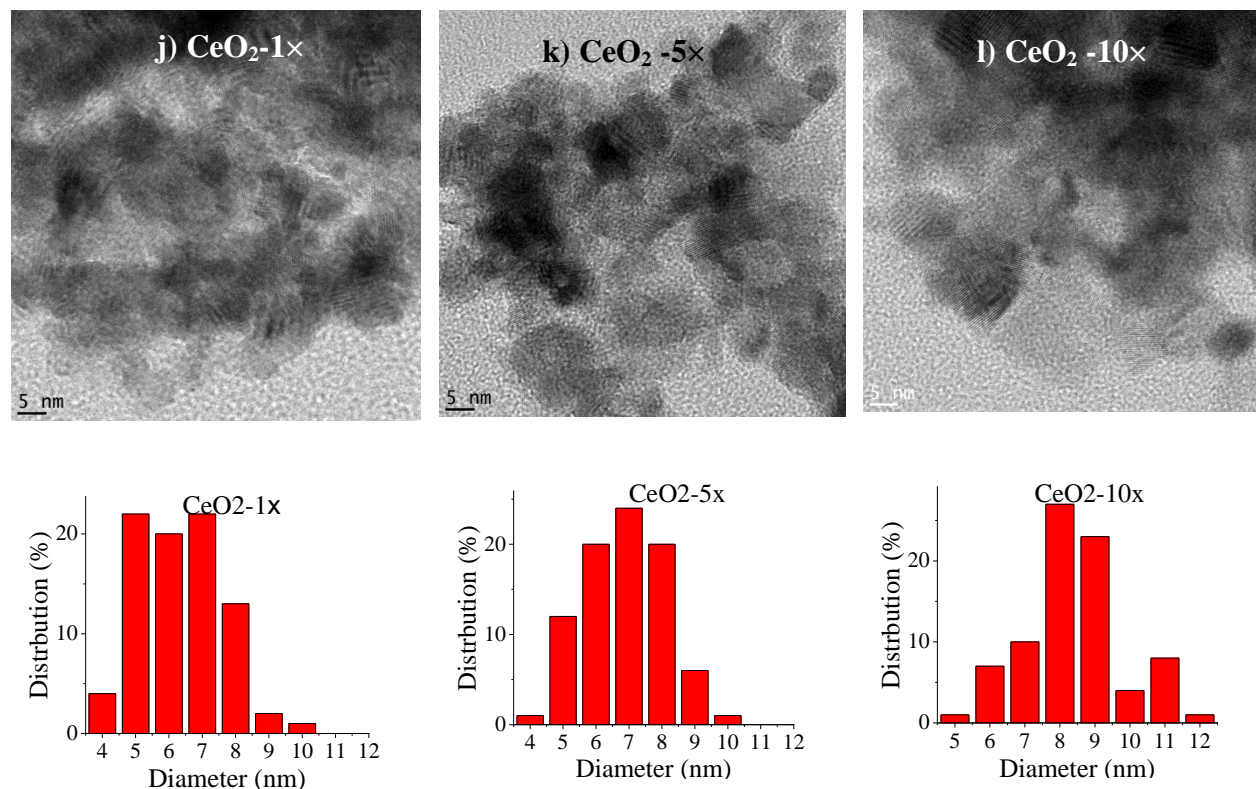
Figure 3. 4 – j) - l) TEM characterization for CeO_2 produced by Pechini method with and without polymeric dilution. The average particle size of CeO_2 is between 6 and 8 nm.

X-ray photoelectron spectroscopy (XPS) is a technique that probes the surface composition and changes in an atom's core level structure, and was used to investigate catalysts. Figure 3.5 a)-i) show the Pt 4f high resolution spectra for all Pt and Pt-CeO_2 catalysts under investigation. The two doublets of Pt 4f, namely $Pt4f_{7/2}$ and $Pt4f_{5/2}$ (Figure 3.5), represent the two degenerated states of Pt separated by 3.33 eV and with an intensity ratio $Pt4f_{7/2}:Pt4f_{5/2}=4/3$

(Table A2.1). The Pt $4f_{7/2}$ peak around 71 eV corresponds to zero-valent Pt^0, while the very low intensity peak at higher binding energy i.e. 72.4 eV is assigned to Pt^{2+} ionized state for the same degeneracy[6].
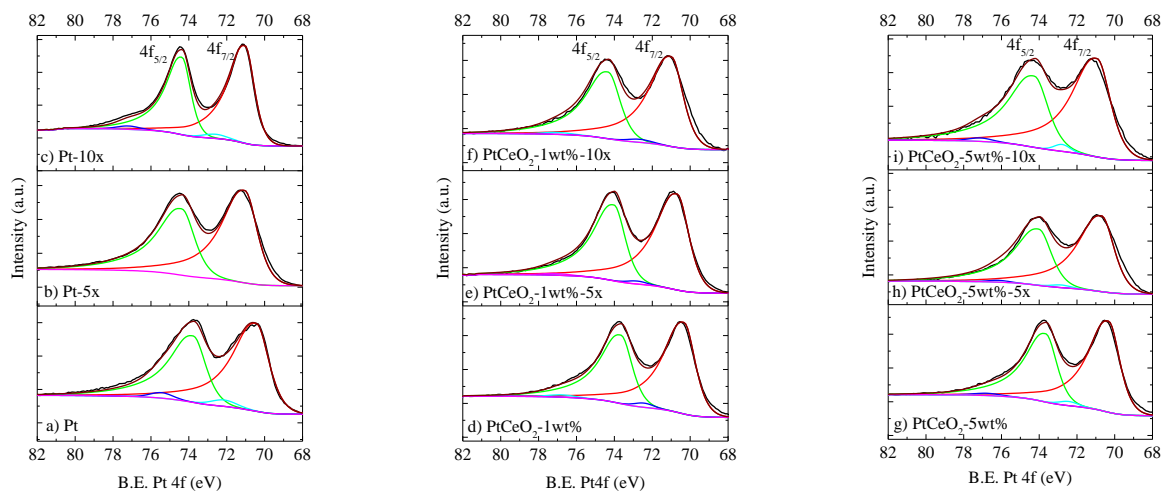
Figure 3. 5 – High resolution ceria spectra for Pt 4f with applied dilutions a)-c) and for Pt 4f in PtCeO$_2$-1wt% electrocatalysts d)-f) and for CeO$_2$ in PtCeO$_2$-5wt% g)-i).

It is long known that a transition metal nanoparticle as Pt, exhibit binding energy variations not only with its particle size but also with the chemical composition[7]. As observed in Figure 3.6 all three series show a negative shift of Pt$4f_{7/2}$ binding energy with the addition of ceria. Initial state effects caused a strong interaction between Pt and Ce is the most probable explanation.
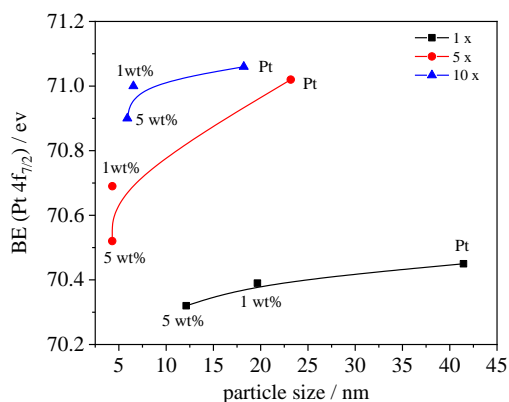
Figure 3. 6 – Binding energy of Pt $4f_{7/2}$ as function of Pt nanoparticles' average particle size. The ceria wt% and of the dilution of the Pt and Ce precursors in the polyester gel are indicated in the figure.

The effect of dilution seems to produce an opposite trend with respect to that of ceria, and positive shifts are observed in the values of the binding energy of Pt $4f_{7/2}$. This shift is especially relevant for pure platinum 1× and 5× (0.6 eV positive shift) where the largest variation of particle size is observed, thus it could be related to a particle size effect by means of relaxation or core hole screening[8-10]. A $e^2/2r$ relationship between the binding energy and particle radius (e is the electron charge=$1.60217662 \times 10^{-19}$ C) has been established[10]. However, this effect is more pronounced on nanoparticles with diameters below 5 nm[11]. Thus, the positive shift may be related to a different structural arrangement of the Pt atoms on the particles' surface[9].

The Ce 3d core level spectra recorded for the $PtCeO_2$ composites and for pure CeO_2 (used as a reference to better understand the interaction between Pt-CeO_2 interaction) are shown in (Figure 3.7 a)-i). The spectra include two main cerium-rich bands that correspond to the $3d_{5/2}$ and $3d_{3/2}$ spin-orbit states. Moreover, the presence of mixed oxidation states results in a complex Ce 3d spectrum although Ce (III) can be differentiated from Ce (IV) due to different line shapes

[12,13]. Namely, v_2/v_2' and u_1/u_1' doublets, separated by 18.6 eV, are assigned to primary photoemission from Ce (IV) and Ce (III), respectively [14]. The v_2/v_2' corresponds to $3d^9 4f^0 O2p^6$ and u_1/u_1' corresponds to the $3d^9 4f^2 O2p^5$ final states of Ce (IV) and Ce(III), respectively. The v_0/v_0' and v_1/v_1' doublets are shake-down features resulting from the transfer of one or two electrons from a filled O 2p orbital to an empty Ce 4f orbital during the Ce (IV) photoemission. These processes are referred as v_0/v_0' Ce(IV) $3d^9 4f^2 O2p^4$ and v_1/v_1' Ce(IV) $3d^9 4f^1 O2p$ [13,15].
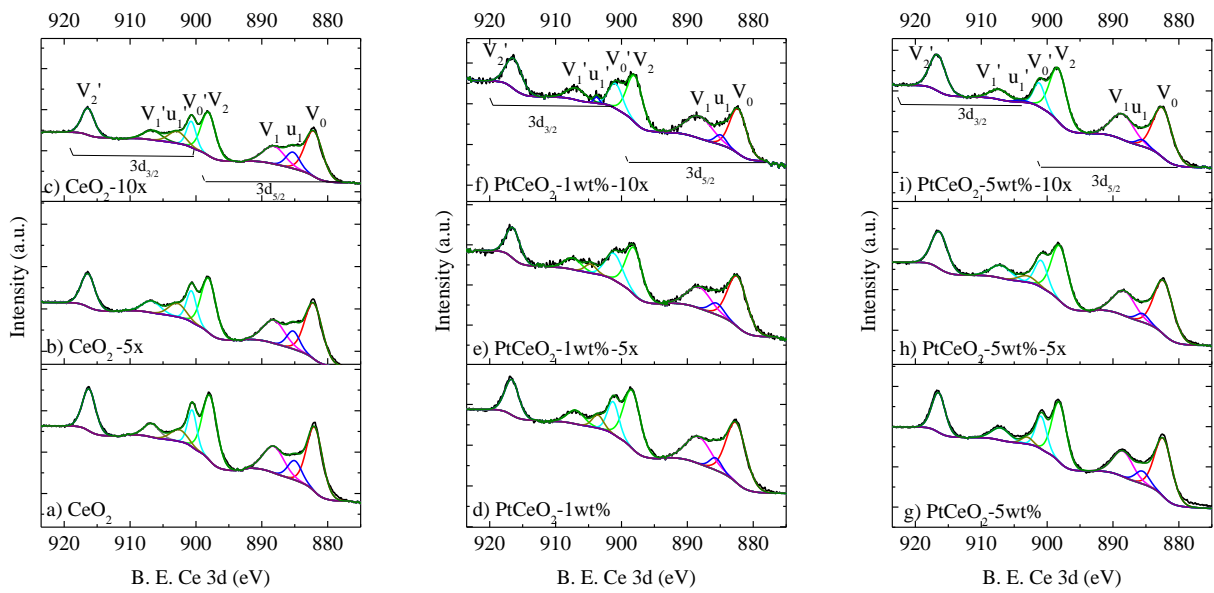
Figure 3. 7 – High-resolution spectra of Ce 3d with 0x, 5x and 10x dilutions for pure ceria a)-c), for $PtCeO_2$-1wt% d)-f) and for $PtCeO_2$-5wt% g)-i).

The several parameters that we can obtain from XPS data analysis are shown in Figure 3.8.
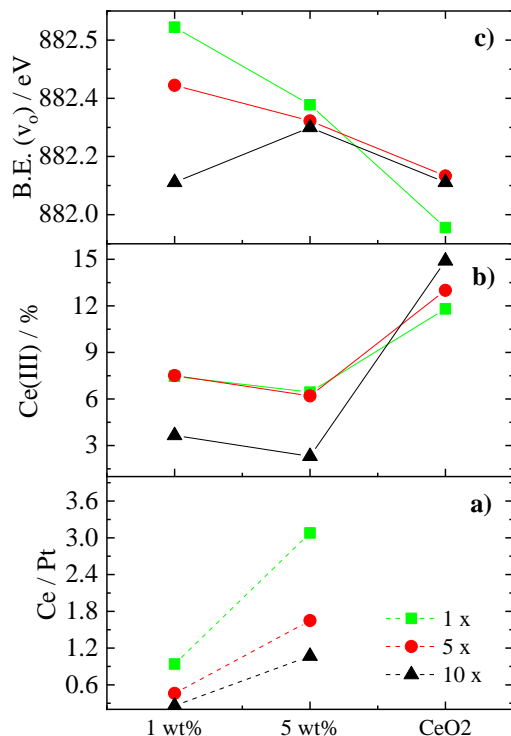
Figure 3. 8 – Binding energy associated to a) u1 Ce (III) and b) v_0 (Ce(IV)) main peaks c) variation of the Ce (III)/Ce (%) and d) Ce/Pt at% ratio.

The surface Ce/Pt atomic ratio was calculated using the at% obtained from the area under the peaks indicated in equation 3.1:

$$\frac{Ce}{Pt} = \frac{v_0+u_1+v_1+v_2+v_0'+u_1'+v_1'+v_2'}{(Pt4f)_{7/2}} \times 100 \qquad \text{(Equation 3.1)}$$

As shown in Figure 3.8 a) the surface Ce/Pt atomic ratio is higher than the nominal values of 0.01 (PtCeO$_2$ 1wt%) and 0.06 (PtCeO$_2$ 5wt%). This is consistent with the TEM images presented in Figure 1 that show the Pt NPs covered by CeO$_2$ NPs. As expected, the catalysts with higher amount of ceria, i.e. with 5wt% show the highest Ce/Pt ratio. The composites from series 1 × have the lowest Ce/Pt ratio and, as expected from TEM analysis, this ratio increases with the

decrease of Pt's average particle size and better dispersion of the Pt NPs within CeO_2 matrix. XPS analysis also revealed that most of the surface cerium species are present as Ce (IV), Figure 3.8 b), which is consistent with the relatively high temperature used in the synthesis (400 °C) and small particle size of the CeO_2 nanoparticles[16].

The %Ce (III), was determined using the at% obtained from the area under the peaks indicated in equation 3.2 [15]:

$$\%Ce(III) = \frac{Ce(III)}{Ce(III)+Ce(IV)} \times 100 = \frac{u1'+u1}{u_1'+u_1+v_0+v_1+v_2+v_0'+v_1'+v_2'} \times 100 \quad \text{Equation 3.2)}$$

As shown in Figure 3.8 b), the %Ce (III) is lower in the Pt-CeO2 composites (between 4 and 10%) compared to pure CeO_2 (between 15 and 21%). Also, peak v0 is shifted to higher binding energy values in the composites with respect to pure CeO2, Figure 3.8 c). As already mentioned, a strong interaction between Pt and CeO_2 explains a more positively charged cerium in the nano-composites than in pure ceria. Interestingly, the effect of the Pt particle size (expressed in the figure as dilution of the metal precursors in the polymer precursor matrix) is more marked for the Pt-CeO$_2$-1wt% catalysts.

3.2.2. Electrochemical characterization

The electrochemical characterization of the catalysts was performed by cyclic voltammetry in 0.5 M H_2SO_4. The typical cyclic voltammogram of polycrystalline Pt was recorded for all catalysts, Figure 3.9. The formation of surface platinum oxides is evidenced at potentials above 0.5 V vs SCE, and their reduction in the 0.3 to 0.7 V vs SCE potential window. In the hydrogen adsorption / desorption region three peaks centered at ca. -0.13 V, ca. -0.01 V and at ca. -0.02 V vs SCE assigned to (110), (100) step and (100) terrace-flat planes[17-19], are

clearly visible. The electrochemical surface area (ESA) values determined from the H-desorption features of the cyclic voltammograms (CV) are reported in Table 3.1.

Table 3. 1 – Electrochemical surface area (ESA) derived from the H-desorption region of the cyclic voltammograms presented in Figure 3.9.

Catalyst	ESA $\times$ 10^{-4} / m^2
Pt - 1 $\times$	0.40
Pt - 5 $\times$	1.46
Pt - 10 $\times$	3.62
Pt-CeO$_2$ 1 wt%- 1 $\times$	1.43
Pt-CeO$_2$ 1 wt% - 5 $\times$	1.17
Pt-CeO$_2$ 1 wt% - 10 $\times$	1.57
Pt-CeO$_2$ 5 wt% - 1 $\times$	0.25
Pt-CeO$_2$ 5 wt% - 5 $\times$	0.42
Pt-CeO$_2$ 5 wt% - 10 $\times$	1.23

The current intensity increased from pure Pt 1 $\times$ to Pt 10 $\times$ in accordance to the decrease of the size of the Pt NPs, as observed in Figure 3.3. A similar effect, but in a lower extent is observed for the Pt-CeO$_2$ electrodes. In fact, the addition of ceria decreases the current intensity as the result of the coverage of the surface of the Pt NPs by the oxide, Figures 3.9 b) and c).
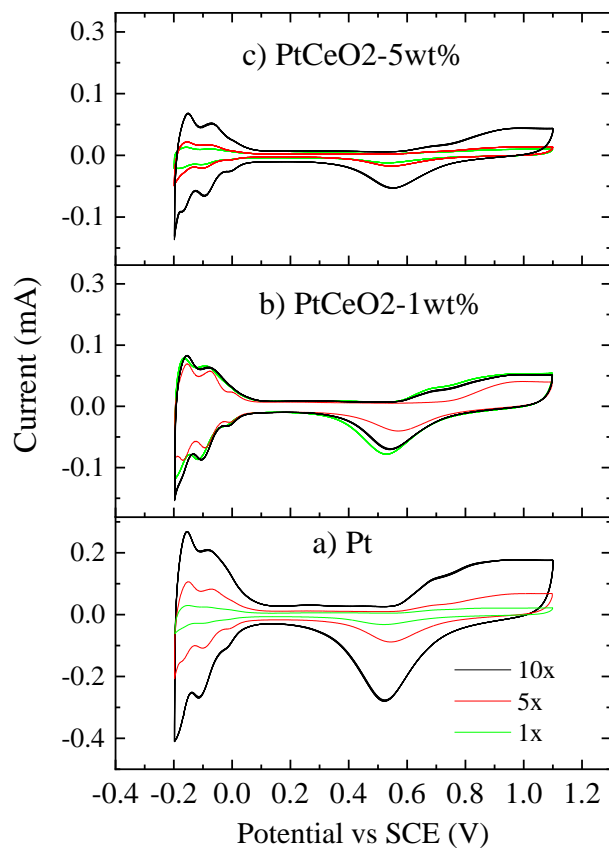
Figure 3. 9 – Cyclic voltammograms in the 0.5M H_2SO_4 electrolyte at $50mVs^{-1}$ for a) pure Pt, b) $PtCeO_2$-1% and c) $PtCeO_2$-5% composites prepared with $1 \times$ (green), $5 \times$ (red) and $10 \times$ (black) dilution in the precursor polyester gel. The current is normalized to Pt's electrochemical surface area.

3.2.1. Ethanol oxidation

The anodic scans for the ethanol electro-oxidation reaction in H_2SO_4 electrolyte are presented in Figure 3.10 and the complete cyclic voltammograms are reported in appendix A5.
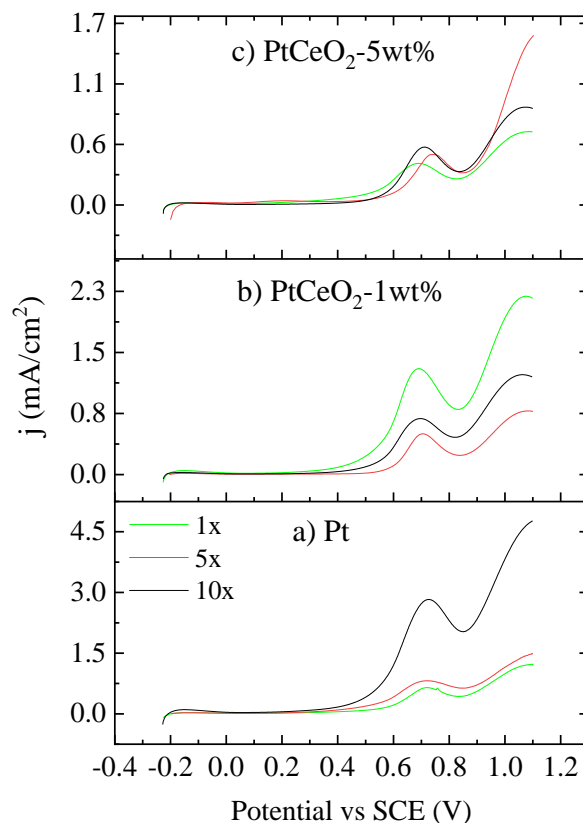
Figure 3. 10 – Cyclic voltammograms recorded in 1 M ethanol in 0.5 M H_2SO_4 electrolyte at 50 mV.s-1 for (a) Pt, (b) Pt-CeO$_2$ 1wt% and (c) Pt-CeO$_2$ 5wt% composites prepared from $1 \times$ (black), $5 \times$ (red) and $10 \times$ (blue) dilution in the precursor polyester gel. The current is normalized to Pt's electrochemical surface area.

In Figure 3.10, the current was normalized to Pt's ESA of the corresponding catalyst. All the voltammetric features are typical of the ethanol electro-oxidation reaction catalyzed by Pt[20]. The adsorption of ethanol on the surface of the catalysts starts at around 0.2V vs SCE, and it is followed by its oxidation to CO_2 from CO_{ads} at ca. 0.65 V vs SCE. Overall, and as expected, higher ethanol current densities were measured for catalysts with higher electrochemical surface area. But, interestingly, there are two singular points. First, Pt $10 \times$ shows a remarkably higher

current with respect to the Pt 1 × and Pt 5 ×. Second, Pt-CeO$_2$ 1wt% - 1 × shows the highest current density for the Pt-CeO$_2$ series.

The trends observed in the cyclic voltammograms were confirmed by chronoamperometry, Figure 3.11. The currents at 900 s normalized to Pt's electrochemical surface area are shown in Figure 3.12.
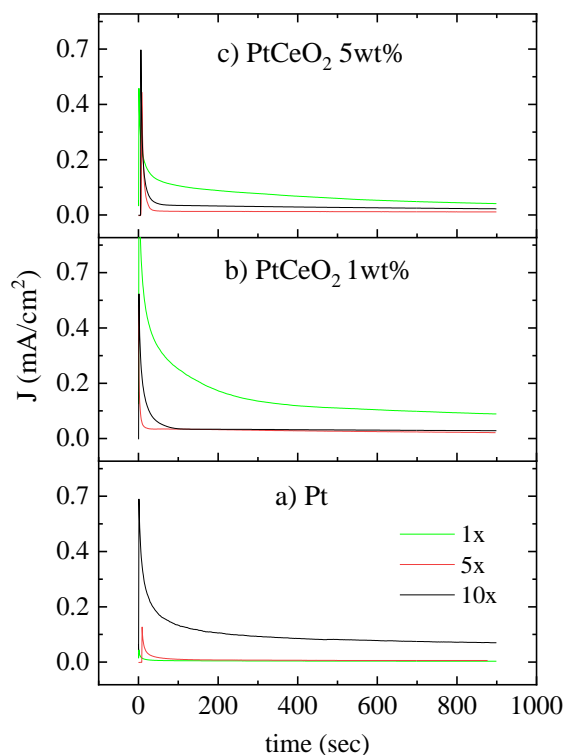
Figure 3. 11 – Chronoamperometric measurements recorded at 0.6 V vs SCE in 1 M ethanol in 0.5 M H$_2$SO$_4$ electrolyte for (a) pure Pt, (b) Pt-CeO$_2$ 1 wt% and (c) Pt-CeO$_2$ 5 wt% composites prepared from 1 ×, 5 × and 10 × dilution in the precursor polyesther gel. The current is normalized to Pt's electrochemical surface area.
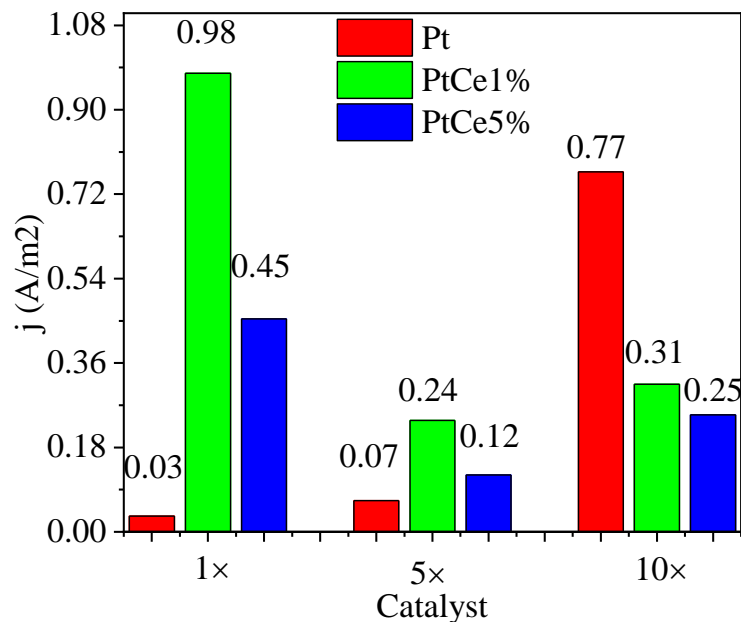
Figure 3. 12 – Current density normalized to the Pt's electrochemical surface area for the Pt, Pt-CeO$_2$ 1 and 5 wt% composites prepared from 1×, 5 × and 10 × dilution in the precursor polyesther gel. The current values were taken at the end (t=900 s) of the chronoamperometric measurements recorded at 0.6 V vs SCE in 1 M ethanol in 0.5 M H$_2$SO$_4$.

For the 1 × series catalysts, the current density increased substantially with the addition of ceria to Pt. This increase corresponds to~20 times for Pt-CeO$_2$ 1wt% and to~10 times Pt-CeO$_2$ 5wt% compared to bare Pt. For the 5 × series a different trend was observed, the current increased 3 times upon the addition of 1 wt% of ceria to Pt and 2 times with the addition of 5 wt% of ceria to Pt. Finally, for the 10 × dilution a different trend was observed and pure Pt shows the highest catalytic activity toward the ethanol oxidation; in fact, the addition of ceria decreases the current density of about 2 times for Pt-CeO$_2$ 1 wt% and to 3 times for Pt-CeO$_2$ 5 wt%. Still, Pt-CeO$_2$ 1wt% always shows a higher current density than that of Pt-CeO$_2$ 5wt%.

Moreover, comparing Pt 10 × and Pt-CeO$_2$ 1wt% 1× which are composed of Pt NPs of similar size, the electrocatalytic activity of the later is 1.3 × higher than that of the former. Differences in the size and agglomeration of the Pt NPs, and the absence of carbon support can justify the lower current densities observed in this work compared to those reported in the literature. The size of these Pt NPs is well above 3 nm, the optimal Pt particle size for ethanol oxidation[21,22], and above the size of the Pt NPs in the Pt/CeO$_2$/C composite catalysts discussed in the Introduction section (typically 5 nm)[16,23-25].

According to these results, few wt% of CeO$_2$ are sufficient to enhance the electrocatalytic activity of Pt NPs for ethanol oxidation. However, this enhancement is more meaningful on samples containing Pt NPs with larger particle sizes (e.g. 20 nm as in Pt-CeO2 1 wt% 1 ×). XPS analysis, Figure 3.6, revealed negative shifts of Pt 4f peaks with the addition of CeO$_2$ and thus, an evidence of an electronic effect between Pt and Ce. A negative shift of the Pt 4f binding energy usually reflects a downshift shift of the Pt 4f d-band center position with respect to the Fermi level[26], which can explain the higher electrocatalytic activity of the Pt-CeO$_2$ 1 wt% catalysts. According to Norskov et al.[27] when the d-band center is shifted upwards in energy scale, new antibond states above the Fermi level are formed. As consequence, the adsorbate-metal interaction is stronger and the electrocatalytic activity related to the catalyst is lower. XPS analysis, Figure 3.8, also revealed that the ceria in these Pt-CeO$_2$ composites is more oxidized than in pure CeO$_2$. As previously reported by Anderson et al.[23] the more oxidized is CeO$_2$ (higher Ce(IV)/Ce(III) ratio), the higher the catalytic activity of Pt for both methanol and ethanol oxidation in acid medium. These positive effects are however hindered by a high coverage of the Pt nanoparticles surface by CeO$_2$ which results in the decrease of active sites. This is the case of

the samples with 5 wt% of CeO_2 or with smaller Pt NPs (higher dilution of the metal precursors in the polyester matrix).

3.3. Conclusions

Pt NPs without and decorated with CeO_2 (1 and 5 wt% with respect to Pt) and with average Pt particle sizes ranging from 40 nm down to 4 nm, were prepared by the Pechini method and their electrocatlytic activity for ethanol electro-oxidation in acid medium investigated. It was found that 1 wt% of CeO_2 can remarkably enhance the activity of 20 nm Pt NPs. This enhancement is due to a strong electronic interaction between Pt and CeO_2 as shown by XPS analysis. Overall, the addition of very small amounts of CeO_2 to Pt resulted in negative shift of Pt's binding energy and a more oxidized CeO_2. These imply, respectively, a weaker interaction between Pt and CO_{ads}–like species and put in evidence the importance of Ce(IV) ions in the oxidative removal of these poisoning species.

3.4. References

1.   Adriane V.Rosario ECP. Comparison of the electrochemical behavior of CeO2–SnO2 and CeO2–TiO2 electrodes produced by the Pechini method. Thin solid films 2002:1-7.

2.   Freitas RG, Oliveira RTS, Santos MC, Bulhões LOS, Pereira EC. Preparation of Pt thin film electrodes using the Pechini method. Materials Letters 2006;60:1906-10.

3.   Tai L-W, Lessing PA. Modified resin-intermediate processing of perovskite powders: Part I. Optimization of polymeric precursors. Journal of Materials Research 1991;7:502-10.

4.   Prasad R, Bella VR. A Review on Diesel Soot Emission, its Effect and Control. 2011 2011:18.

5.   Nagai Y, Hirabayashi T, Dohmae K, et al. Sintering inhibition mechanism of platinum supported on ceria-based oxide and Pt-oxide–support interaction. Journal of Catalysis 2006;242:103-9.

6.   Lewera A, Timperman L, Roguska A, Alonso-Vante N. Metal–Support Interactions between Nanosized Pt and Metal Oxides (WO3 and TiO2) Studied Using X-ray Photoelectron Spectroscopy. The Journal of Physical Chemistry C 2011;115:20153-9.

7.   Verykios XE, Stein FP, Coughlin RW. Metal-support interaction effects of silver catalysts during ethylene oxidation. Journal of Catalysis 1980;66:147-54.

8.   Isaifan RJ, Ntais S, Baranova EA. Particle size effect on catalytic activity of carbon-supported Pt nanoparticles for complete ethylene oxidation. Applied Catalysis A: General 2013;464–465:87-94.

9.   Radnik J, Mohr C, Claus P. On the origin of binding energy shifts of core levels of supported gold nanoparticles and dependence of pretreatment and material synthesis. Physical Chemistry Chemical Physics 2003;5:172-7.

10.   Bagus PS, Nelin CJ, Kay E, Parmigiani F. Reply to the comment by DiCenzo and Wertheim on "core binding energies for clusters⋯". Journal of Electron Spectroscopy and Related Phenomena 1987;43:C13-C8.

11.   Claus P, Brückner A, Mohr C, Hofmeister H. Supported Gold Nanoparticles from Quantum Dot to Mesoscopic Size Scale: Effect of Electronic and Structural Properties on Catalytic Hydrogenation of Conjugated Functional Groups. Journal of the American Chemical Society 2000;122:11430-9.

12.   Paparazzo E, G.M.lngo, Zacchetti N. X-ray induced reduction effects at Ce02 surfaces: An x-ray photoelectron spectroscopy study. J Vac Sci Technology A 1991; 9:1416-20.

13.   Avramova I, Suzer S, Guergova D, Stoychev D, Stefanov P. CeOx/Al2O3 thin films on stainless steel substrate — Dynamical X-ray photoelectron spectroscopy investigations. Thin solid films 2013;536:63-7.

14.   Moulder JF, Sickle WF, Sobol PE, Bomben KD. Handbook of X-ray Photoelectron Spectroscopy: A Reference Book of Standard Spectra for Identification and Interpretation of XPS Data: Physical Electronics Division, Perkin-Elmer Corporation; 1992.

15.   Zhang C, Grass ME, McDaniel AH, et al. Measuring fundamental properties in operating solid oxide electrochemical cells by using in situ X-ray photoelectron spectroscopy. Nature materials 2010;9:944.

16.   Yu L, Xi J. CeO2 nanoparticles improved Pt-based catalysts for direct alcohol fuel cells. International Journal of Hydrogen Energy 2012;37:15938-47.

17.   Markovic NM, Gasteiger HA, Ross PN. Oxygen Reduction on Platinum Low-Index Single-Crystal Surfaces in Sulfuric Acid Solution: Rotating Ring-Pt(hkl) Disk Studies. The Journal of Physical Chemistry 1995;99:3411-5.

18.   Attard GA, Gillies JE, Harris CA, et al. Electrochemical evaluation of the morphology and enantioselectivity of Pt/graphite. Applied Catalysis A: General 2001;222:393-405.

19.   Gómez R, Clavilier J. Electrochemical behaviour of platinum surfaces containing (110) sites and the problem of the third oxidation peak. Journal of Electroanalytical Chemistry 1993;354:189-208.

20.   Moghaddam RB, Pickup PG. Support effects on the oxidation of ethanol at Pt nanoparticles. Electrochimica Acta 2012;65:210-5.

21.   Perez J, Paganin VA, Antolini E. Particle size effect for ethanol electro-oxidation on Pt/C catalysts in half-cell and in a single direct ethanol fuel cell. Journal of Electroanalytical Chemistry 2011;654:108-15.

22.   Corradini PG, Santos NA, Silva GC, Perez J. Pt–rare earth catalysts for ethanol electrooxidation: modification of polyol synthesis. Journal of Solid State Electrochemistry 2016;20:2581-7.

23.   Anderson JM, Patel J, Karakoti AS, Greeneltch N, Díaz DJ, Seal S. Aging effects of nanoscale ceria in ceria–platinum composite electrodes for direct alcohol electro-oxidation. Electrochimica Acta 2011;56:2541-5.

24.   De Souza RFB, Flausino AEA, Rascio DC, et al. Ethanol oxidation reaction on PtCeO2/C electrocatalysts prepared by the polymeric precursor method. Applied Catalysis B: Environmental 2009;91:516-23.

25.   Díaz D, Greenletch N, Solanki A, Karakoti A, Seal S. Novel Nanoscale Ceria–Platinum Composite Electrodes for Direct Alcohol Electro-Oxidation. Catal Lett 2007;119:319-26.

26.   Rigsby MA, Zhou W-P, Lewera A, et al. Experiment and Theory of Fuel Cell Catalysis: Methanol and Formic Acid Decomposition on Nanoparticle Pt/Ru. The Journal of Physical Chemistry C 2008;112:15595-601.

27.   Hammer B, Norskov JK. Electronic factors determining the reactivity Surface Science () 1995;343:211-20.

4. Electro-oxidation of ethanol with Pt and PtCeO$_2$ prepared by the Reduction Method

4.1. Summary

As seen in the previous chapter, the Pechini method is very versatile offering a combination of parameters to play with and allowing the preparation of Pt particles of different sizes. Moreover, it can produce homogeneous composite catalysts with high catalytic activity, and formed by a very small amount of one phase (CeO$_2$) dispersed on a second one (Pt), such as Pt-CeO$_2$ 1wt%. However, the control over the size of Pt NP is limited by the heating process, which sinters the nanoparticles leading to their growth. Alternatively, a more straightforward method such as a reduction method using NaBH$_4$ can be used to obtain Pt NPs in the range of 2-3 nm, which is the optimum Pt particle size for the ethanol oxidation[1]. The chemical reduction method is a low temperature technique allowing the production of large amounts of nanoparticles, with relatively narrow size distribution[2]. Moreover, the synthesis of Pt-CeO$_2$ NPs using a second method allowed us to confirm the positive effect found before in Chapter 3 for 1wt% CeO$_2$ on Pt particles of smaller size.

Because in solution techniques, the particles may diffuse, attach to the surface of other particles and grow, we used a stabilizing agent to try to further limit the growth of the nanoparticles. In the present case we used sodium citrate, and the physicochemical and electrotacalytic properties of the Pt and Pt-CeO$_2$ particles are compared with those of pristine citrate-free nanoparticles. For the study of the electrocatalytic properties, the catalysts were characterized by cyclic voltammetry (with and without ethanol) and by chronoamperometry in

the presence of ethanol. The main liquid products oxidation, i.e. acetaldehyde and acetic acid, were subsequently analyzed by ^{H}NMR.

4.2. Physicochemical characterization of the PtCeO$_2$ nanoparticles

Figure 4.1 shows the diffractograms of Pt and Pt-CeO$_2$ samples prepared by the reduction method in the presence and absence of citrates. All diffraction peaks are indexed to a face centered cubic (fcc) phase of platinum (JCPDS#04-0802) with the main peaks at 2θ=39.7 (111), 2θ=46.2 (200), 2θ=67.5 (220), 2θ=81.3 (311) and 2θ=85.7^{o} (222). The lattice parameter calculated using each diffraction angle is practically constant and equal to 3.91 Å for all samples and close to lattice parameter as bulk Pt (3.92 Å)[3]. No diffraction peaks related to the CeO$_2$ phase are observed even for the highest concentration of CeO$_2$ (5 wt%), meaning that probably ceria is amorphous as its temperature of crystallization is around 400-460°C[4,5]. For comparison, the XRD of ceria produced by reduction method (black) at room temperature and crystallized ceria produced by the Pechini method at 400 °C (blue) are shown in appendix A7. Ceria produced by reduction method at room temperature is amorphous and the result is an x-ray scattering curve showing nothing more than one broad maxima (black line) in appendix A7. On the contrary, an imposed temperature treatment at 400 °C leads to a periodical structure arrangement, nucleation and grain growth resulting in a yellow crystalline powder with fcc structure (blue line)[6].

The same amount of sample (15 µL) was used in all cases to compare the samples intensity. Pure platinum synthesized without citrate has the highest peak intensity to hich a more crystalline structure is associated. The addition of ceria decreases the peaks intensity, thus following the order : Pt > PtCeO$_2$-1wt% > PtCeO$_2$-5wt%. In the presence of citrate, a similar

trend was observed: Pt (cit) > PtCeO$_2$-1wt% (cit) > PtCeO$_2$-5wt% (cit). In addition, all the catalysts with citrate show lower peak intensities than those citrate-free. In this sense other authors have already suggested a decrease inintensity associated with some residual stabilizer agent in this case, organic citrate.[7].
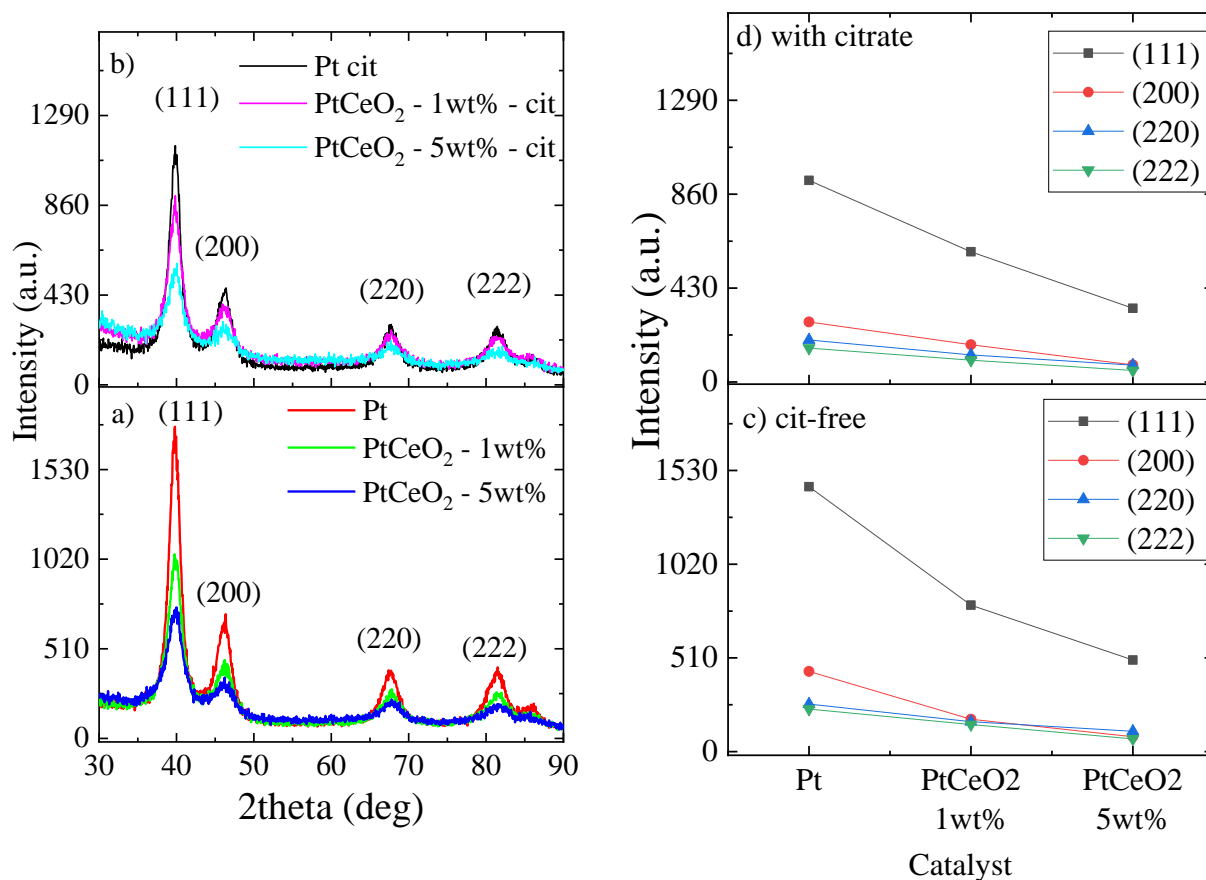
Figure 4. 1 – X-Ray diffractograms of the synthesized Pt-CeO$_2$ catalysts and analysis of the (111) and (220) peaks with no citrate a), c) and with citrate b), d).

The particles' morphology and particle size distribution were assessed by TEM and representative images of the nanoparticles are shown in Figure 4.2. The statistics for particle size

distribution was done from 20 nm scale images having approximately a distribution of 100 particles (Appendix A4). Pure platinum shows a mean particle size of 5.9 ± 1.3 nm which agrees well with the literature value of 5.0 ± 1.3 nm for Pt/C produced by the reduction method[8], whereas the nanocomposites show an average particle size of 3.2 ± 0.6 nm for Pt-CeO$_2$ 1wt% and 3.3 ± 0.7 nm for Pt-CeO$_2$ 5wt%, Figure 4.2 (a), (c) and (e). The nanoparticles prepared in the presence of citrate also showed a decrease in the particle size from 3.7 ± 0.9 nm for pure Pt to 2.3 ± 0.5 nm for PtCeO$_2$ 1wt% and 2.2 ± 0.5 nm for PtCeO$_2$ 5wt%, Figure 4.2 (b), (d) and (f).

As for the Pechini method, these results show that very small amounts of ceria are effective in decreasing the particle size of Pt nanoparticles. Some authors have shown that ceria could also stabilize ionic species of platinum. This has been attributed to the interaction between these two species such as O^{2-}-Ce^{4+}-O^{2-}-Pt^{n+}-O^{2-} with n=2 or 4, which explains the strong ceria and platinum interactions[1].

Overall, the nanoparticles synthesized with citrate are slightly more homogeneous in terms of size distribution (relatively narrower histograms) than those prepared in the absence of citrate. Due to the amorphous character of ceria, one cannot distinguish it from Pt, so we performed EDX analysis on both PtCeO$_2$ (with 1 and 5 wt% of CeO$_2$) to confirm the composition, Figure 4.2 c) and e). Later on, we will show how such changes with respect to the size morphology and structure will influence the catalytic activity.

a) Pt

b) Pt-cit

c) PtCeO$_2$-1wt%

d) PtCeO$_2$-1wt%-cit

e) PtCeO$_2$-5wt%

f) PtCeO$_2$-5wt%-cit

92
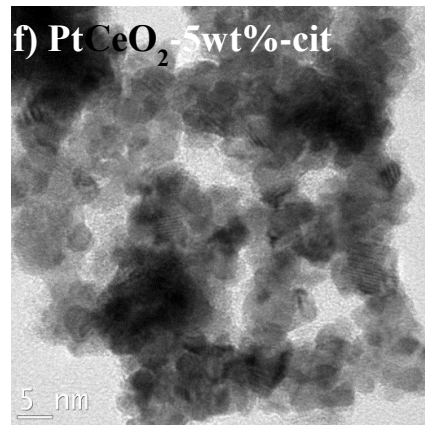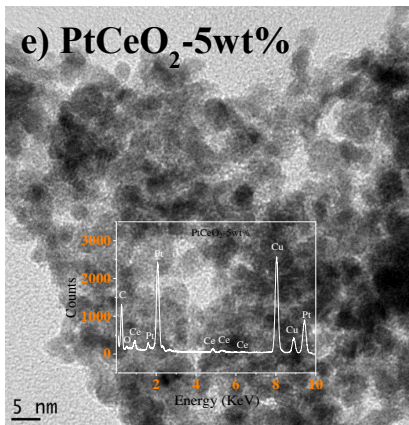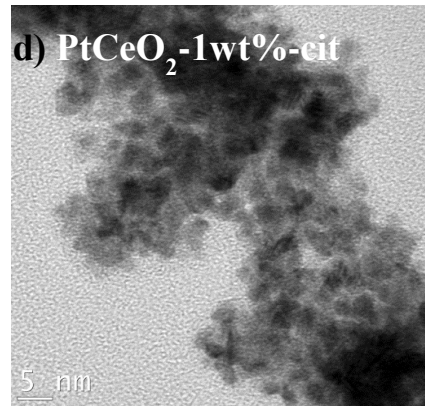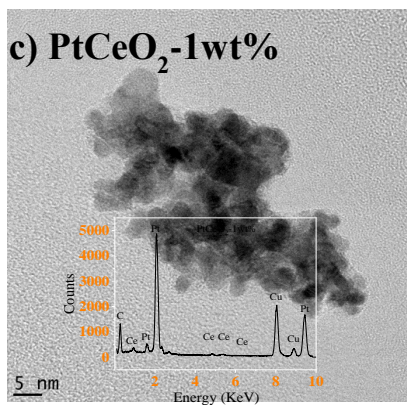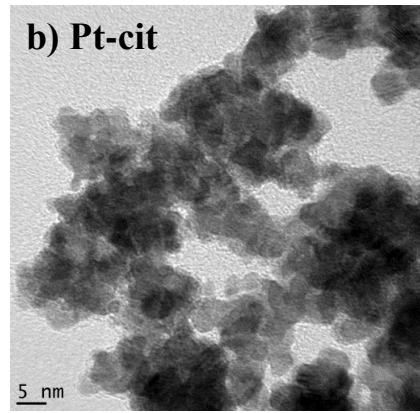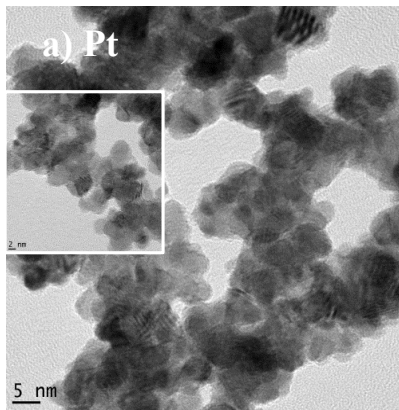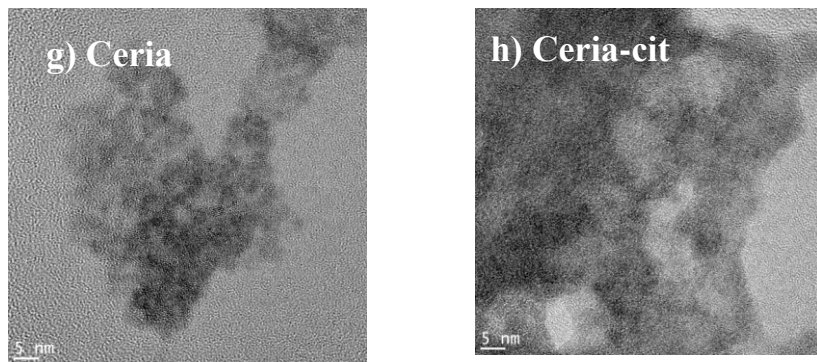
Figure 4. 2 – TEM micrographs of Pt (a, b), Pt-CeO$_2$ 1 wt% (c, d) EDX analysis in inset, Pt-CeO$_2$ 5wt% with EDX analysis in inset (e, f) and (g, h) pure ceria prepared in the absence (left column) and presence (right column) of citrate.
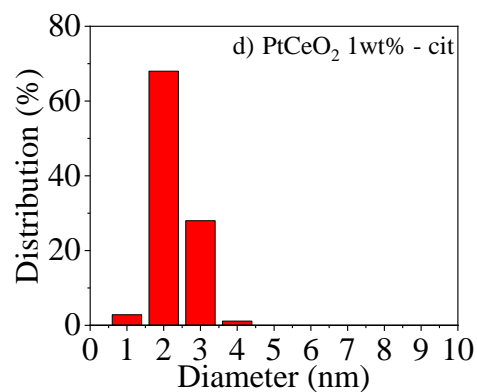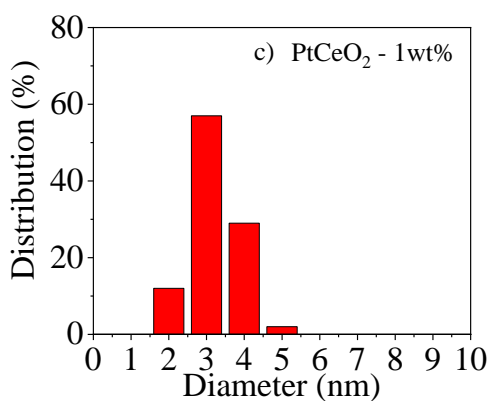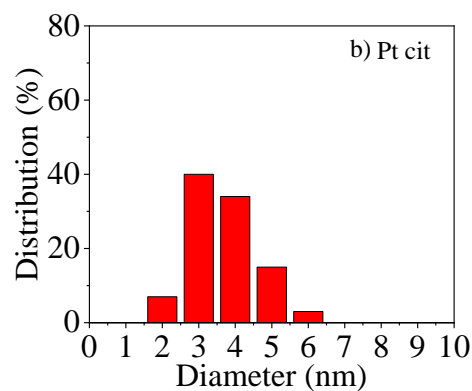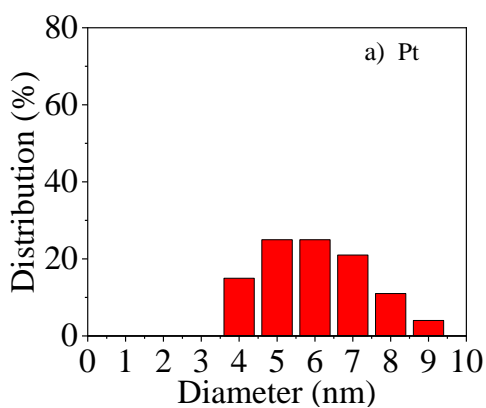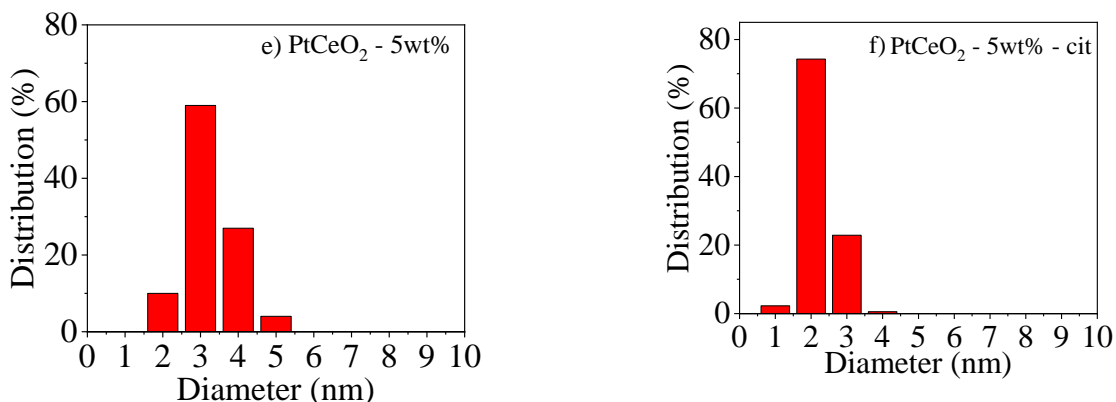
Figure 4. 3 – Statistics for particle size distribution from 20 nm scale images having approximately a distribution of 100 particles for Pt (a, b), Pt-CeO$_2$ 1 wt% (c, d), Pt-CeO$_2$ 5wt% (e, f) prepared in the presence (left column) and absence (right column) of citrates.

Similarly to the previous chapter, all catalysts were analysed by XPS, and Figure 4.4, shows the Pt 4f high resolution spectra. The spectra contain two distinct peaks assigned to Pt 4f$_{7/2}$ and Pt4$_{5/2}$, separated by 3.33 eV, (Table A 2.2). Each peak was deconvoluted considering two different oxidation states: Pt (0) and Pt (II). The Pt 4f$_{7/2}$ peak around 71 eV corresponds to zero-valent Pt, while the peaks around 72-73 eV could be assigned to Pt (II) ionized state[9]. The Pt (II) peak areas are slightly higher on catalysts prepared without citrate, but the difference is not significant.

The Pt 4f peaks of the catalysts produced by the reduction method appear at binding energy values 1 eV higher than those observed for Pt 4f peaks of all samples prepared with the Pechini method (see figure 3.5). This could be related with the sample preparation which was different in the two cases. The powders obtained by the Pechini method were put in direct contact with the Cu tape (section 2.5.3). In the present case, a small volume of the suspension containing the NPs was drop casted on a glass surace (section 2.5.3). Some residual differential

charge across the glass surface which is an isolating material might have not been compensated in spite of use of a ground connection to conduct the excess of charge.
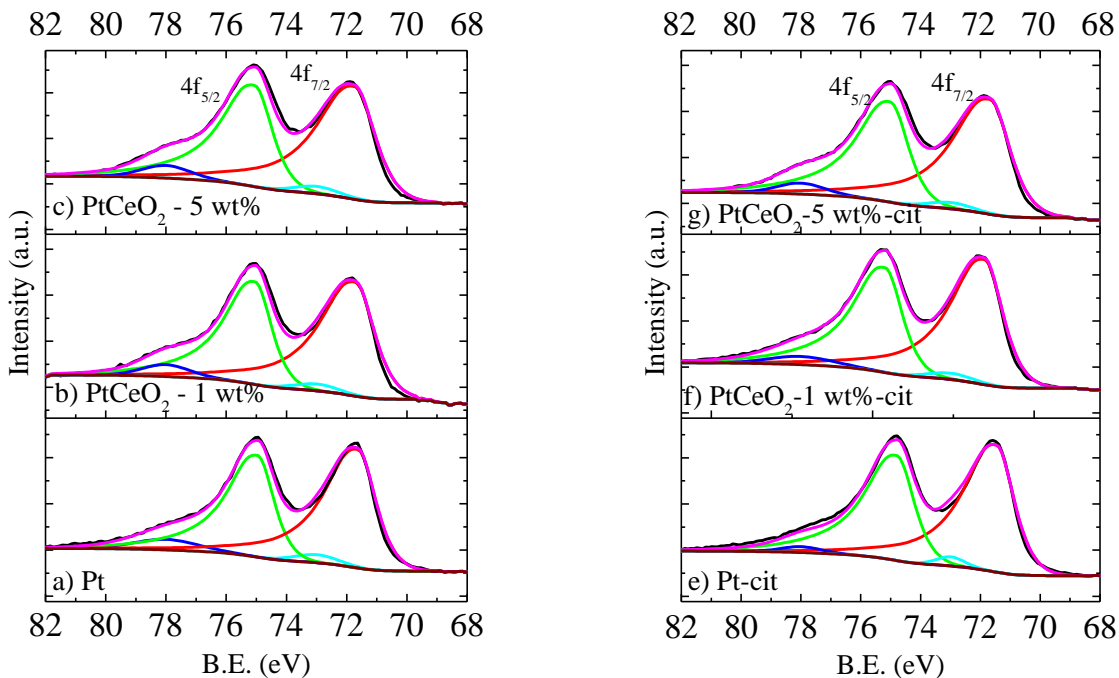
Figure 4. 4 – Core level spectra of Pt 4f for $PtCeO_2$ 1 and 5 wt% in the absence (a, b, c), and in presence of citrate (e, f, g).

It is well known that transition metal nanoparticles exhibit binding energy variations by means of core level shifts because of two main contributions: initial state effect and final state effects[10] as was explained in more detail in section 2.5.2. Briefly, the former contribution is related to the evolution of the chemical and electronic structure of the metal. The latter is related to the screening of the photoemission core hole which depends strongly on the size and shape, and on the nature of the substrate[11]. Thus, to better understand the effect of ceria and of the particle size on the Platinum binding energy core level shifts, these were correlated and the results presented in Figure 4. 5 a)-b).
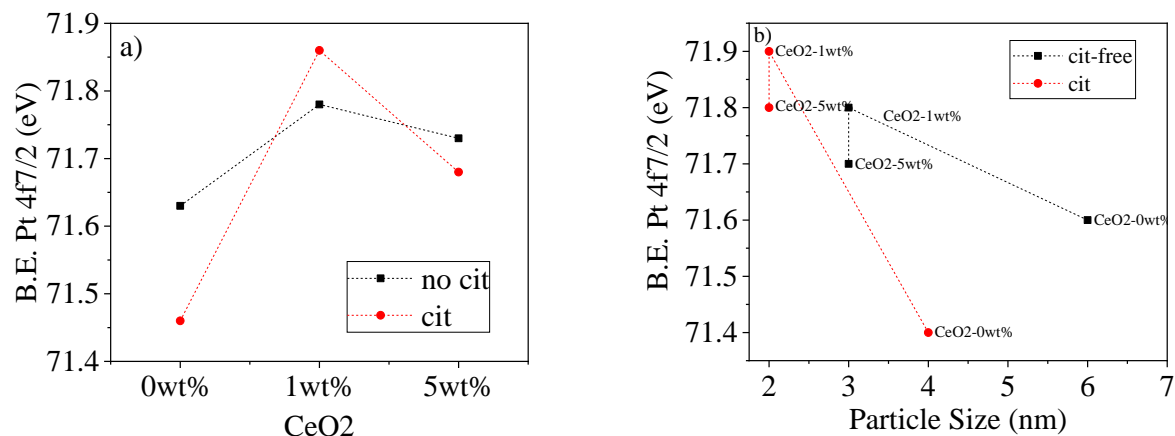
Figure 4. 5 – a) Binding energy (B.E.) of the component (Pt 4f$_{7/2}$) of all catalysts as a function of (a) ceria's amount; (b) Pt's average particle size for the samples with citrate and citrate-free.

The addition of 1 wt% of CeO$_2$ to Pt shifts the Pt4f$_{7/2}$ B.E. to higher values: from 71.6 eV to 71.8 eV for samples prepared with no citrate, and from 71.4 eV to 71.9 eV for the series prepared in the presence of citrate Further addition of 5 wt% CeO$_2$ contributes to the B.E. decrease to 71.7 and 71.8 eV for the samples prepared without and with citrates respectively. It is interesting to note that Pt-CeO$_2$-1wt% presents a maximal value of B.E.. Figure 4.5 a). This was also observed previously with the nanocomposites prepared by the Pechini method (Figure 3.6).

As shown in figure 4.5 b), the B.E. values decrease as the average size of the Pt NPs increases. This inverse relationship between the particle size and the B.E. is even more pronounced when considering the catalysts prepared in the presence of citrates, since these nanoparticles are the smallest of all: from Pt-cit to PtCeO$_2$-1wt%-cit and PtCeO$_2$-5wt%-cit the particle size decreased from 3.6 ±0.9 to 2.3 ± 0.4 nm and 2.2 ± 0.4 nm, but the B.E. increased 0.5 eV and 0.4 eV respectively. It can be concluded that in the case of the catalysts prepared by the

reductor method, the effect of the particle size on the values of the B.E. prevails over a possible electronic effect due to a strong interaction between ceria and Pt as observed for samples prepared by the Pechini method (Figure 3.6: a clear negative B.E. shift with the amount of ceria and decrease of particle size was verified for all catalysts). It is reported that the size effect more notorious for Reduction method, is more pronounced on nanoparticles with diameters below 5 nm which is the case[12]. A detailed comparison of the shifts in the binding energy values and electrocatalytic activity of all catalysts investigated in this thesis is presented at the end of Chapter 5.

The high resolution Ce 3d spectra are shown in Figure 4.6. The spectra of pure CeO_2 prepared under similar conditions are also shown as reference. In spite of the very small amount of ceria in the composites, Figure 4.6 shows well-defined peaks that can be attributed to both Ce (IV) and Ce (III) species.
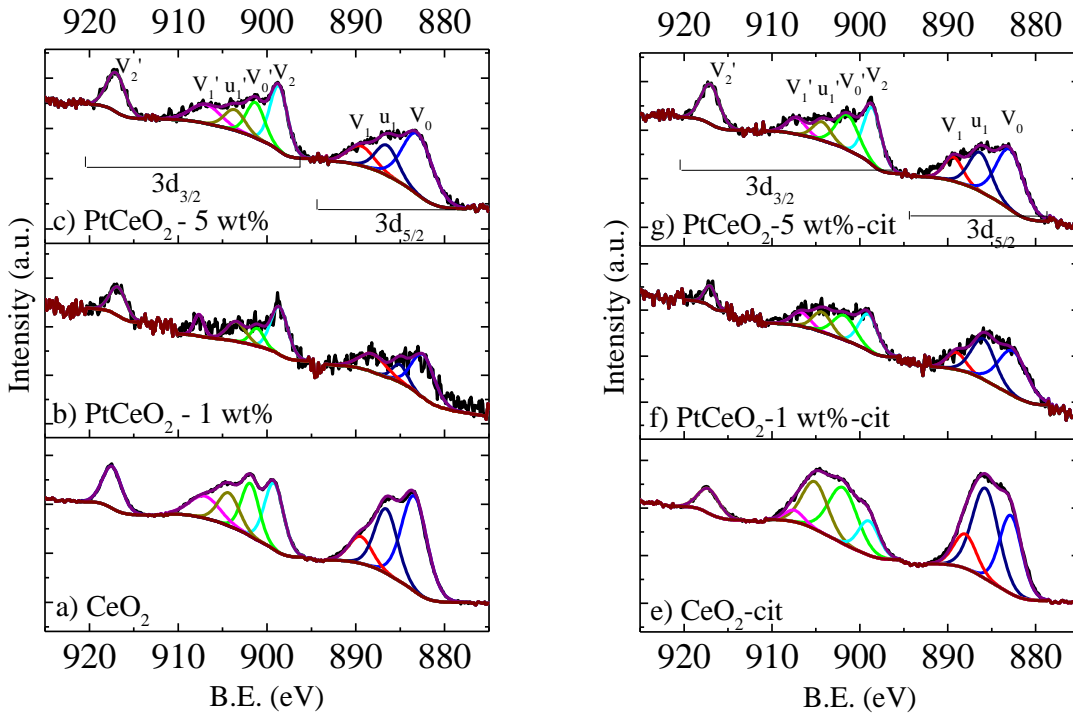
Figure 4. 6 – Ce 3d core level spectra of Pt and PtCeO$_2$ 1 and 5wt% in the absence (a, b, c), and in presence of citrate (e, f, g).

As explained in the previous chapter, the peaks labeled V$_0$ and V$_0$' represent the 3d$_{5/2}$ and 3d$_{3/2}$ ionizations of cerium in the oxidation state (IV). This assignment implies a 3d multiplet splitting (V$_0$, V$_0$') of 18.7 eV. The contribution of Ce (III) is represented by u$_1$ and u$_1$'. The Ce 3d spectrum also shows two additional sets of weaker peaks (V$_1$, V$_1$' and V$_2$, V$_2$'). Comparison between Figure 4.6 a) - c) and d) - f) reveals that the relative intensity of peak u$_1$ with respect to V$_0$ is higher for the series prepared with citrate. This is especially pronounced in the case of CeO$_2$-cit and PtCeO$_2$-1wt%-cit, meaning that these samples have a higher % Ce (III) with respect to CeO$_2$ and Pr-CeO$_2$-1wt%.

Figure 4.8 shows the different information that can be extracted from the Ce 3d XPS data analysis. Firstly, we analyze a) Ce/Pt ratio, b) secondly, the relative peak areas of Ce(III)/Ce(IV),

and finally c) the shift in binding energies of the V_0 main peak of Ce(IV) respectively, Figure 4.7 a) - c).
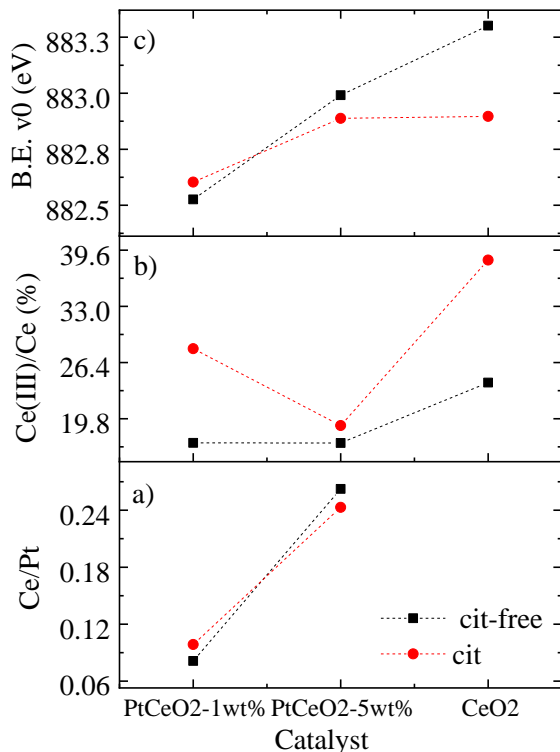
Figure 4. 7 – a) (Ce/Pt) at% ratio b) Ce (III) at % surface ratio c) B.E. of component (v_0) from Ce (IV) $3d_{5/2}$ for the citrate and citrate-free samples.

The Ce/Pt atomic ratio was calculated from the area under the peaks using equation 3.1 presented in Chapter 3. As shown in Figure 4.7 a), the Ce/Pt ratios are larger than the corresponding nominal atomic ratios, that is, above 0.01 and 0.06 for both 1 and 5 wt% CeO_2, respectively. The catalysts with 5 wt % of ceria have a slightly higher Ce/Pt surface ratio than the ones with 1 wt% of ceria although the difference is not very significant. Comparatively the Ce/Pt ratio obtained in Figure 4.7 a) is lower than the obtained for the Pechini method, Figure3.8 a).

The percentage of Ce (III), Figure 4.8 b) can be estimated by XPS data using equation 3.2 from Chapter 3. As shown in Figure 4.8 b), ca. 17% of cerium is present with oxidation state (III), for Pt with 1 and 5 wt% of CeO_2, whereas the % Ce (III) on pure ceria is 24%. For the samples prepared in the presence of citrate, the % Ce (III) decreases from 28 to 19% in the nanocomposites with 1 an 5wt% of ceria and increasing to 38% for pure ceria. In fact, the nanocomposite's % Ce (III) is higher for the reduction method than for Pechini method.

The analysis of the B.E. values of the Ce (IV) $3d_{5/2}$ well-defined peak V_0 centered at around 882.6 eV is shown respectively in Figure 4.8 c). The position of this peak is shifted to higher binding energy values in the composites with respect to pure CeO_2. It is important to remember at this point that an opposite shift is observed for Pechini method, Figure 3.8 c) where a negative shift toward pure ceria was observed and it suggested a strong interaction between Pt and ceria by means of initial state effects. For the reduction method other factors like the smaller size of the nanoparticles, may promote final state effects to those related with initial state effects already observed for Pechini method.

4.3. Electrochemical characterization

Figure 4.9 displays the cyclic voltammograms recorded in 0.5 M H_2SO_4 electrolyte for all prepared catalysts, (a) citrate-free and (b) with citrate. The peaks centered between – 0.1 and – 0.05 V in the forward scan are assigned to hydrogen desorption and they are followed by Pt oxidation between 0.6 and 0.9 V. In the reverse scan, the reduction of PtO_x to Pt occurs between 0.7 and 0.5 V, followed by hydrogen adsorption peaks at around 0.05 and -0.1V from which the catalyst electrochemical surface area can be estimated[13-15]. The Pt-CeO_2 catalysts show lower current than pure Pt, and the current decreases with increasing CeO_2 content; this occurs

regardless of the presence of citrate during the synthesis, and is explained by the increase in the coverage of the surface of Pt NPs as ceria is added. Similar trend was found for the catalysts prepared by the Pechini method.
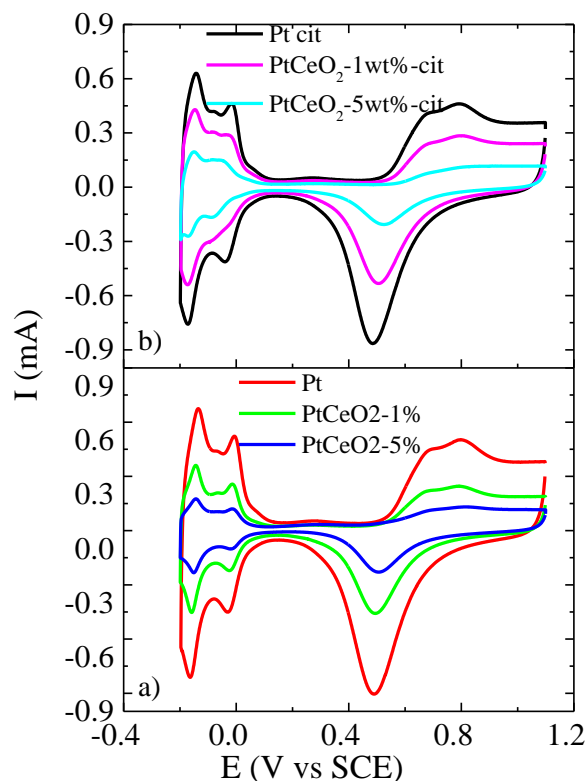
Figure 4. 8 – Cyclic Voltammetry curves for Pt, PtCeO$_2$-1%, PtCeO$_2$-5% prepared (a) without and (b) with citrate.

Thus, pure platinum shows an ESA of 32.9 m^2/g and when ceria is added this value decreases to 17.5 for 1 wt% CeO$_2$ and to 9.1 m^2/g for 5 wt% CeO$_2$. In the presence of citrate, similar trend is observed for which pure Pt shows an ESA of 29.2 m^2/g that decreases to 20.2 and 10.5 m^2/g for the nanocomposites with 1 and 5wt% of ceria, respectively. Thus, no meaningful difference in terms of ESA is observed between the series prepared with and without citrate.

The forward scan for the ethanol oxidation reaction in H_2SO_4 is illustrated in Figure 4.9 (a) without citrate and (b) with citrates. Ethanol starts to adsorb on the surface of the catalysts at around 0.4-0.6 V vs. SCE, and its oxidation to products such as acetaldehyde occurs at around 0.65-0.67 V vs SCE [16]. Acetaldeyhde is an interesting by-product since it can be further oxidized to produce CO_2 or acetic acid.
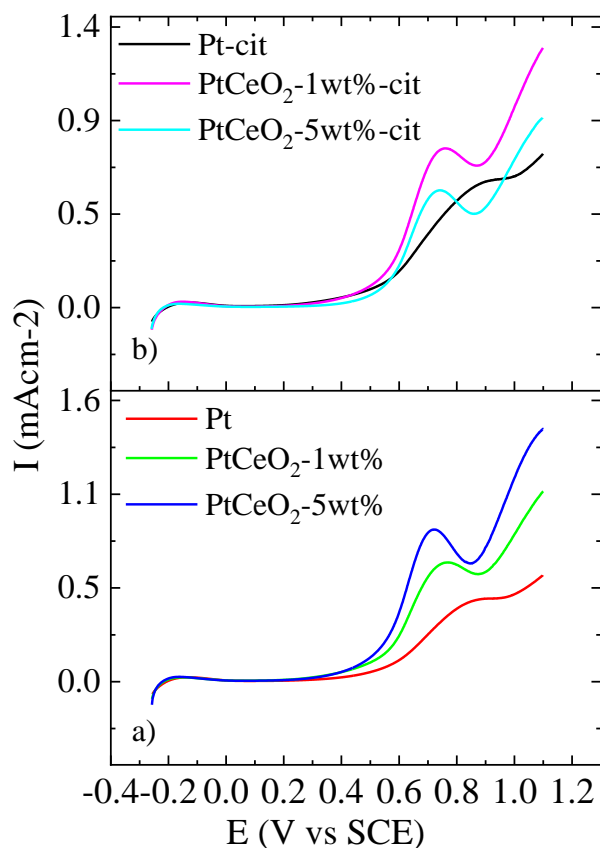
Figure 4. 9 – Forward scans of the currents for all catalysts (a) as prepared without citrate and (b) with citrate in EtOH/H_2SO_4. Full scans are shown in appendix A6.

As can be seen in Figure 4.9 a) the Pt nanocomposites with 1 and 5 wt% of ceria have their peaks for ethanol oxidation shifted from 0.9V (for pure Pt) to 0.76 and to 0.72 V,

respectively. Similar shifts are observed for the catalysts prepared in the presence of citrate: from 0.93V for Pt-cit to 0.75 and 0.73V for PtCeO2 1 wt% cit and 5 wt% cit, respectively. Independently of the presence of citrate, the nanocomposites with 5 wt% of ceria show remarkably lower peak potential for the ethanol oxidation than platinum. This contrasts with the previous chapter (Pechini method) where no major shifts in the peak potential were observed in the nanocomposites.

The positive effect of the addition of CeO_2 to Pt on the ethanol oxidation was confirmed by chronoamperometry at 0.6 V as illustrated in Figures 4.10 a) and b). The current values at the end of 900 s normalized to the electrochemical surface area for the batch synthesized without and with citrate are reported in Figures 4.10 c) and d) respectively.
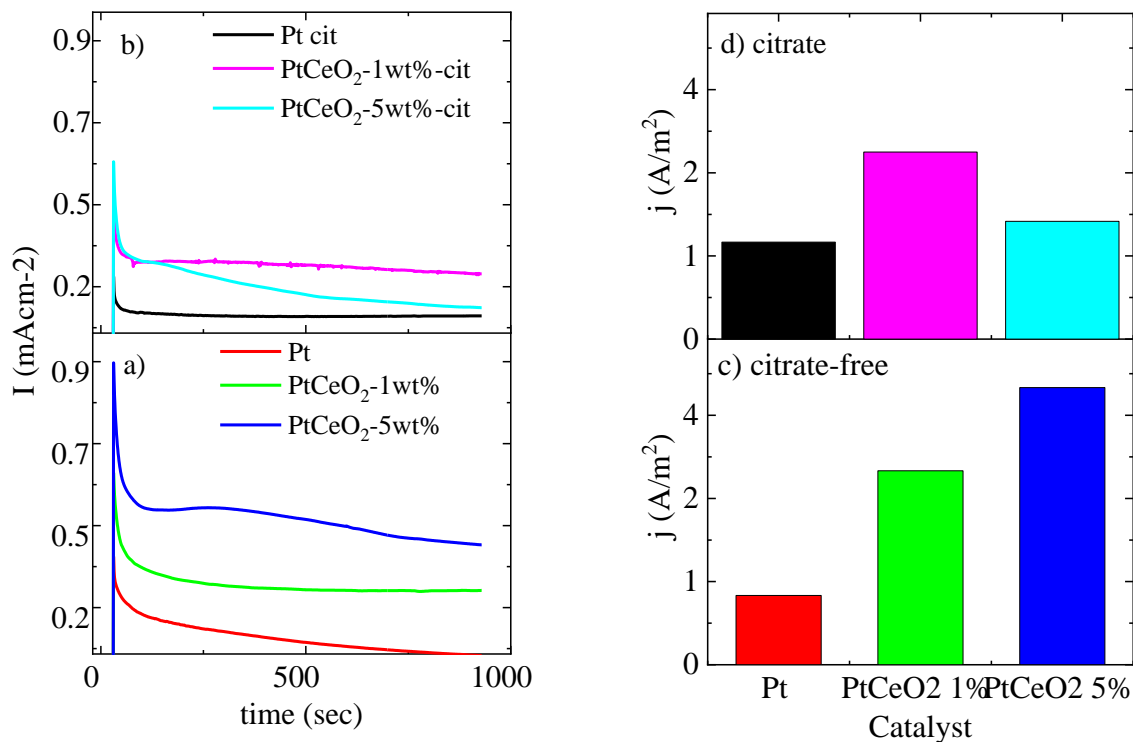
Figure 4. 10 – Chronoamperometric measurements at 0.6 V vs SCE for the catalysts prepared (a) without and (b) with citrates. Current density at 900 s normalized to the ESA for c) citrate-free and d) with citrate batch.

Figure 4.10 a)-b) shows the current vs. time response generated in a chronoamperometric experiment. As 1 wt% of ceria is added to Pt, the current density at 900s increases from 1 to 2.8 Am^{-2} (about 280%), and when 5 wt% of ceria is added it increases from 1 to 4 Am^{-2} (about 400%), Figure 4.10 a) and c). In addition, the current value after 350 s is fairly constant in the case of $PtCeO_2$-1wt% (less for $PtCeO_2$-5wt%) when compared with pure Pt which shows a strong current decay. It can be concluded that the catalysts with ceria have a higher resistance to poisoning than Pt. As 1 wt% of ceria is added to Pt synthesized in the presence of citrate, the current density at 900s increases from 1.4 to 2.7 $mAcm^{-2}$ (about 192 %) and when 5 wt% of ceria is added to Pt, it increases from 1.4 to 1.7 $mAcm^{-2}$ (about 121%), with respect to Pt. In addition, the current value after 230 s starts to slowly decay in the case of $PtCeO_2$-5wt%. Remarkably pure Pt-cit shows a stable current. According to this results few wt% of CeO_2 are sufficient to enhance the electrocatalytic activity of Pt NPs for ethanol oxidation. However, this enhancement is more meaningful on samples containing Pt NPs with a particle size close to 3 nm, i.e. the Pt-CeO_2 1 wt% and 5 wt% prepared in the absence of citrates. Overall the data presented in Figure 4.10 c) and d) may suggest that increasing the amount of CeO_2 from 1 to 5wt% promotes the activity of the Pt NPs, whereas the presence of citrate reduces and stabilizes the Pt particle size specially when considering 1 wt% of ceria. In fact, these NPs exhibit a particle size close to the optimum one for ethanol oxidation[1] (3 nm).

XPS analysis of Pt 4f 7/2, Figure 4.5 a), revealed a positive shift of Pt 4f with increased addition of 1 of ceria and decreasing for further addition of 5wt%. Instead the position of the peak V_0 of the Ce3d spectra shifts to higher BE with the addition of ceria, Figure 4.7 c). The opposite trend was observed for Pechini method showing evidence for initial state effects. Thus it is possible that the Pt to Ceria interaction for the reduction method is not as strong as verified for Pechini method. As discussed above, a particle size effect by means of final state effects may predominate in reduction method. Although it is not clear how small should the particles be in order to produce a particle size effect, it is generally accepted that the physical and electronic properties of transition metal nanoparticles as Pt exhibit strong variations with their size[11,17-19] and here, Pt is almost totalitarian in the catalyst's composition. Thus, as we will see in Chapter 5, the current enhancement verified for the best catalyst, PtCeO$_2$-5wt%, may be related to the modification of the electronic properties in addition to its optimal size.

Similarly to this work, Yang et al.[20] prepared Pt/C catalysts with 10, 20, 30, 35 and 40wt% of CeO$_2$ by reduction method. The author found out that when the mass ratio of CeO$_2$ to Pt/C catalysts was 35%, the catalysts showed the highest catalytic activity for methanol oxidation. The author explains that the positive effect of CeO$_2$ on platinum activity is in that case assigned to bifunctional mechanism, meaning that ceria works as Ru does in Pt-Ru/C catalysts. Thus the author proposes the following mechanism:

$$CeO_2 + H_2O \rightarrow CeO_2-(OH)_{ads} + H^+ + e^-,$$

$$Pt\text{-}CO_{ads} + CeO_2-(OH)_{ads} \rightarrow Pt + CeO_2 + CO_2 + H^+ + e-$$
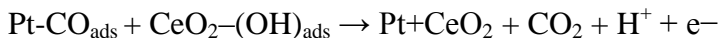
The formation of OH$_{ads}$ species at lower potentials can transform CO-like poisoning (CO$_{ads}$) on Pt to CO$_2$ that evolves away from the solution. Thus, Pt active sites will be available for further electrochemical ethanol oxidation reaction.

It is important to bear in mind that one of the catalysts with highest activity i.e. PtCeO$_2$-1wt%-cit (2.8 A/m^2, Figure4.10 c)) coincide with the catalyst with highest %Ce(III) (25%, Figure4.7b). In this sense, Kopelent reported that the rate of Ce (III) formation during the Ce(III)/Ce(IV) redox cycle is enhanced when Pt–CeO$_2$ is in the vicinity of Pt-CO with oxygen transference from Pt-CeO$_2$ to Pt-CO similar to what is proposed in the bifunctional effect[21,22]. In this sense because the % of Ce (III) is superior for Reduction than for the Pechini method it may suggest that bifunctional method predominates for the first method than for the second one.

4.4. Ethanol oxidation – ^{H}NMR products characterization

The selectivity of each catalyst toward ethanol oxidation to liquid products was evaluated through extended electrolysis for 5h at 0.67 V vs SCE and analysis of the electrolyte by ^{H}NMR. It is well-known that incomplete ethanol oxidation yields to acetaldehyde and acetic acid[23]. The concentration of each of these reaction products is shown in Figure 4.12 together with the current recorded over time. An optimization study was first performed by carrying out electrolysis at several potentials (from 0.6 V to 0.7V) and the optimal potential was established to be 0.67 V (appendix A2).
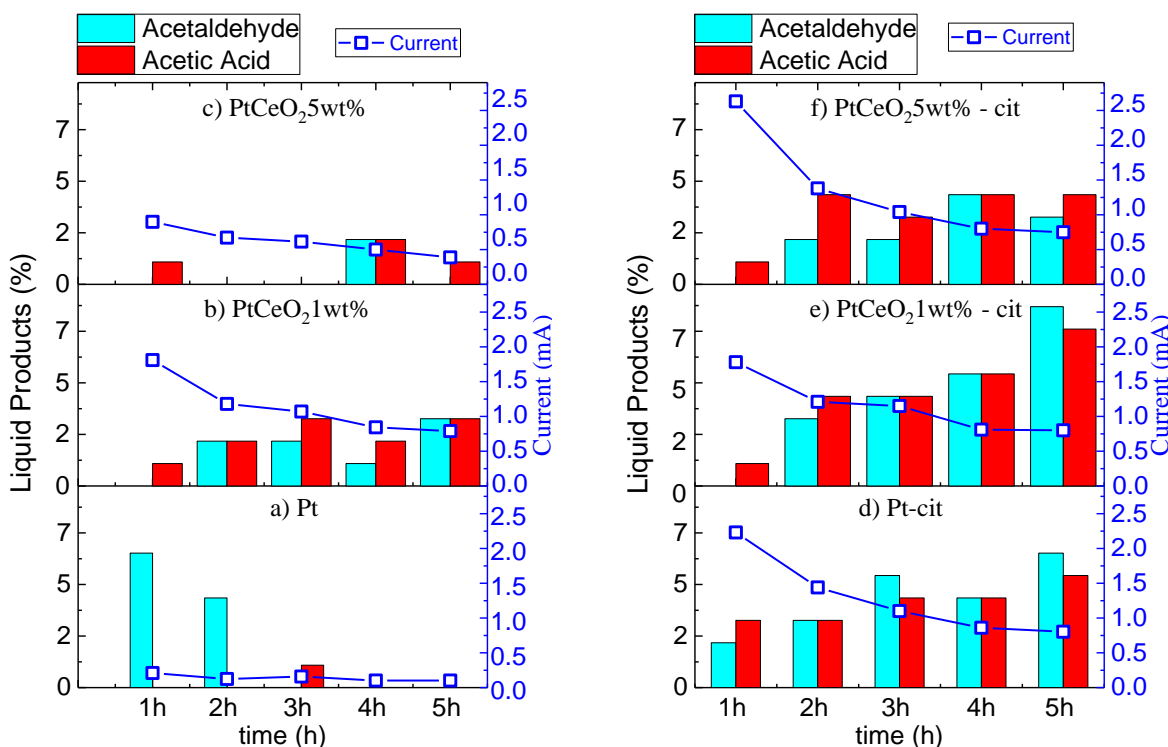
Figure 4. 11 – Ethanol oxidation liquid products by Pt and $PtCeO_2$-1 and 5 wt% prepared in the (a,b,c) absence of citrates and (d,e,f) in the presence of citrates at 0.67V vs SCE.

As can be seen in Figure 4.11 a), pure Pt clearly favors the acetaldehyde production to acetic acid. This could suggest the further oxidation of acetaldeyde to CO_2 since no other products are detected. In fact, the excess of acetaldehyde compared to acetic acid, which is a dead-end product, may probe the presence of a more selective surface catalyst toward oxidation to CO_2 [16]. It has been reported that pure Pt is more selective to CO_2 production than when alloyed to Ru, Sn, Os and Mo with exception of Rh[24]. However, the lack of liquid products after 3h of electrolysis is probably due to the catalyst deactivation as seen in Figure 4.11 a). For $PtCeO_2$-1wt% an increased electrocatalytic activity and a more stable current allowed the detection of acetaldehyde and acetic acid continuously through the electrolysis. The trend is less clear for $PtCeO_2$-5wt% that showed an inferior activity and stability compared to $PtCeO_2$-1wt%. The

catalysts, Pt-cit, $PtCeO_2$-1wt%-cit and $PtCeO_2$-5wt%-cit show an increased amount of liquid products with time. This culminated with a maximum of acetaldehyde and acetic acid at the end of 5h electrolysis for $PtCeO_2$-1wt%-cit.

In general terms, comparing Figure 4.11 (a-c) with 4.11 (d-f), it is clear that the particles prepared with citrate result in reaction mixtures with more liquid products. This clearly results from the more stable currents recorded with these catalysts compared to those obtained with the catalysts prepared in the absence of citrate. A relevant difference between Pt and Pt-cit particle sizes, (6±1 nm) and (4±1 nm) respectively, seems to explain these results. Because smaller NPs are known for their increased reactivity, more products are expected for Pt-cit than for Pt. De souza et al. synthesized by Pechini method PtSnCe/C catalysts for ethanol oxidation in acid medium. For the catalyst with the best catalytic activity (current density= 17 mAmg^{-1}) which had a 68:22:10 ratio composition (10wt% of Ce) and a particle size of 3.7 nm, the only detected products were acid acetic and CO_2[25]. Interestingly the author also compared this catalyst with the parent PtSn concluding that the presence of cerium was necessary to activate the catalyst and to convert ethanol preferably to acetic acid in the fuel cell. The author concludes that 10 wt.% Ce caused a significant increase in the amount of CO_2 that is produced and whose signals coincide with a high level of acetaldehyde production. This result again suggests that acetaldehyde can be converted into CO_2. However, these results were attained at potentials (0.8 V RHE) higher than the ones corresponding to the range of maximum power density for a fuel cell (0.5 V vs RHE). Table 1 from Chapter 1, shows some of the most representative publications on the ethanol oxidation yields by means of CO_2, acetic acid (AA) and acetaldehyde (AAL) in acidic medium. It is clear that there is no consensus on the reported product analysis and some are even conflicting. While Arico et al.[26] have reported a 96% conversion of ethanol to CO_2 for a DEFC

(145 °C) for a Pt anode, Rousseau et al.[27] reported 20%, 7.7% and 9.8% yields of CO_2, for Pt/C, PtSn/C and PtSnRu/C respectively on DEFC at 80 °C. Thus acetic acid and acetaldehyde are the two major reaction products for most of the Pt based catalysts (Table 1 from Chapter 1). Interestingly in a fuel cell study in alkaline medium, at 60 ºC, 0.1 M ethanol and with a Pt anode, the CO_2 production was estimated to be around 55%; in acid medium, under similar conditions and using the same anode catalyst, it is only 2%[28,29]. This indicate that the C-C bond scission rates are much higher in alkaline than in acid medium and with a different mechanism of ethanol oxidation.

From both batches produced by Reduction method, $PtCeO_2$-1wt%-cit and $PtCeO_2$-5wt% showed the highest currents, Figure 4.10 c)-d). This means that the ethanol oxidation reaction was more efficient for these catalysts. Most of the literature reviews agree that liquid products as acetaldehyde and acetic acid are the major products of ethanol oxidation compared to CO_2. However it is well-known that acetaldehyde is able to be further oxidized to CO_2 but acetic acid is not. It is interesting that the best catalyst i.e. $PtCeO_2$-5wt% produced only a small amount of acetic acid followed by $PtCeO_2$-1wt%-cit that showed the highest amounts acetaldehyde and acetic acid. This suggests that two different mechanisms were involved on the ethanol oxidation for both series. Hence, for the series without citrate, $PtCeO_2$-5wt% which possess the best current density (Figure 4.10), seems to participate in the ethanol oxidation reaction via-acetaldehyde that was consumed in the process. It is remarkable the particle size of this catalyst (3 nm) is reported as the ideal size for ethanol oxidation (section 1.5).

We have correlated the amount of Ce (III) on the surface of the catalysts obtained by XPS (Figure 4.7 b), with the amount of liquid products (after 5h electrolysis, Figure 4.12) and we obtain the results presented in Figure 4.12. Before discussing the figure, it should be reminded

that the ESA of Pt in the catalysts decreases with increasing CeO_2 content, and that for each composition the citrate did not have an impact the ESA values (Figure 4.8).
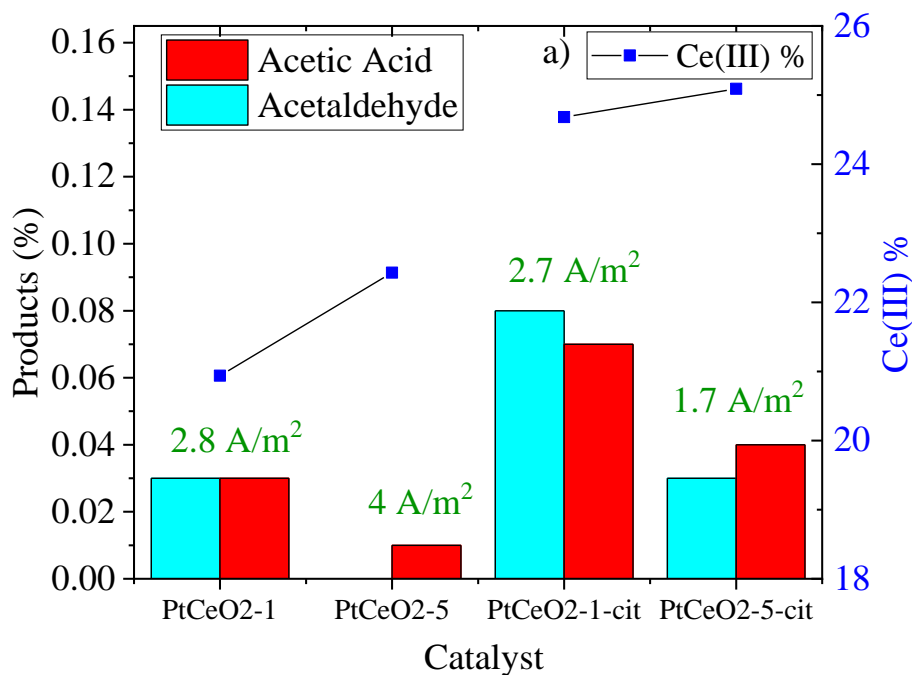
Figure 4. 12 – Selectivity of each nanocomposite catalyst toward ethanol oxidation to liquid products at the end of 5h electrolysis, according to the corresponding Ce(III) %. The corresponding current densities are indicated in green.

The lower current density, the higher values of Ce (III), and the higher amount of liquid products for the citrate stabilized series suggest that Ce (III) favors the acetic acid/acetaldehyde pathways. On the one hand, it is possible that the oxidation of ethanol to acetaldehyde and especially to acetic acid is favored by the presence of oxygen-containing species as ceria. On the other hand, it is well-established that CeO_2 participates in the CO oxidation to CO_2, thus the importance of a higher fraction of Ce (IV) species on the surface of the catalyst[21,22], equation 4.1:

$$Pt\text{-}CO_{ads} + 2\ CeO_2 + 2H^+ + 2e^- \rightarrow Ce_2O_3 + Pt + CO_2 + H_2O \quad (\text{Equation } 4.1)$$

It should be emphasized that in this correlation the amount of Ce (III) estimated by XPS may not correspond to the real surface Ce (III) the electrolysis tests. Distinctly for the catalyst series with no citrate, the lower Ce (III) content may suggest detrimental effect between Pt and Ce (III) and stronger particle size effect.

4.5. Conclusions

Two series of catalysts of $PtCeO_2$ catalysts were prepared by the reduction method, one using citrate as stabilizer and a second one without. A variation of the particle size with the addition of CeO_2 is found for the stabilized series which corresponds to the smallest nanoparticles sizes (2nm). However 3 nm is reported in literature as the ideal particle size for ethanol oxidation which corresponds to $PtCeO_2$-5wt%. In addition, from both series, $PtCeO_2$-5wt% presents the highest current for ethanol oxidation (4 A/m^2 at E= 0.6 V vs SCE) followed by $PtCeO_2$-1wt%-cit with 2.7 A/m^2. The ^{H}NMR analysis of the liquid products obtained from a 5h ethanol oxidation reaction showed different product selectivity for the series with and without citrate. This fact may evidence different mechanisms for ethanol oxidation to $CO_2.$ The series with citrate is associated with a higher amount of Ce (III) and of liquid products than the other one prepared in the absence of citrate. The ^{H}NMR analysis of the liquid products obtained from a 5h ethanol oxidation reaction showed different selectivity: $PtCeO_2$-1wt%-cit produced slightly more acetaldehyde than acetic acid, whereas $PtCeO_2$-5wt% produced only a small amount of acetic acid. As $PtCeO_2$-1wt%-cit revealed a higher amount of Ce (III) and liquid products, it is possible that Ce (III) favors the ethanol oxidation to acetaldehyde and acetic acid.

4.6. References

1.   Perez J, Paganin VA, Antolini E. Particle size effect for ethanol electro-oxidation on Pt/C catalysts in half-cell and in a single direct ethanol fuel cell. Journal of Electroanalytical Chemistry 2011;654:108-15.

2.   Van Rheenen PR, McKelvy MJ, Glaunsinger WS. Synthesis and characterization of small platinum particles formed by the chemical reduction of chloroplatinic acid. Journal of Solid State Chemistry 1987;67:151-69.

3.   Bommersbach P, Chaker M, Mohamedi M, Guay D. Physico-Chemical and Electrochemical Properties of Platinum−Tin Nanoparticles Synthesized by Pulsed Laser Ablation for Ethanol Oxidation. The Journal of Physical Chemistry C 2008;112:14672-81.

4.   Rupp JLM, Scherrer B, Harvey AS, Gauckler LJ. Crystallization and Grain Growth Kinetics for Precipitation-Based Ceramics: A Case Study on Amorphous Ceria Thin Films from Spray Pyrolysis. Advanced Functional Materials 2009;19:2790-9.

5.   Chen Z, Kronawitter CX, Yang X, Yeh Y-w, Yao N, Koel BE. The promoting effect of tetravalent cerium on the oxygen evolution activity of copper oxide catalysts. Physical Chemistry Chemical Physics 2017;19:31545-52.

6.   Cullity BD. Elements of X-Ray Diffraction. 2 ed: Addison-Wesley Publishing Company, Inc.; 1978.

7.   Farrell BP, Sevonkaev IV, Goia DV. Preparation of Dispersed Spherical Platinum Particles with Controlled Size and Internal Structure. Platinum Metals Review 2013;57:160-8.

8.   Moghaddam RB, Pickup PG. Support effects on the oxidation of ethanol at Pt nanoparticles. Electrochimica Acta 2012;65:210-5.

9.   Hüfner S, Wertheim GK. Core-line asymmetries in the x-ray-photoemission spectra of metals. Physical Review B 1975;11:678-83.

10.   Verykios XE, Stein FP, Coughlin RW. Metal-support interaction effects of silver catalysts during ethylene oxidation. Journal of Catalysis 1980;66:147-54.

11.   Henry CR. Surface studies of supported model catalysts. Surface Science Reports 1998;31:231-325.

12.   Claus P, Brückner A, Mohr C, Hofmeister H. Supported Gold Nanoparticles from Quantum Dot to Mesoscopic Size Scale: Effect of Electronic and Structural Properties on Catalytic Hydrogenation of Conjugated Functional Groups. Journal of the American Chemical Society 2000;122:11430-9.

13.   Markovic NM, Gasteiger HA, Ross PN. Oxygen Reduction on Platinum Low-Index Single-Crystal Surfaces in Sulfuric Acid Solution: Rotating Ring-Pt(hkl) Disk Studies. The Journal of Physical Chemistry 1995;99:3411-5.

14.   Attard GA, Gillies JE, Harris CA, et al. Electrochemical evaluation of the morphology and enantioselectivity of Pt/graphite. Applied Catalysis A: General 2001;222:393-405.

15.   Gómez R, Clavilier J. Electrochemical behaviour of platinum surfaces containing (110) sites and the problem of the third oxidation peak. Journal of Electroanalytical Chemistry 1993;354:189-208.

16.   Lai SCS, Kleijn SEF, Öztürk FTZ, et al. Effects of electrolyte pH and composition on the ethanol electro-oxidation reaction. Catalysis Today 2010;154:92-104.

17.   Isaifan RJ, Ntais S, Baranova EA. Particle size effect on catalytic activity of carbon-supported Pt nanoparticles for complete ethylene oxidation. Applied Catalysis A: General 2013;464–465:87-94.

18.   Bagus PS, Nelin CJ, Kay E, Parmigiani F. Reply to the comment by DiCenzo and Wertheim on "core binding energies for clusters···". Journal of Electron Spectroscopy and Related Phenomena 1987;43:C13-C8.

19.   Radnik J, Mohr C, Claus P. On the origin of binding energy shifts of core levels of supported gold nanoparticles and dependence of pretreatment and material synthesis. Physical Chemistry Chemical Physics 2003;5:172-7.

20.   Yang Y, Zhang Z, Hu Z. Activity improvement of Pt/C catalysts by adding CeO2 nanoparticles. Journal of Rare Earths 2011;29:58-63.

21.   Kopelent R, van Bokhoven JA, Szlachetko J, et al. Catalytically Active and Spectator Ce3+ in Ceria-Supported Metal Catalysts. Angewandte Chemie International Edition 2015;54:8728-31.

22.   Artiglia L, Orlando F, Roy K, et al. Introducing Time Resolution to Detect Ce3+ Catalytically Active Sites at the Pt/CeO2 Interface through Ambient Pressure X-ray Photoelectron Spectroscopy. The Journal of Physical Chemistry Letters 2017;8:102-8.

23.   Wang H, Jusys Z, Behm RJ. Ethanol electrooxidation on a carbon-supported Pt catalyst-reaction kinetics and product yields. Journal of Physical chemistry B 2004;108:19413-24.

24.   Ghumman A, Vink C, Yepez O, Pickup PG. Continuous monitoring of CO2 yields from electrochemical oxidation of ethanol: Catalyst, current density and temperature effects. Journal of Power Sources 2008;177:71-6.

25.   De Souza RFB, Parreira LS, Silva JCM, et al. PtSnCe/C electrocatalysts for ethanol oxidation: DEFC and FTIR "in-situ" studies. International Journal of Hydrogen Energy 2011;36:11519-27.

26.   Aricò AS, Cretı̀ P, Antonucci PL, Antonucci V. Comparison of Ethanol and Methanol Oxidation in a Liquid-Feed Solid Polymer Electrolyte Fuel Cell at High Temperature. Electrochemical and Solid-State Letters 1998;1:66-8.

27.   Rousseau S, Coutanceau C, Lamy C, Léger JM. Direct ethanol fuel cell (DEFC): Electrical performances and reaction products distribution under operating conditions with different platinum-based anodes. Journal of Power Sources 2006;158:18-24.

28.   Rao V, Hariyanto, Cremers C, Stimming U. Investigation of the Ethanol Electro-Oxidation in Alkaline Membrane Electrode Assembly by Differential Electrochemical Mass Spectrometry. Fuel Cells 2007;7:417-23.

29.   Fujiwara N, Siroma Z, Yamazaki S-i, Ioroi T, Senoh H, Yasuda K. Direct ethanol fuel cells using an anion exchange membrane. Journal of Power Sources 2008;185:621-6.

5. Comparison of the Pt and Pt-CeO$_2$ catalysts prepared by the reduction and Pechini methods

5.1. Comparison of the two preparation methods

The main objective of this thesis was to verify the effect of the addition of very small amounts of ceria on the electrocatalytic activity of Pt toward ethanol oxidation in acid environment. In order to understand and to compare the effect of ceria on Pt nanoparticles with different sizes, catalysts with the same composition were synthesized by the Pechini and reduction methods. For the first method, Pt NPs with sizes ranging from 4 to 40 nm were obtained, although clustering of the NPs forming large Pt masses could still be spotted in some cases. Nevertheless, most of the small and individual Pt NPs in the Pt-CeO$_2$ samples were well dispersed in a CeO$_2$ matrix. In reduction method, much smaller Pt nanoparticles were always obtained, with sizes varying between 2 and 6 nm. Another major difference between the samples obtained by the two methods is the crystallinity of the Pt and CeO$_2$ phases. While CeO$_2$ is crystalline in Pechini method, for the Reduction method it is amorphous.

On the first part of this chapter we will globally analyze the effect of the Pt particle size and of the addition of ceria on the Pt 4f 7/2 binding energy, and then we will try to attain a more detailed cause-effect analysis. Figure 5.1 shows the shift in the Pt $4f_{7/2}$ of all the catalysts produced in this work as a function of the Pt average particle size.
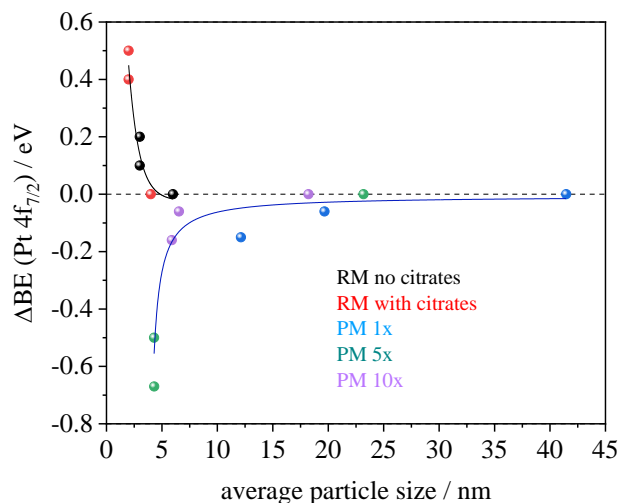
Figure 5. 1 – Shift in the binding energy of Pt $4f_{7/2}$ (ΔB.E.) as a function of the average particles sizes (nm) of the particles produced in this work, using the reduction method (RM) and the Pechinni method (PM)

As shown in the top part of Figure 5.1, for the samples prepared by the reductor method the B.E. values decrease as the average size of the Pt NPs increases. This inverse relationship between the particle size and the B.E. is even more pronounced when considering the catalysts prepared in the presence of citrates, since these nanoparticles are the smallest of all. For instance, from Pt-cit to $PtCeO_2$-1wt%-cit and $PtCeO_2$-5wt%-cit the particle size decreased from 3.6 ±0.9 to 2.3 ± 0.4 nm and 2.2 ± 0.4 nm, and the B.E. increased 0.5 eV and 0.4 eV with respect to pure Pt. However no such inverse relationship is verified for the Pechini method where larger particles with average particle sizes ranging from 40 nm down to 4 nm, were synthesized at high temperature. Thus, distinctly to what was observed for the reduction method, for Pechini method a decrease in the B.E. (negative shift) with decrease of particle size is observed, Figure 5.1 and 3.6.

It is well documented that the smaller the nanoparticles the more significant the influence of the metal relaxation energies, and particle size effects may take place on Pt. Thus, in this work the particle size effects are especially relevant for the citrate stabilized nanoparticles which are the smallest ones produced. Wertheim[1] established a $e^2/2r$ relationship between the binding energy and particle radius of a spherical nanoparticle (e the electric charge) as explained in more detail in section 2.5.2. It is reported that this relaxation is more pronounced on nanoparticles with diameters below 5 nm[2], which is the case for those produced in the reduction method. This fact leaded us not to neglect aspects related to the screening of the photoemission core hole which depends strongly on the particle size, shape or even support[3-5]. Since in this work the nanoparticles are unsupported we can better correlate the observed shifts with the particle size or ceria effects, excluding the carbon or other support effects. It is known that the support can modify the electronic properties (then the reactivity) of the particles and in some cases creating strong metal-support interactions[5].

The remaining question concerning the particle size effect is that there is no sharp discrimination between what is a large and a small nanoparticle. Henry[5] synthesized by vapor deposition method, collections of metal particles with control of the nucleation and growth. In specific the author studied the Pd $3d_{5/2}$ core level shifts as a function of the size (measured by TEM) showing clearly a dependency on the size and cluster shape. The author observed slightly higher binding energies shifts on the Pd $3d_{5/2}$ binding energy, measured by XPS, for Pd clusters as a function of their size (ranged from 1.5 to 3 nm) determined by TEM. The author concluded that the BE decreases when the cluster size increases by means of final state effects. Although it is very difficult to separate the initial from final state effects, the author mentioned that for a

spherical cluster, the final state effect (size effect) can be simply analyzed assuming the Wertheim's equation as explained in more detail in section 2.5.2.

The observed core level binding energy shifts in Figure 5.1, are intrinsically explained by means of initial-state or final-state effects in the field of photoelectron spectroscopy as described in detail in section 2.5.2. Initial state effects due to changes in the electronic structure (changes in the chemical or in the geometric environment) are better depicted in the Figure 5.2 that represents the Pt $4f_{7/2}$ B.E. variation in function of the increased amount of ceria for all catalysts.
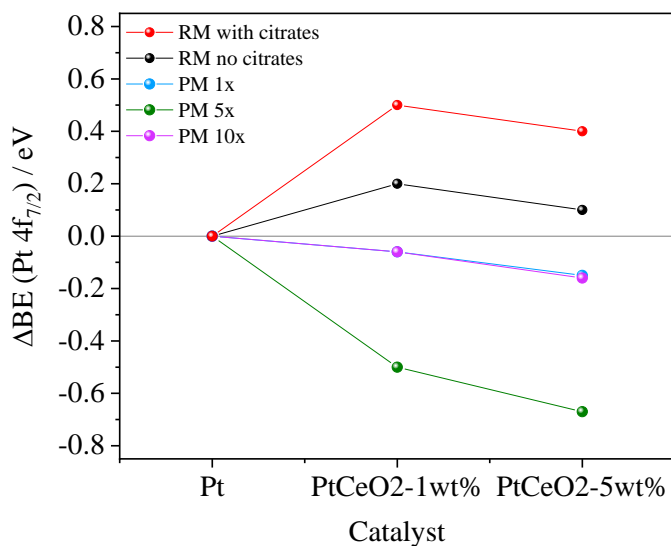
Figure 5. 2 – Shift in the Pt 4f7/2 B.E. as a function of the increased amount of ceria in the Pt nanocomposite catalysts. Catalysts were prepared by the reduction method (RM) and the Pechinni method (PM).

As can be seen in Figure 5.2, for the Pechini method, the addition of very small amounts of CeO_2 to Pt resulted in a negative shift of Pt's binding energy whereas for the Reduction method the opposite trend, i.e. a positive shift, was observed. For the Pechini method, initial state

effects due to changes in the electronic structure (changes in the chemical or in the geometric environment) are observed by the Pt $4f_{7/2}$ negative shifts as ceria is being added to Pt. The lower part of Fig 5.2 shows best this effect. On the contrary final state effects that occur due to screening of the core hole created after photoemission caused by a decrease in the particle size are observed in the upper part of Figure 5.2 (Reduction method). It is interesting that a sharp distinction of the size (Figure 5.1) and ceria effect (Figure 5.2) can be related with the so called final and initial-state effects, respectively. Figure 5.3 shows that these results are not an artifact and that the ceria's B.E. also changes with increased addition to Pt.
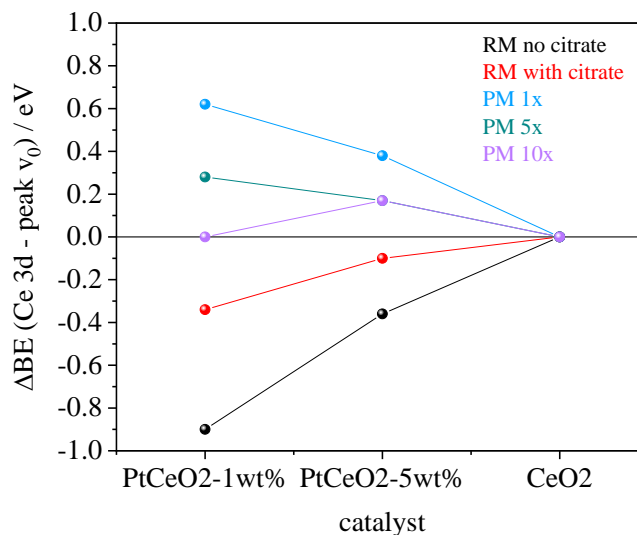
Figure 5. 3 – Shift in the B.E. of Ce 3d main peak (v_0) as a function of increased amount of ceria in the Pt nanocomposite catalysts. Catalysts were prepared by the reduction method (RM) and the Pechinni method (PM).

It can be concluded that in the case of the catalysts prepared by the redutor method, the effect of the particle size on the values of the B.E. prevails over a possible electronic effect. However the samples prepared by the Pechini method, evidence a stronger electronic interaction

between ceria and Pt than a particle size effect. The knowledge of the electronic properties of the catalysts is important to understand and compare their chemical reactivity. According to our results few wt% of CeO_2 are sufficient to enhance the electrocatalytic activity of Pt NPs for ethanol oxidation. However, this enhancement is more meaningful on samples containing in Pt-CeO_2 1 wt%-cit and in Pt-CeO_2-5wt% with current densities of 2.7 Am^{-2} and 4 Am^{-2} respectively. Figure 5.4 describes the influence of the Pt's particle size on the ethanol electro-oxidation in acid medium, with catalysts prepared by reduction method generating substantially higher currents than those obtained by the Pechini method. Thus, the highest currents are reached for the smallest nanoparticles i.e. for Pt-CeO_2 1 wt%-cit (2.3 ± 0.4 nm) and for Pt-CeO_2-5wt% (3.2 ± 0.6) whose size is close to the optimum for ethanol oxidation (3 nm)[6]. This fact is ascribed by Perez et al.[7] as the size that best compromise between structural and electronic effects and/or oxophilicity effects of the Pt surface in order to favor the formation of CO_2, as reported in section 1.5 from Chapter 1. Moreover it is well reported that in the case of very small particles the electronic (initial effects) and size effects (final effects) can be very different relatively to bulk material. Based on these observations, final state effects play the most exponential role on the PtCeO_2 5-wt% produced by reduction method (the best catalyst of this thesis). However for the catalysts prepared by the Pechini method, there is a strong evidence of an electronic effect (by means of initial state effects) between Pt and CeO_2. This is especially relevant for PtCeO_2-1wt% 1× that reached a current value of 1 Am^{-2} with a particle size of 20 nm which resulted in higher electrocatalytic activity, Figure 5.4. Moreover such particles are too large to observe size effects and it is well documented that in the range 10-50 nm no size effects are observable[5].
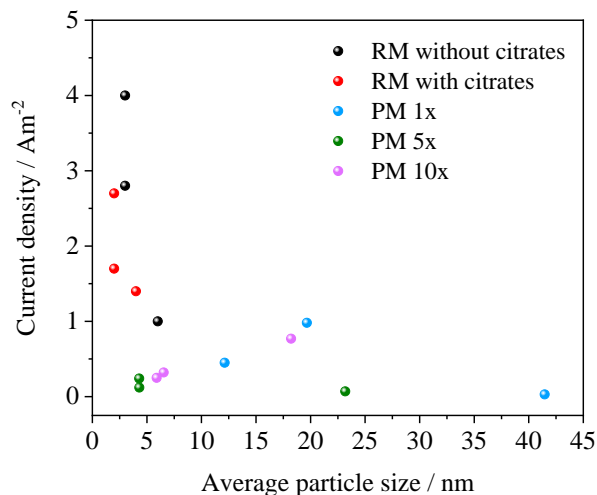
Figure 5. 4 – Current density as a function of the particle size for all catalysts produced in this work showing that for the catalysts prepared by the reduction method (RM) the particle size effect is predominant relatively to those prepared by the Pechini method (PM).

The higher reactivity of $PtCeO_2$-1wt% $1\times$ means that 1 wt% of ceria is enough to weaken the Pt-CO bond. On the basis of initial state effects, the shifts in the core-level B.E. spectra are linked to shifts in the position of the center of the Pt d-band, making it possible to use XPS to observe changes in surface electronic structure of Pt. According to Nørskov's d-band center theory[8], these effects lead to narrowing or widening of the d-band, and a subsequent shift in its center toward or away from the Fermi level (the Fermi level is located at a higher energy level than both valence or core levels) to conserve energy and maintain a constant filling of the d-band. Thus, the negative shifts of the Pt 4f binding energy reflects a downshift shift of the Pt 4f *d*-band center position with respect to the Fermi level[9], which can explain the higher electrocatalytic activity of the Pt-CeO$_2$ 1 wt% catalysts. According to Norskov et al.[8] when the *d*-band center is shifted upwards in energy scale, new antibond states above the Fermi level are formed. As consequence, the adsorbate-metal interaction is stronger as (in the case in the case of

Pt-CO bond) and the electrocatalytic activity related to the catalyst is lower due to higher poisoning of the Pt sites.

5.2. Conclusion

Pt NPs without and modified by CeO_2 (1 and 5 wt% with respect to Pt) and with average Pt particle sizes ranging from 40 nm down to 2 nm, were prepared by the Pechini and by Reduction methods. Their electrocatalytic activity for ethanol electro-oxidation in acid medium was investigated. For the Pechini method, the catalysts with the highest activity were those formed by Pt nanoparticles with average sizes between 10 and 20 nm. In particular, it was found that 1 wt% of CeO_2 can remarkably enhance the activity of 20 nm Pt NPs. This enhancement was explained in terms of a strong electronic interaction between Pt and CeO_2 as shown by XPS analysis. The addition of very small amounts of CeO_2 to Pt resulted in negative shift of Pt's binding energy and a more oxidized CeO_2. This suggests, a weaker interaction between Pt and CO_{ads} – like species and put in evidence the importance of Ce^{4+} ions in the oxidative removal of these poisoning species. For the Reduction method, it was found that 5 wt% of CeO_2 remarkably enhanced the activity of 3 nm Pt NPs. This enhancement was explained in terms of size effect. Contrary to the Pechini method, we observed a positive shift of Pt's binding energy as the particle size becomes smaller. This means that size, or final state effects, played a predominant role over electronic effects in the Reduction method. In the total absence of citrates during the synthesis, the increase in the ceria content is directly related with the increase in the current density.

Overall, the highest electrocatalytic activity for the ethanol oxidation was obtained for $PtCeO_2$-5wt% produced by the reduction method.

123

5.3. Future perspectives

To find the best catalyst for DEFC it is necessary to control its particle size but also its structure and defects. To achieve this goal, it is necessary to integrate electrochemical measurements with physico-chemical characterization studies as XRD, XPS, TEM and other relevant techniques. In particular, performing Rietveld analysis on the XRD data could provide us with additional information on the effect of the addition of CeO_2 on the micro-strain and substitutions/vacancies on the Pt nanoparticles and correlate these effects with the XPS analysis and electrochemical results[10,11]. This work has already started in collaboration with Profs. Ernesto Pereira and Renato Freitas from University of Sao Carlos, Brazil. Moreover, and since there is a lack of information in the literature on the decoupling between the Pt particle size and ceria effects, it would be interesting to synthesize and characterize nanoparticles with other ceria compositions and using other methodologies in order to clearly separate those two effects.

Ethanol can be produced from biomass (by numerous agricultural and municipal wastes) and is a sustainable fuel; 2) it has about two-thirds of the energy density of gasoline and one-quarter of that of pure hydrogen; 3) it is safe and in many countries there is already infrastructure for its distribution which shortens the path for the ethanol direct conversion into energy inside a fuel cell. However, the oxidation of any organic molecule is much more challenging in acid medium than in basic medium due to the slower kinetics. This challenge justified this work and other attempts to find the best catalyst for ethanol oxidation in acid medium. However, since the kinetics of ethanol oxidation is faster in alkaline medium, it is expected an even better performance of synthesized $PtCeO_2$ catalysts at higher pH. Other authors refer that going from acidic to alkaline medium the CO_2 current efficiency may increase from 2 to 55%[12] which increases the potential of DEFC. Previously, we prepared anionic exchange membranes[13,14] to

operate specifically in alkaline medium. One possibility would be to test the performance of a direct ethanol fuel cell composed with these membranes along with the catalysts prepared in this work. These tests would be carried out having in mind that, temperature, performance and the constraints on materials need to be addressed for best power density, durability, cost and for installation/application purposes so that prototype cells based on these materials can be developed.

5.4. References

1.   Bagus PS, Nelin CJ, Kay E, Parmigiani F. Reply to the comment by DiCenzo and Wertheim on "core binding energies for clusters⋯". Journal of Electron Spectroscopy and Related Phenomena 1987;43:C13-C8.

2.   Claus P, Brückner A, Mohr C, Hofmeister H. Supported Gold Nanoparticles from Quantum Dot to Mesoscopic Size Scale: Effect of Electronic and Structural Properties on Catalytic Hydrogenation of Conjugated Functional Groups. Journal of the American Chemical Society 2000;122:11430-9.

3.   Isaifan RJ, Ntais S, Baranova EA. Particle size effect on catalytic activity of carbon-supported Pt nanoparticles for complete ethylene oxidation. Applied Catalysis A: General 2013;464–465:87-94.

4.   Bagus PS, Ilton ES, Nelin CJ. The interpretation of XPS spectra: Insights into materials properties. Surface Science Reports 2013;68:273-304.

5.   Henry CR. Surface studies of supported model catalysts. Surface Science Reports 1998;31:231-325.

6.   Perez JM, Beden B, Hahn F, Aldaz A, Lamy C. "In situ" infrared reflectance spectroscopic study of the early stages of ethanol adsorption at a platinum electrode in acid medium. Journal of Electroanalytical Chemistry and Interfacial Electrochemistry 1989;262:251-61.

7.   Perez J, Paganin VA, Antolini E. Particle size effect for ethanol electro-oxidation on Pt/C catalysts in half-cell and in a single direct ethanol fuel cell. Journal of Electroanalytical Chemistry 2011;654:108-15.

8.   Hammer B, Norskov JK. Electronic factors determining the reactivity Surface Science () 1995;343:211-20.

9.   Rigsby MA, Zhou W-P, Lewera A, et al. Experiment and Theory of Fuel Cell Catalysis: Methanol and Formic Acid Decomposition on Nanoparticle Pt/Ru. The Journal of Physical Chemistry C 2008;112:15595-601.

10.   Jones J, Xiong H, DeLaRiva AT, et al. Thermally stable single-atom platinum-on-ceria catalysts via atom trapping. Science 2016;353:150-4.

11.   Pylypenko S, Peterson EJ, Halevi B, Champagne E, Olson TS, Atanassov P. Hierarchically Structured Pt–Alloy Ethanol Oxidation Electrocatalysts. Electrocatalysis 2012;3:334-45.

12.   Rao V, Hariyanto, Cremers C, Stimming U. Investigation of the Ethanol Electro-Oxidation in Alkaline Membrane Electrode Assembly by Differential Electrochemical Mass Spectrometry. Fuel Cells 2007;7:417-23.

13.   Paulo M, Matos B, Ntais S, Fonseca F, Tavares A. Effect of monobutylether ethylene glycol on Mg/Al layered double hydroxide: a physicochemical and conductivity study. J Nanopart Res 2013;15:1-14.

14.   Paulo MJVR, Tavares A. Novel hydrotalcite composites membranes for alkaline fuel cells. ECS Transactions 2011;35:21-8.

A1. Résumé: Cataliseurs de platine et platine ceria pour l'electro-oxidation de l'ethanol

Avant l'utilisation généralisée des combustibles fossiles, la composition de l'atmosphère en termes de quantité de dioxyde de carbone (CO_2) était équilibrée entre les plantes absorbant le CO_2 et produisant de l'oxygène, et les animaux produisant du CO_2 et absorbant l'oxygène. Mais l'exploitation et la combustion de combustibles fossiles en grandes quantités depuis la révolution industrielle créent un énorme apport de CO_2 dans l'atmosphère. En 2014, la concentration de CO_2 dans l'atmosphère a franchi pour la première fois les 400 ppm (410 ppm) depuis au moins 2,5 millions d'années. La combustion des combustibles est de loin la principale cause du problème, causant 57% des émissions mondiales[1]. En fait, le dioxyde de carbone reste dans l'atmosphère beaucoup plus longtemps que le méthane, les deux gaz à effet de serre les plus connus. Le premier reste dans l'atmosphère une centaine d'années tandis que le second n'y séjourne qu'une douzaine d'années. Par contre le méthane représente un potentiel de réchauffement global (PRG) 25 fois plus puissant que le CO_2[2]. Les conséquences négatives de ces gaz provoquent un effet de serre qui fait augmenter la température de l'atmosphère, au fur et à mesure de l'augmentation des leur niveaux dans l'atmosphère.

Les carburants liquides organiques alternatifs, issus des déchets végétaux et animaux, représentent un potentiel énergétique continuellement reconstitué et renouvelé[3]. Par exemple, les déchets de la biomasse provenant d'activités domestiques, commerciales et industrielles peuvent être convertis en éthanol. Ceux-ci comprennent les déchets solides municipaux (papier, tissu, débris de jardin) et les déchets commerciaux et industriels (papier, matériaux d'emballage,

textiles, bois de démolition). L'éthanol est un hydrocarbure liquide qui peut être distribué via l'infrastructure existante. Il n'est pas toxique et ne nécessite pas de conteneurs de stockage mobiles avancés comme c'est le cas avec le H_2 comprimé. L'utilisation d'éthanol avec ou sans essence réduit les émissions de CO_2. De plus, le CO_2 libéré lorsque l'éthanol est utilisé dans les véhicules peux être recyclé pour produire des cultures de blé qui captent la même quantité de CO_2 [4].

Les piles à combustible sont des dispositifs électrochimiques conçus pour convertir l'énergie chimique d'un carburant en énergie électrique. L'intérêt principal d'étudier la conversion directe de cette énergie porte sur la recherche de nouvelles et meilleures façons de convertir les formes actuelles d'énergie primaire (thermique, radiante, mécanique et chimique) en électricité, tout en améliorant l'efficacité de la conversion.

Les émissions de CO_2 d'une voiture sont proportionnelles à sa consommation de carburant. Les piles à combustible peuvent convertir l'énergie chimique avec moins de pertes. Un schéma d'une pile à combustible à éthanol direct est présenté à la figure A1.1.
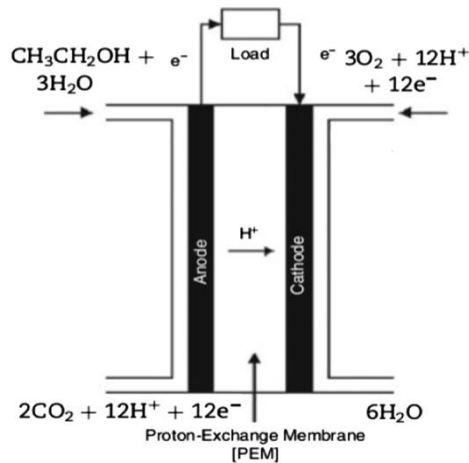
Figure A1. 1 – Pile à combustible éthanol directe (en millieu acide) de Zakaria *et al.* [4]

Les deux demi-réactions et la réaction globale, qui se produisent dans une pile à combustible à éthanol directe (DEFC) en milieu acide (25 ° C), sont présentées dans les équations 1.1 et 1.2. La réaction globale est résumée dans l'équation 1.3.

Anode $\qquad C_2H_5OH + 3H_2O \rightarrow 2CO_2 + 12H^+ + 12e^- \qquad E^0 = 0.084V$ (eq. 1.1)

Cathode $\qquad 2O_2 + 12H^+ + 12e^- \rightarrow 6H_2O \qquad E^0 = 1.23V$ (eq. 1.2)

Globale $\qquad C_2H_5OH + 3O_2 \rightarrow 2CO_2 + 3H_2O \qquad E^0 = 1.146 V$ (eq. 1.3)

Le carburant (éthanol) est oxydé à l'anode produisant 12 H^+ (équation 1.1) qui sont conduits à travers un électrolyte à la cathode. À la suite, les protons réagissent avec l'oxygène et, par conséquent, produisent de l'eau (équation 1.2). Les 12 électrons ainsi libérés lors de l'oxydation de l'éthanol, voyagent à travers un circuit externe vers la cathode en fermant le circuit électrique. La réaction globale pour produire de l'électricité est indiquée à l'équation 1.3. Puisque la tension de la cellule est en théorie de 1,146 V (à 25 °C) , l'éthanol pourrait être entièrement oxydé en CO_2 et en eau[5].

L'oxydation d'alcools et d'autres petites molécules organiques tels que des aldéhydes, des cétones et des acides carboxyliques fait partie des réactions d'oxydation les plus étudiées sur les surfaces de catalyseurs à base de métaux de transition comme le platine (Pt). Le Pt est un bon catalyseur pour plusieurs réactions électrochimiques, non seulement en raison de sa stabilité dans les milieux acide et basique, mais aussi à cause de sa réactivité envers la plupart des réactions d'oxydation et de réduction d'un grand nombre de molécules[6,7]. Cependant, il est bien rapporté que pendant l'oxydation des petites molécules organiques, le CO s'adsorbe de manière irréversible sur la surface du Pt, bloquant les sites actifs dans l'étape finale de la réaction d'oxydation de l'éthanol. Le CO se lie fortement au platine avec le temps jusqu'à une saturation

totale de la surface du catalyseur. Ce phénomène est connu sous le nom d'empoisonnement du platine. En conséquence, la fixation d'une molécule de CO sur le catalyseur réduit la surface disponible pour les réactions d'oxydation. Afin de surmonter ce problème, un second métal est ajouté au platine pour aider à catalyser la réaction d'oxydation. Ce second métal devrait :

a) être capable de former des espèces oxygénées (métal-OH) à des potentiels inférieurs à celui du Pt pur ; ou,

b) affaiblir électroniquement la liaison platine-CO.

Les catalyseurs à base de métaux nobles et d'oxyde de cérium font partie des systèmes connus pour présenter de fortes interactions entre le catalyseur et le co-catalyseur[8]. Parmi les métaux qui peuvent être utilisés, Ru[9] a été largement étudié en raison de la formation de Ru-OH. Un rapport Pt: Ru de 60:40 semble être proche de la composition optimale pour l'oxydation de l'éthanol. La présence de petites quantités de Ru n'a aucun effet sur le courant d'oxydation de l'éthanol. La densité de courant de Ru augmente pour une concentration minimale de 20%.

Le CeO_2 a également été proposé comme co-catalyseur du Pt pour l'oxydation de petites molécules organiques[10]. Quant à eux, De Souza et al.[11] observent deux pics maximaux de la performance catalytique du platine vers l'oxydation de l'éthanol à 25% et à 80% de Ce. Ce comportement est complètement différent de celui observé pour les catalyseurs Pt-Ru.

L'objectif principal de notre travail est d'étudier l'effet de l'addition de très petites quantités de CeO_2 ($\leq$ 5% en poids) sur l'activité électrocatalytique du Pt vers l'oxydation de l'éthanol en milieu acide. Nous chercherons également à mieux comprendre les changements perceptibles dans les propriétés électroniques et structurelles des particules de ces catalyseurs en fonction de leur taille et des énergies de liaison associées. Des nanoparticules de Pt et $PtCeO_2$ avec des quantités de CeO_2 de 1% ou de 5% en poids, ont d'abord été synthétisées par la méthode

du précurseur polymérique (également connue sous le nom de méthode Pechini, une méthode sol-gel). Comme dans la méthode Pechini une étape de calcination peut provoquer la coalescence et l'agrégation des nanoparticules métalliques, la méthode de réduction est aussi explorée comme une alternative pour produire des nanoparticules plus petites. La méthode de réduction étant une technique de basse température, elle minimise l'agrégation des particules et permet la production de grandes quantités de produit, avec une distribution granulométrique relativement étroite[12]. L'effet de la taille des nanoparticules de Pt sur l'électro-oxydation des alcools et de leurs dérivés est bien connu. Par exemple, Arenz et al.[13] ont montré que la vitesse de production du CO_2 dépend fortement de la taille des nanoparticules de Pt avec un ordre de $1 \leq 2 < 5 << 30$ nm. Ainsi, dans ce travail, nous comparons l'activité électrocatalytique des nanoparticules de petite taille obtenues par la méthode de réduction avec celles de plus grande taille synthétisées à haute température comme pour la méthode de Pechini[14]. Finalement, dans ce travail, nous considérons la variation de l'énergie de liaison des électrons du cœur de l'atome dû aux variations de la taille des particules.

A 1.2 Résultats

La figure A1.2 illustre la variation du décalage associé à l'énergie de liaison du Pt 4f $_{7/2}$ pour les composites $Pt-CeO_2$ par rapport à celle des nanoparticules de Pt, en fonction de la taille respective des nanoparticules de Pt pour les deux séries de catalyseurs produits par la méthode de Pechini et par la méthode de Réduction.
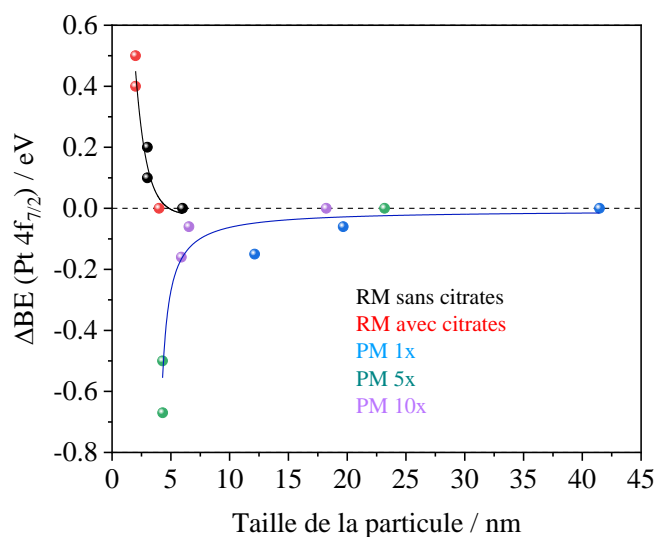
Figure A1.2 – Variation de l'énergie de liaison du pic du Pt $4f_{7/2}$ dans les composites Pt-CeO$_2$ par rapport à celle du Pt pour les catalyseurs préparés par la méthode de Pechini (PM) et par la méthode de réduction (RM).

Pour la méthode de réduction, tous les nanocomposites ont des valeurs d'énergie de liaison Pt $4f_{7/2}$ décalées vers des valeurs plus élevées. Il existe une relation inverse intéressante entre la taille des particules de Pt et l'énergie de liaison. Pour la méthode Pechini, contrairement à la méthode de réduction, le décalage devient plus négatif avec la diminution de la taille de la particule. Un décalage négatif de l'énergie de liaison Pt 4f reflète généralement un décalage vers le bas de la position centrale de la bande *d* du Pt par rapport au niveau de Fermi[15], ce qui peut expliquer l'activité électrocatalytique plus élevée des catalyseurs Pt-CeO$_2$ à 1% en poids. D'après Norskov *et al.*[16], lorsque le centre de la bande *d* est décalé vers des valeurs d'énergies plus hautes, de nouveaux états antiliants au-dessus du niveau de Fermi sont formés. En conséquence,

l'interaction entre le métal et l'adsorbant est plus fort. L'interaction pourrait être une preuve d'un effet électronique entre Pt et Ce.

Par la méthode de réduction quand la taille des particules diminue, l'énergie de liaison augmente, spécialement pour les plus petites particules obtenues dans ce travail, c'est-à-dire une taille de particules d'environ 2 nm. Il est connu qu'un criblage des électrons peut avoir lieu, l'expérience ayant déjà démontré que plus les particules sont petites, plus l'influence du processus de relaxation sera importante[17]. La question restante est qu'il n'y a pas de discrimination nette entre ce qui c'est une grande et une petite nanoparticule. En ce sens, Wertheim[18] établit une relation de type $e^2/2r$ entre l'énergie de liaison et le rayon (r) des particules (e c'est la charge électrique). L'auteur considère qu'un changement d'énergie de liaison de 1 eV ou plus, est fortement lié aux effets de l'état final, mais une question demeure sur la taille de la nanoparticule, pour qu'une telle variation d'énergie de liaison soit produite.

Les variations d'énergie de liaisons observées dans la figure A1.2 sont expliquées de manière intrinsèque en termes d'effets d'état initial ou d'état final dans le domaine de la spectroscopie photoélectronique, comme décrit en détail à la section 2.5.2. Les effets d'état initial sont dus à des modifications de la structure électronique (modifications de l'environnement chimique ou de l'environnement géométrique) et sont mieux décrits à la figure A1.3 a), qui représente la variation de l'énergie de liaison du Pt $4f_{7/2}$ en fonction de la quantité d'oxyde de cerium pour tous les catalyseurs. Il est intéressant d'observer, à la figure A1.3 b), que ces résultats ne sont pas un artefact et que l'énergie de liaison de l'oxyde de cerium change également avec l'ajout de Pt.
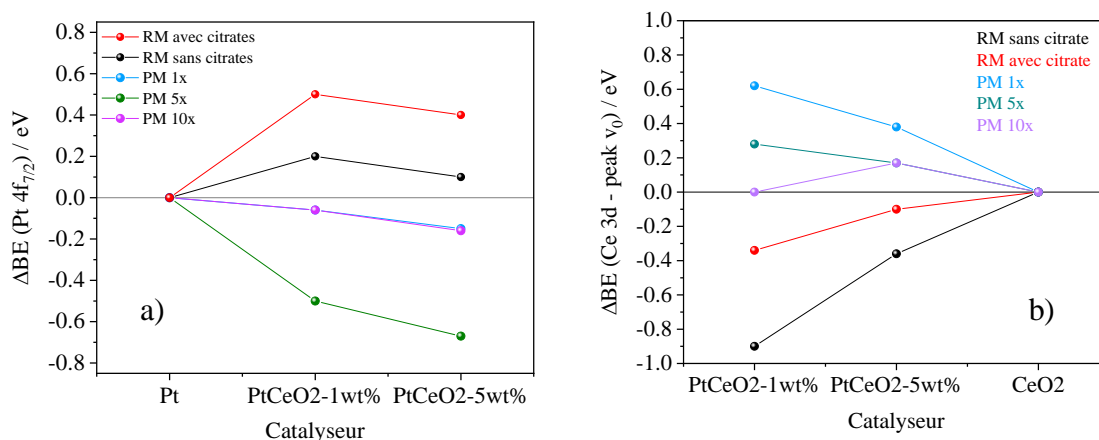
Figure A1.3 – Déplacements de l'Énergie de Liaison (ΔBE) du pic a) Pt $4f_{7/2}$ et b) du pic (v_0) de Ce 3d en fonction de la quantité de CeO_2 dans les nanocomposites de Pt-CeO_2 pour la Méthode de Réduction (RM) et pour la Méthode de Pechini (PM).

On peut en conclure que, dans le cas des catalyseurs préparés par la méthode réducteur, l'effet de la taille des particules sur les valeurs d'énergie de liaison prévaut sur un éventuel effet électronique. Sur la base des effets d'état initiaux, les changements dans les spectres du Pt $4f_{7/2}$ sont liés aux changements de centre de la bande d du Pt, ce qui permet d'utiliser XPS pour observer les changements dans la structure électronique de surface de Pt. Cependant, les échantillons préparés par la méthode de Pechini ont mis en évidence une interaction électronique entre l'oxyde de cérium et le platine plus forte que l'effet de la taille des particules.

La connaissance des propriétés électroniques des catalyseurs est importante pour comprendre et comparer leur réactivité chimique. Selon nos résultats, quelques % en poids de CeO_2 sont suffisants pour améliorer l'activité électrocatalytique des nanoparticules en Pt pour l'oxydation de l'éthanol. Cependant, cette amélioration est plus significative pour les échantillons produits par la méthode de Réduction contenant 1%-cit et 5% en poids de CeO_2 avec des

densités de courant de 2,7 Am^{-2} et 4 Am^{-2} respectivement. Ainsi, les courants les plus élevés sont atteints pour les plus petites nanoparticules, à savoir pour le Pt-CeO$_2$ 1%-cit (2,3 ± 0,4 nm) et pour Pt-CeO$_2$-5% (3,2 ± 0,6), dont la taille est proche de l'optimum pour l'oxydation à l'éthanol (3 nm)[19]. Ce fait est attribué par Perez et al.[20] à la taille qui concilie le mieux les effets structurels et électroniques et / ou les effets d'oxophilicité de la surface du Pt afin de favoriser la formation de CO_2, comme indiqué à la section 1.5 du Chapitre 1. De plus, il est bien connu que, dans le cas de très petites particules, les effets électroniques (effets initiaux) et de taille (effets finaux) peuvent être très différents par rapport au matériau massique. Sur la base de cette observation, les effets d'état final jouent un rôle plus important sur le PtCeO$_2$ 1-wt%-cit produit par la méthode de réduction. Cependant, pour les catalyseurs préparés par la méthode de Pechini, il existe une forte évidence d'un effet électronique (au moyen d'effets d'état initial) entre Pt et CeO$_2$. Ceci est particulièrement pertinent pour PtCeO$_2$-1w% 1 × qui a atteint une valeur actuelle de 1 Am^{-2} avec une taille de particule de 20 nm, ce qui a lui a conféré une activité électrocatalytique élevée, Fig. A1.4. De plus, ces particules sont trop grosses pour observer des effets de taille et il est bien documenté qu'entre 10 à 50 nm aucun effet de taille avec l'énergie de liaison n'est observable[14].
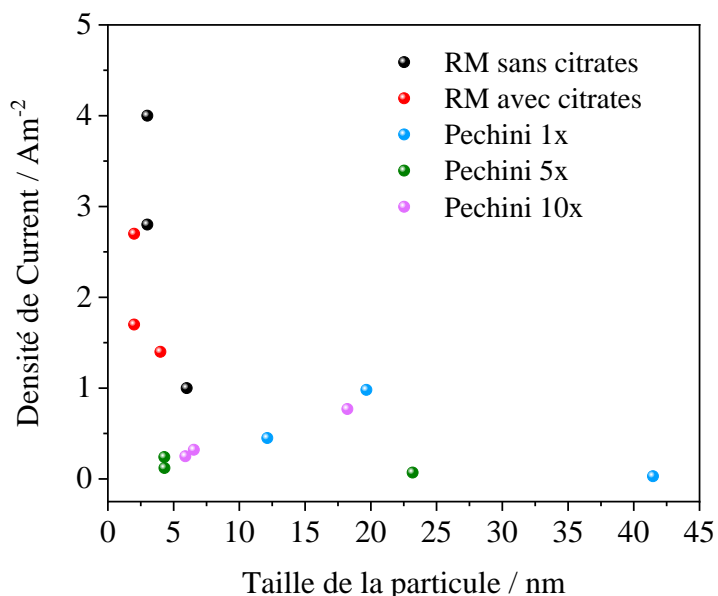
Figure A1.4 – Densité de courant en fonction de la taille des particules produites par la méthode de réduction (RM) et par la méthode de Pechini (PM).

A1.3 Conclusions

Des nanoparticules de Pt sans et avec CeO_2 (1 et 5% en poids par rapport au Pt) et avec des tailles de particules de Pt moyennes allant de 2 nm à 40 nm ont été préparées par la méthode de Pechini et de Réduction. Leur activité électrocatalytique pour l'électro-oxydation à l'éthanol en acide moyen a été étudiée. Pour la méthode de Pechini, il a été constaté que 1% en poids de CeO_2 peut améliorer remarquablement l'activité des NPs de Pt à 20 nm. Cette amélioration est due à une forte interaction électronique entre Pt et CeO_2, comme le montre l'analyse XPS. La réactivité plus élevée de $PtCeO_2$-1% en poids 1 × signifie que 1% en poids d'oxyde de cérium est suffisant pour affaiblir la liaison Pt-CO.

Globalement, l'ajout de très petites quantités de CeO_2 au Pt a entraîné un déplacement négatif de l'énergie de liaison du Pt pour rapport à la méthode de Pechini e positif pour la

137

méthode de Réduction. Par la méthode de Réduction, quand la taille des particules diminue, l'énergie de liaison augmente. Ainsi, les courants les plus élevés de 2.7 et 4 Am^{-2}, sont atteints pour le Pt-CeO$_2$ 1%-cit (2,3 ± 0,4 nm) et pour Pt-CeO$_2$-5% (3,2 ± 0,6), dont la taille est proche de l'optimum pour l'oxydation à l'éthanol (3 nm). Les meilleurs résultats électrochimiques sont obtenus par la méthode de Réduction, ce qui suggère que l'effet de particule semble être plus important au niveau de l'électrocatalyse de l'éthanol par des nanoparticules de platine avec une baisse de pourcentages d'oxyde de cérium.

A1.4 Références

1.   https://350.org/science/.

2.   https://www.futura-sciences.com/planete/questions-reponses/rechauffement-climatique-gaz-effet-serre-co2-methane-pire-565/.

3.   Duff SJB, Murray WD. Bioconversion of forest products industry waste cellulosics to fuel ethanol: A review. Bioresource Technology 1996;55:1-33.

4.   Zakaria Z, Kamarudin SK, Timmiati SN. Membranes for direct ethanol fuel cells: An overview. Applied Energy 2016;163:334-42.

5.   Soloveichik GL. Liquid fuel cells. Beilstein journal of nanotechnology 2014;5:1399.

6.   Lamy C, Belgsir EM. Other direct-alcohol fuel cells. In: Handbook of Fuel Cells: John Wiley & Sons, Ltd; 2010.

7.   Sharma S, Singh P, Hegde MS. Electrocatalysis and redox behavior of Pt2+ ion in CeO2 and Ce0.85Ti0.15O2: XPS evidence of participation of lattice oxygen for high activity. Journal of Solid State Electrochemistry 2011;15:2185-97.

8.   Ostroverkh A, Johánek V, Kúš P, Šedivá R, Matolín V. Efficient Ceria–Platinum Inverse Catalyst for Partial Oxidation of Methanol. Langmuir 2016;32:6297-309.

9.   Watanabe M, Motoo S. Electrocatalysis by ad-atoms. Part III. Enhancement of the oxidation of carbon monoxide on the platinum ruthenium ad-atoms. Electroanalytical Chemistry and Interfacial Electrochemistry 1975;60:275-83.

10.   Trovarelli A. Catalysis by Ceria and Related Materials: Imperial College Press; 2002.

11.   De Souza RFB, Flausino AEA, Rascio DC, et al. Ethanol oxidation reaction on PtCeO2/C electrocatalysts prepared by the polymeric precursor method. Applied Catalysis B: Environmental 2009;91:516-23.

12.   Van Rheenen PR, McKelvy MJ, Glaunsinger WS. Synthesis and characterization of small platinum particles formed by the chemical reduction of chloroplatinic acid. Journal of Solid State Chemistry 1987;67:151-69.

13.   Arenz M, Mayrhofer KJJ, Stamenkovic V, et al. The Effect of the Particle Size on the Kinetics of CO Electrooxidation on High Surface Area Pt Catalysts. Journal of the American Chemical Society 2005;127:6819-29.

14.   Henry CR. Surface studies of supported model catalysts. Surface Science Reports 1998;31:231-325.

15.   Rigsby MA, Zhou W-P, Lewera A, et al. Experiment and Theory of Fuel Cell Catalysis: Methanol and Formic Acid Decomposition on Nanoparticle Pt/Ru. The Journal of Physical Chemistry C 2008;112:15595-601.

16.   Corcoran CJ, Tavassol H, Rigsby MA, Bagus PS, Wieckowski A. Application of XPS to study electrocatalysts for fuel cells. Journal of Power Sources 2010;195:7856-79.

17.   Isaifan RJ, Ntais S, Baranova EA. Particle size effect on catalytic activity of carbon-supported Pt nanoparticles for complete ethylene oxidation. Applied Catalysis A: General 2013;464–465:87-94.

18.   Bagus PS, Nelin CJ, Kay E, Parmigiani F. Reply to the comment by DiCenzo and Wertheim on "core binding energies for clusters···". Journal of Electron Spectroscopy and Related Phenomena 1987;43:C13-C8.

19.   Perez JM, Beden B, Hahn F, Aldaz A, Lamy C. "In situ" infrared reflectance spectroscopic study of the early stages of ethanol adsorption at a platinum electrode in acid medium. Journal of Electroanalytical Chemistry and Interfacial Electrochemistry 1989;262:251-61.

20.   Perez J, Paganin VA, Antolini E. Particle size effect for ethanol electro-oxidation on Pt/C catalysts in half-cell and in a single direct ethanol fuel cell. Journal of Electroanalytical Chemistry 2011;654:108-15.

A2 Appendix – XPS binding energy values for the calculation of Pt4f$_{7/2}$

Table A2.1 – Pt 4f$_{7/2}$ binding energy (B.E.), ΔBE of Pt4f$_{5/2}$ – Pt4f$_{7/2}$ (ΔBE), Intensity ratio of Pt4f$_{7/2}$:Pt4f$_{5/2}$ (I ratio) for the Pechini method.

Catalyst	1x			5x			10x		
	B.E. (eV)	I ratio	ΔBE (eV)	B.E. (eV)	I ratio	ΔBE (eV)	B.E. (eV)	I ratio	ΔBE (eV)
Pt	70.45	1.33	3.33	71.02	1.33	3.33	71.06	1.33	3.33
PtCeO$_2$-1wt%	70.39	1.33	3.33	70.52	1.33	3.33	71	1.33	3.33
PtCeO$_2$-5wt%	70.30	1.33	3.33	70.5	1.33	3.33	70.09	1.33	3.33

Table A2.2 – Pt 4f$_{7/2}$ binding energy (B.E.), ΔBE of Pt4f$_{5/2}$ – Pt4f$_{7/2}$ (ΔBE), Intensity ratio of Pt4f$_{7/2}$:Pt4f$_{5/2}$ (I ratio) for the Reduction method.

Catalyst	Zero citrate			Citrate		
	B.E.(eV)	I ratio	ΔBE (eV)	B.E. (eV)	I ratio	ΔBE (eV)
Pt	71.63	1.27	3.33	71.46	1.25	3.33
PtCeO$_2$-1wt%	71.78	1.27	3.33	71.06	1.27	3.33
PtCeO$_2$-5wt%	71.73	1.27	3.33	71.83	1.27	3.33

A3 Appendix – ^{1}HNMR spectra

A3.1 Optimization of parameters

For the ^{H}NMR analysis of the ethanol oxidation reaction with the catalysts produced by the reduction method, several chronoamperometries with a range of optimization from 0.63 to 0.73V vs SCE were performed. The potential for analysis was chosen corresponding to the highest amount of liquid product formation corresponding to 0.67 V. This potential was determined knowing that the charge (q) flowing through the cell (electricity), is directly proportional to the mass of substance (m) produced at the electrode by the Faraday's law of electrolysis (q = n mol F ; q is the charge (q=Ixt), n mol is the moles of electrons involved in the reaction and F is the Faraday constant=96500 Cmol^{-1}). This means that the catalyst with highest charge (q) will favor the right conditions to produce acetic acid and acetaldehyde with the highest amount.
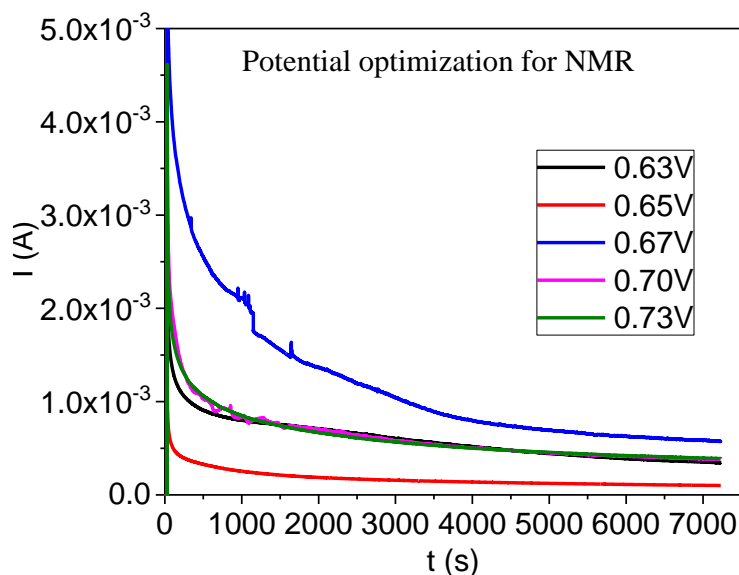
Optimization electrolysis at several potentials from 0.63 to 0.73 V vs SCE being the optimal potential established at 0.67 V. Table A 2.1 shows the potential optimization for best charge or current production for optimal acetaldehyde and acetic acid formation.

Table A3.1 – Measured currents at the end of 7200s for several testing potentials (0.63-0.73) and corresponding charge (Q)

Sample	E (V) vs SCE	t (s)	i (A)	Q= i×t (C)
0	0.6	7200	1.422×10^{-4}	1.024
1	0.63	7200	3.291×10^{-4}	2.370
2	0.65	7200	9.584×10^{-5}	0.690
3	0.67	7200	5.619×10^{-4}	4.045
4	0.70	7200	3.820×10^{-4}	2.750
5	0.73	7200	3.941×10^{-4}	2.837

A3.2 ^{1}HNMR spectra

The following are the [H]NMR spectra for the collected samples (Chapter 4). Analysis was performed with a 600 MHz - NMR– Varian Inova at UQAM, Montreal.
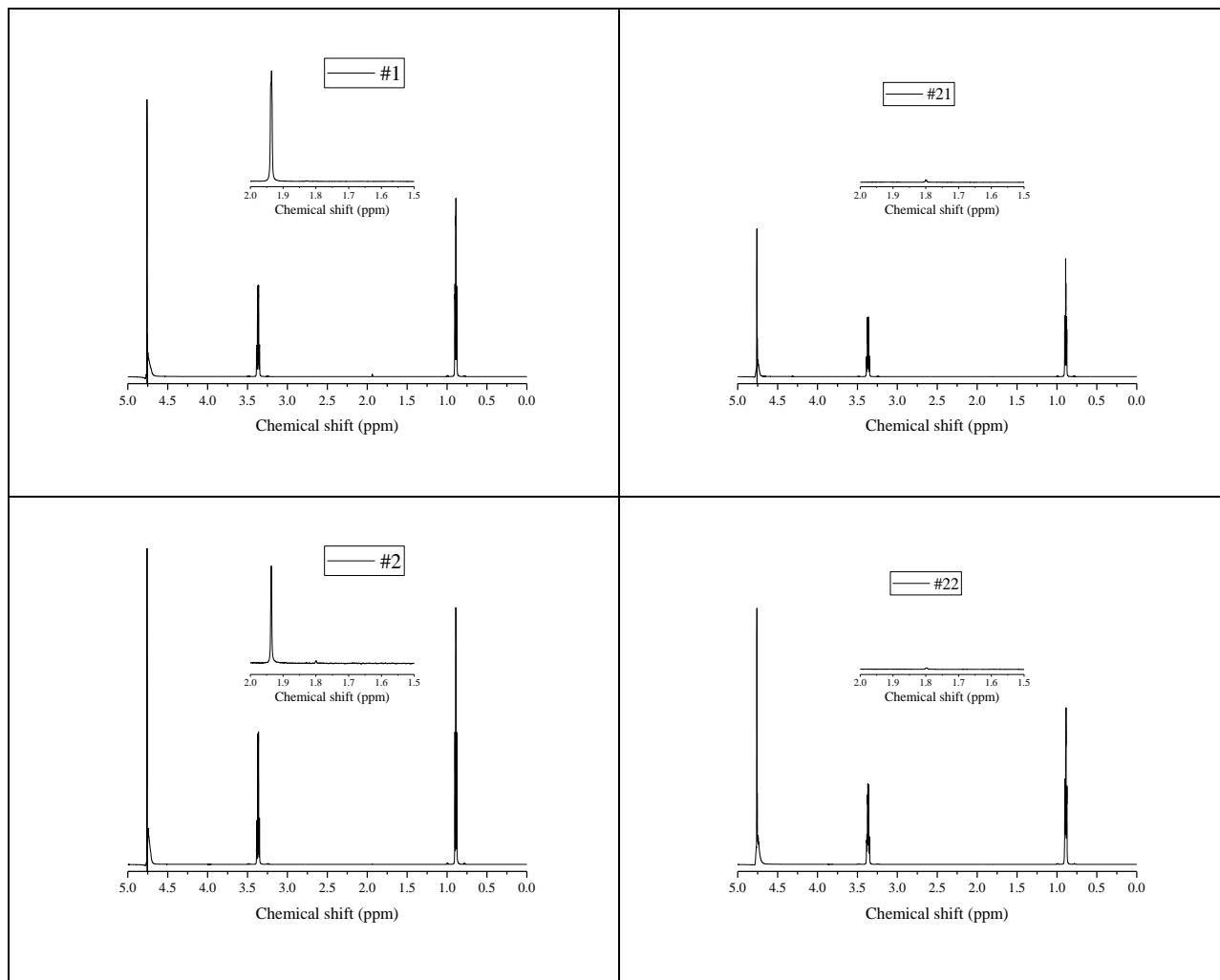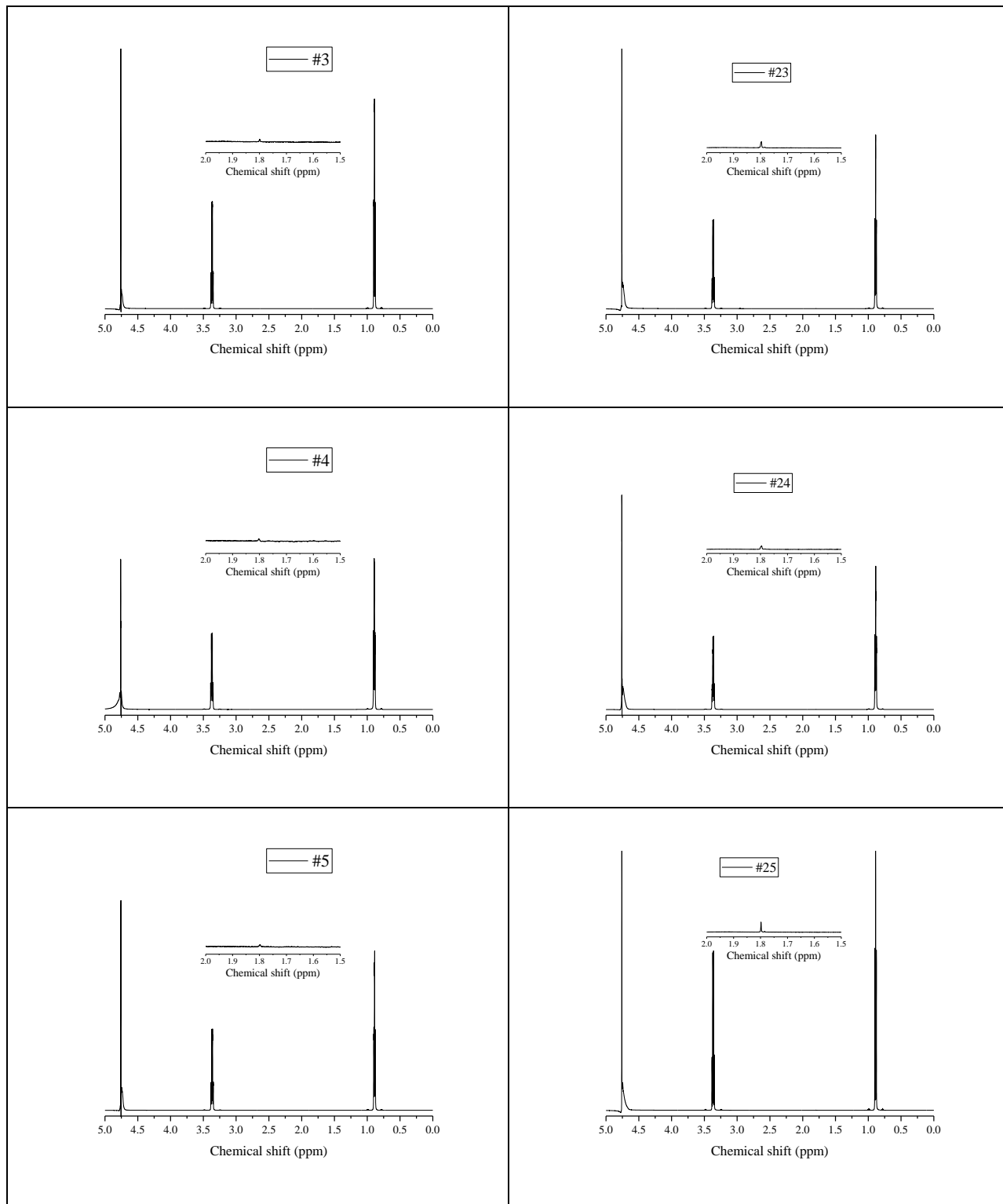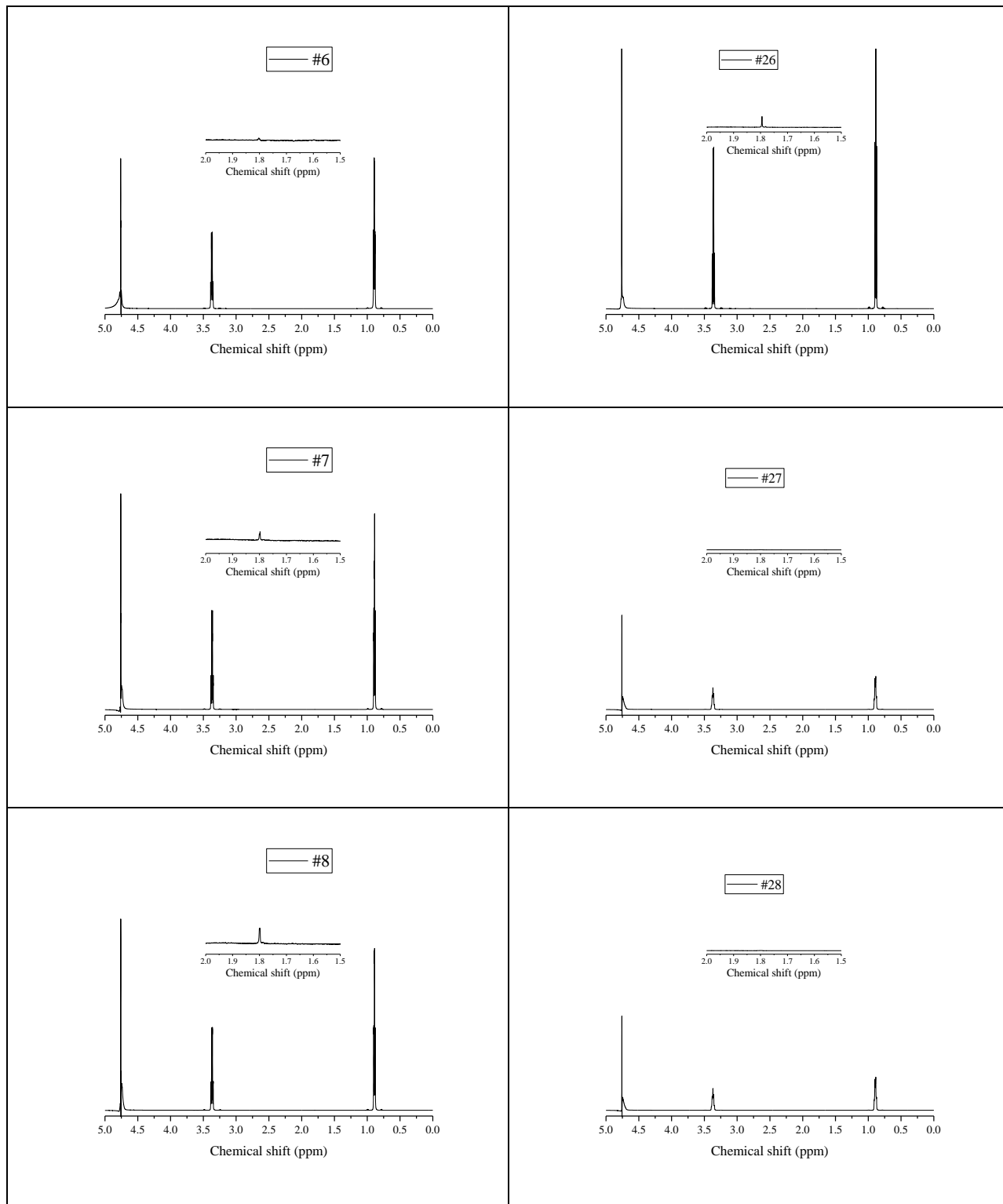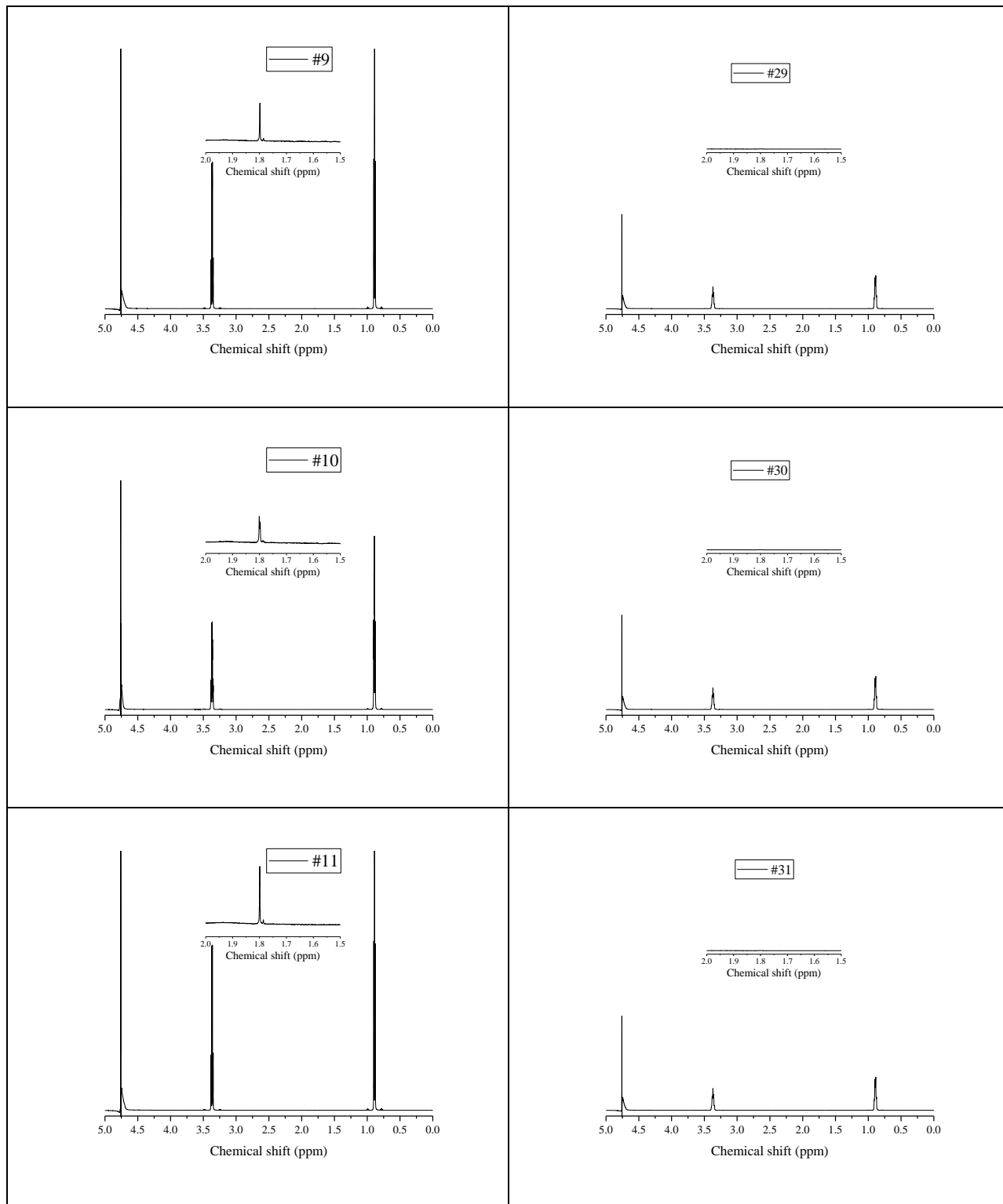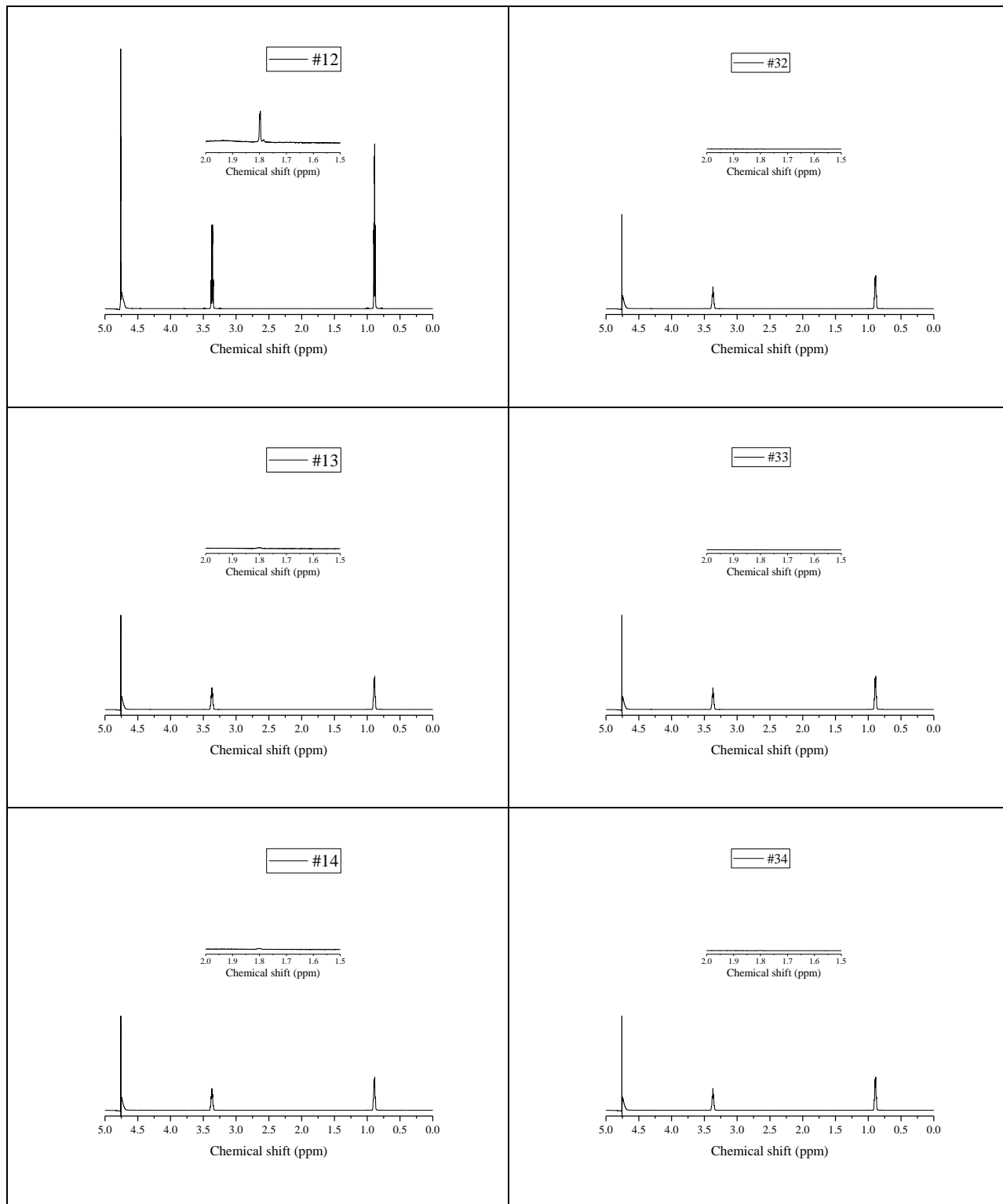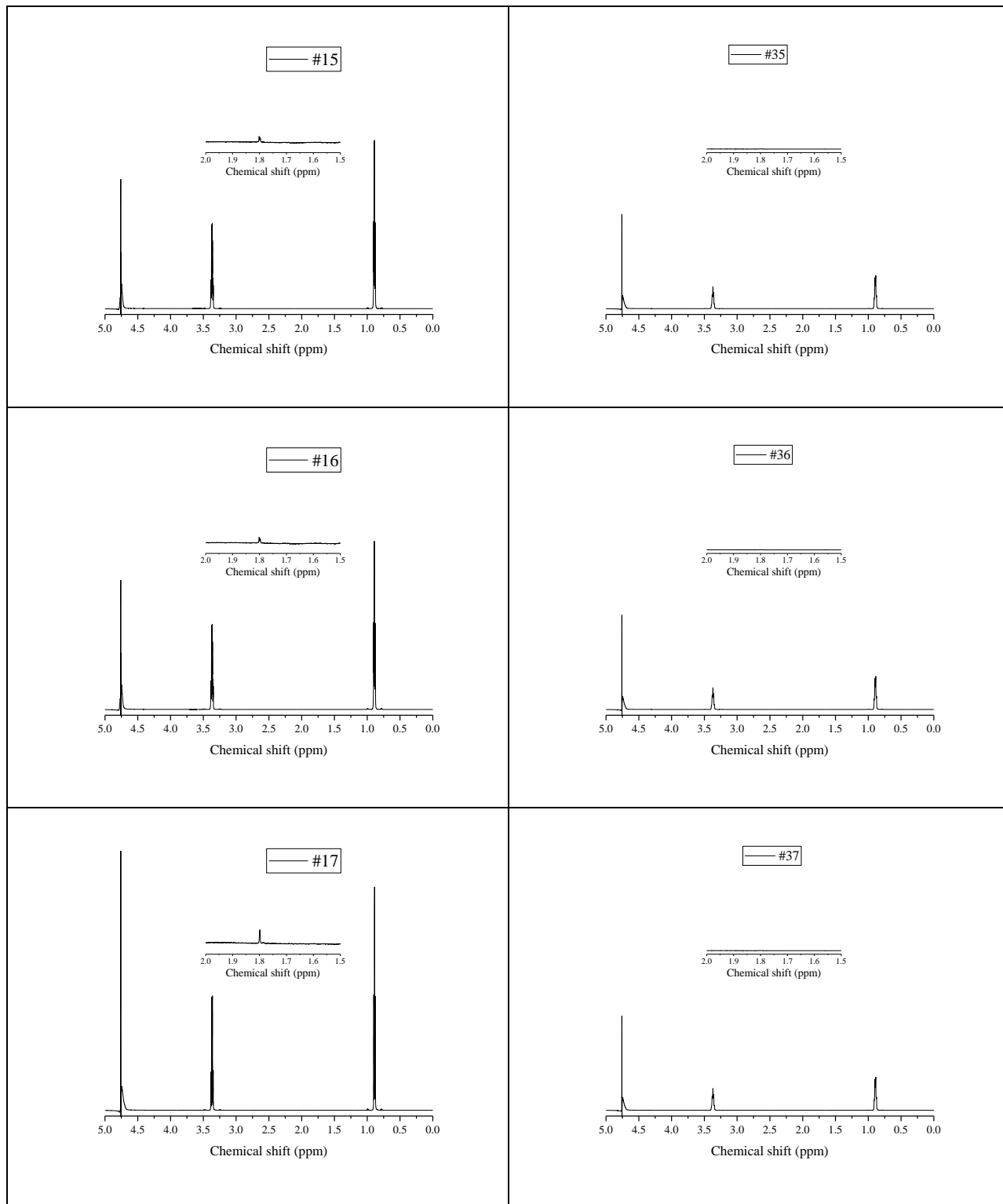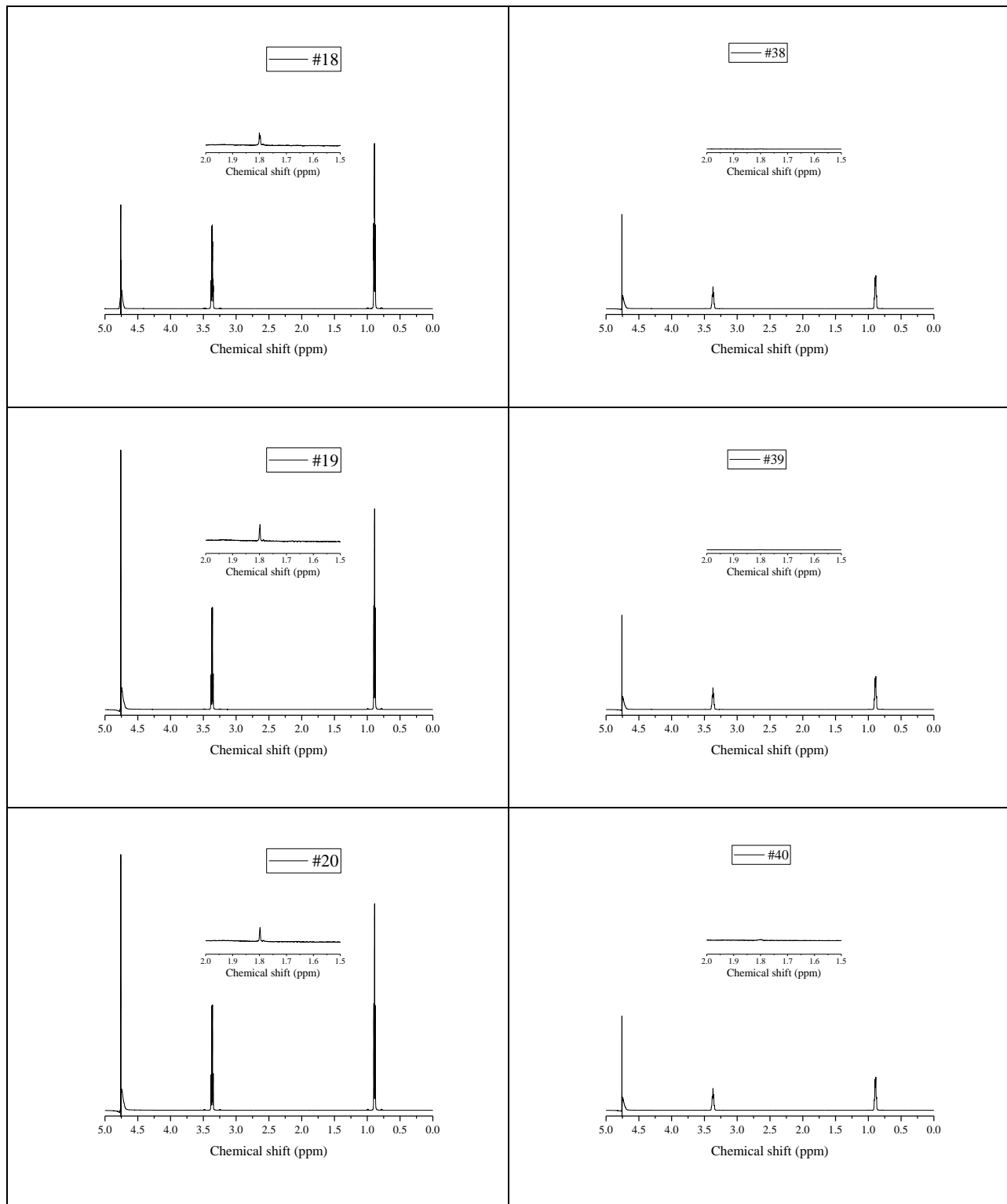
A4 Appendix – TEM images (Pechini method)

Below are the TEM images used for the measurement of the particle size of the catalysts prepared with the Pechini method (Chapter 3).

e)PtCeO$_2$-5wt%-5× f)PtCeO$_2$-5wt%-10×

20 nm
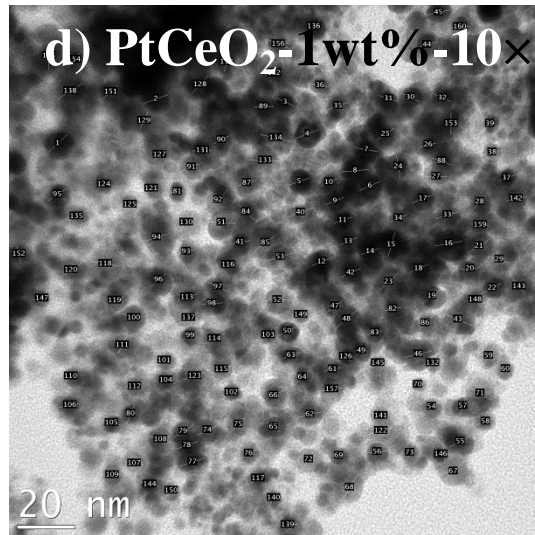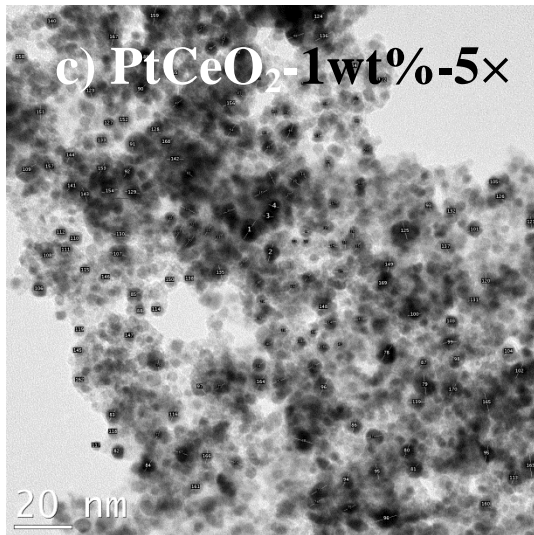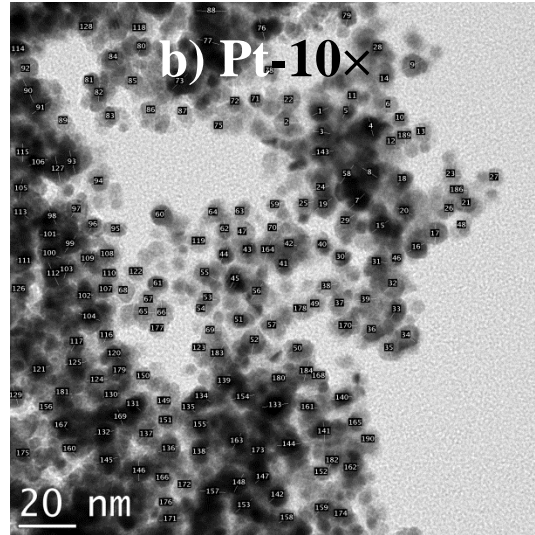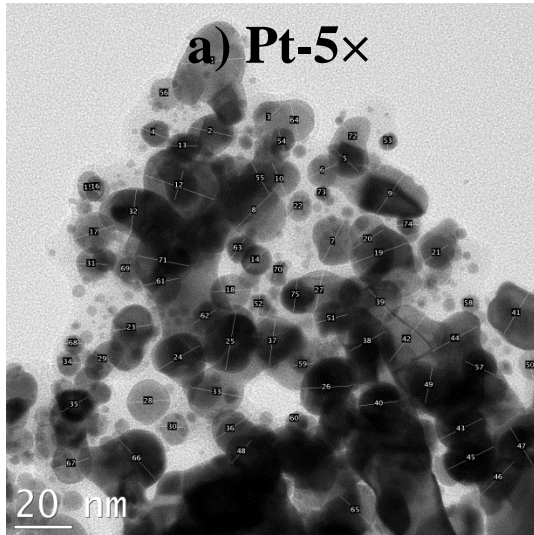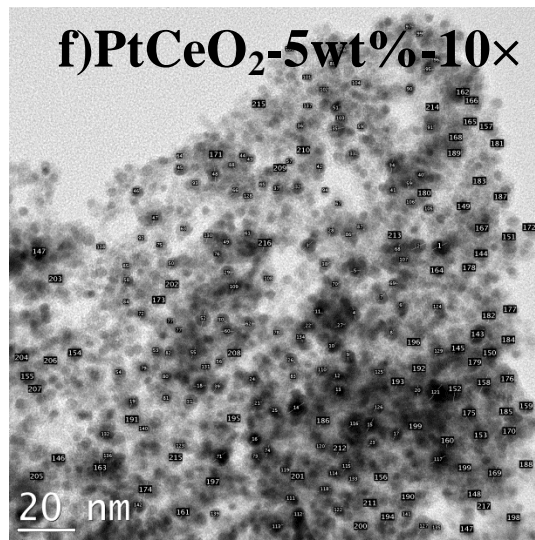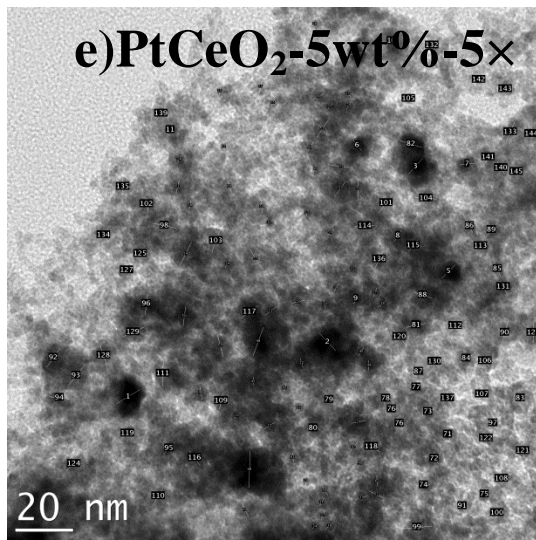
A5 Appendix – TEM images (Reduction method)

Below are the TEM images used for the measurement of the particle size of the catalysts prepared with the reduction method (Chapter 4).

a) Pt

b) Pt-cit

c) PtCeO$_2$-1wt%

d) PtCeO$_2$-1wt%-cit

e) PtCeO$_2$-5wt%

f) PtCeO$_2$-5wt%-cit
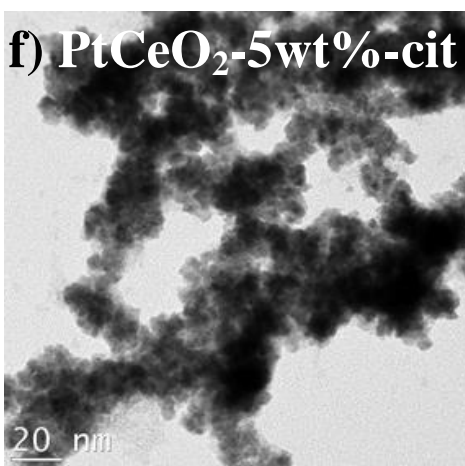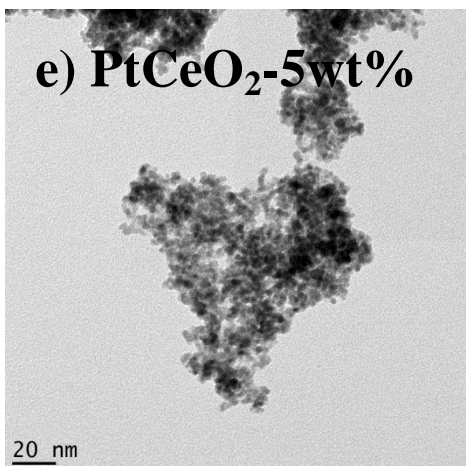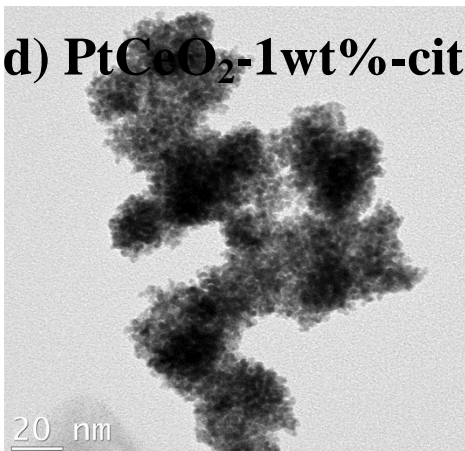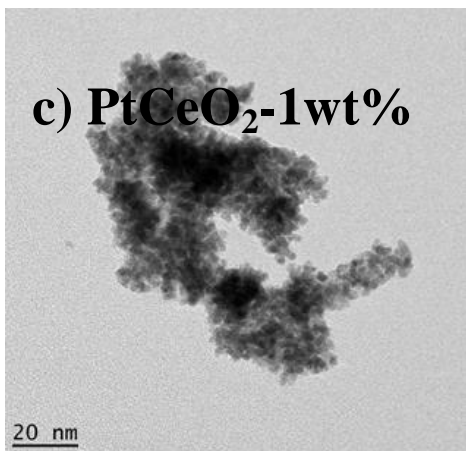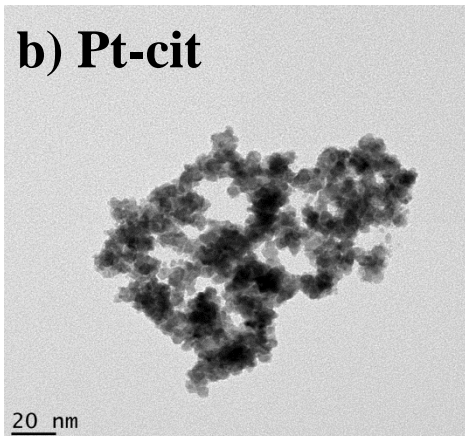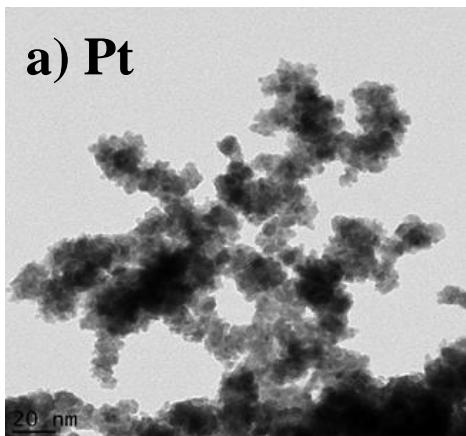
A6 Appendix – Cyclic voltammetry (Pechini method)

Below are the forward and backward current scans in EtOH/H$_2$SO$_4$ for the catalysts prepared by Pechini method; (a) as prepared without dilution, (b) with 5x dilution and (c) with 10x dilution.
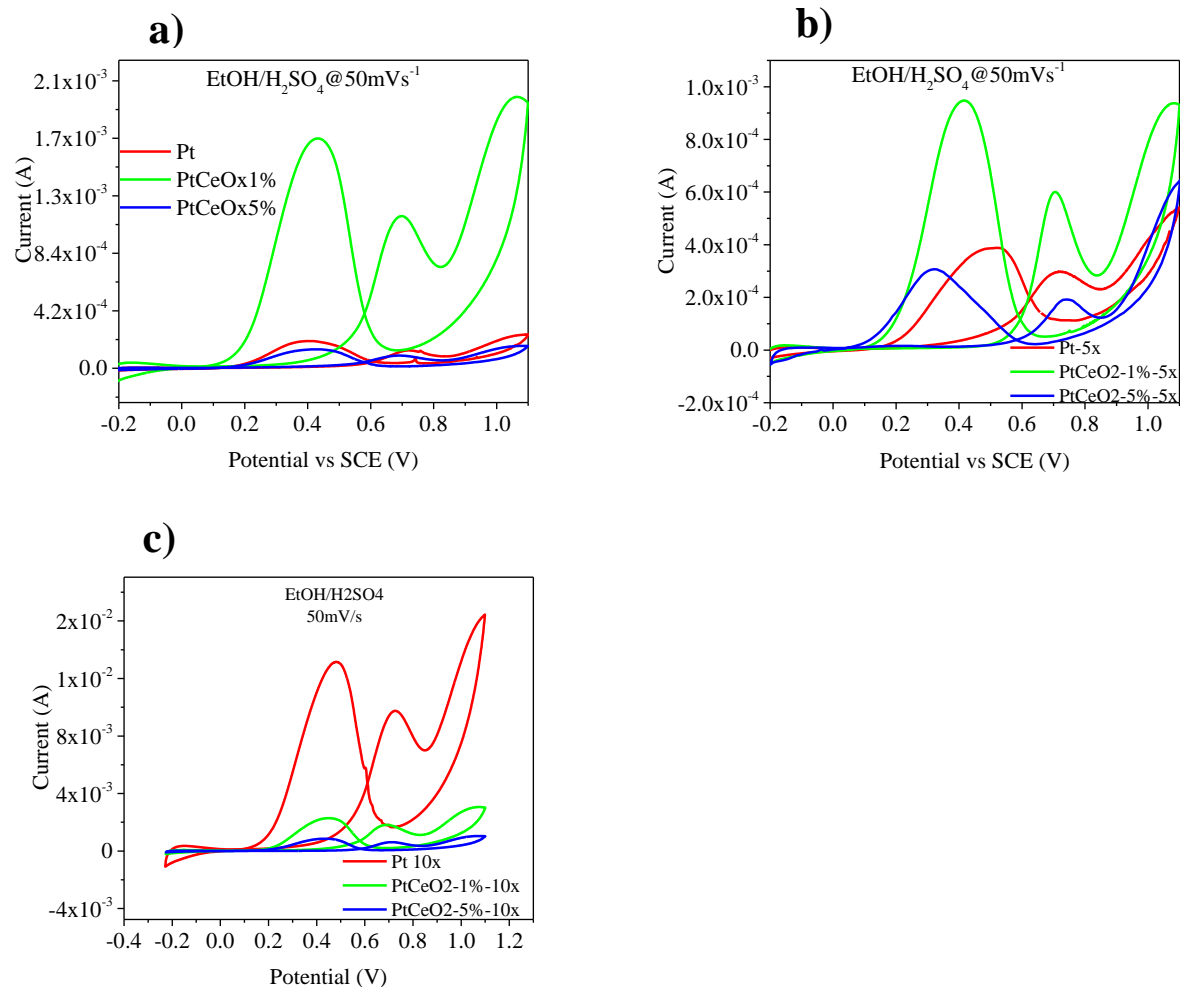
A7 Appendix – Cyclic voltammetry (Reduction method)

Below are the forward and backward scans of the currents for all catalysts (a) as-prepared without citrate and (b) with citrate in EtOH/H_2SO_4.
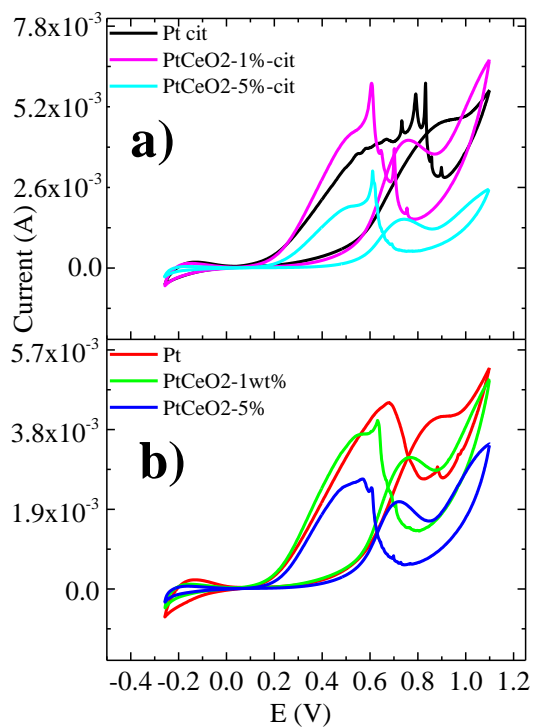
A8 Appendix – XRD

Below is the XRD of non-crystallized (amorphous ceria) prepared by reduction method (black) vs crystallized ceria prepared by the Pechini method at 400°C (blue).
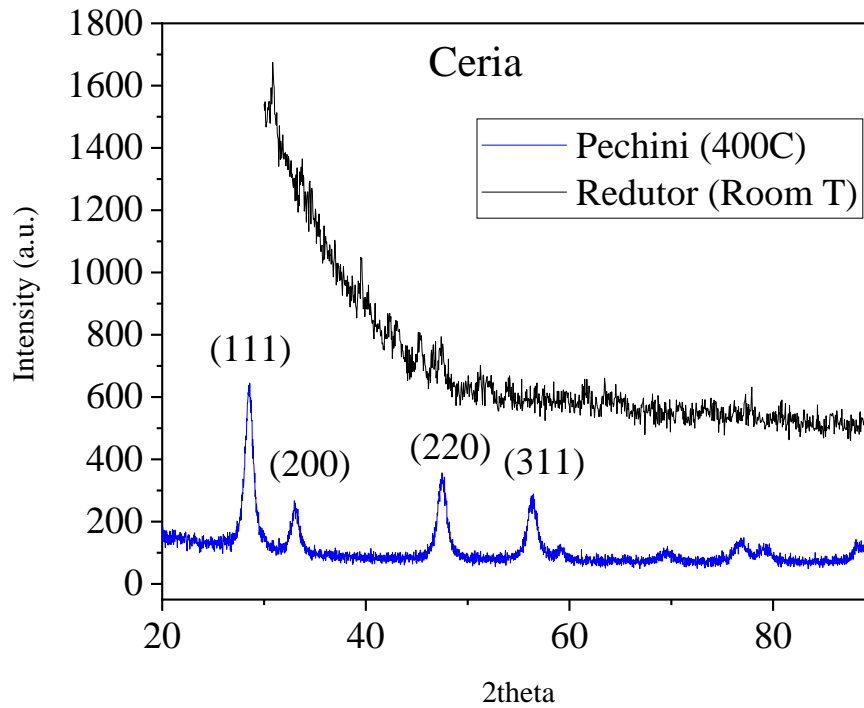
B. Publications during PhD

Peer reviewd papers:

Paulo MJVR, Tavares A. Novel hydrotalcite composites membranes for alkaline fuel cells. ECS Transactions 2011;35:21-8. (Msc work)

Paulo M, Matos B, Ntais S, Fonseca F, Tavares A. Effect of monobutylether ethylene glycol on Mg/Al layered double hydroxide: a physicochemical and conductivity study. J Nanopart Res 2013;15:1-14. (submitted and finalized during my PhD)

Paulo MJ, Freitas RG; Pereira E; Tavares AC, Investigation of the electrocatalytic activity for ethanol oxidation of Pt nanoparticles modified with small amount (≤ 5 wt%) of CeO_2, Journal of Electroanalytical Chemistry, JELECHEM-D-18-01421, under revision.

Carneiro JF, **Paulo MJ**, Siaj M, Tavares AC, Lanza MRV. Nb_2O_5 nanoparticles supported on reduced graphene oxide sheets as electrocatalyst for the H_2O_2 electrogeneration. Journal of Catalysis 2015;332:51-61. (Contribution in XPS and TEM analysis.)

Carneiro JF, **Paulo MJ**, Siaj M, Tavares AC, Lanza MR. Zirconia on Reduced Graphene Oxide Sheets: Synergistic Catalyst with High Selectivity for H_2O_2 Electrogeneration. ChemElectroChem 2017;4:508-13. (Contribution in XPS and TEM analysis.)

Oral comunications:

M. J. Paulo, E. Tchomgui Kamga, B. Arfaoui, S. Ntais, A. C. Tavares, Structure & ionic conductivity of meixnerite modified with mono butyl ether ethylene glycol (mbeeg), Session: New Materials for Energy Applications, ICACC'15 Daytona Beach, Florida, January 27th, 2015;

M. J. Paulo, Renato G. Freitas, Ernesto C. Pereira, Ana C. Tavares, Development of Pt-CeO2 electrocatalysts via sol-gel (Pechini) and chemical reduction for Direct Ethanol Fuel Cells, New Materials for Energy Applications, ICACC'15 Daytona Beach, Florida, January 28th, 2015.